

UC Davis

UC Davis Electronic Theses and Dissertations

Title

Elucidating Molecular Interactions of Fruit and Fungal Pathogens in a Postharvest Context

Permalink

<https://escholarship.org/uc/item/0411897n>

Author

Mesquida Pesci, Saskia Desiree

Publication Date

2024

Supplemental Material

<https://escholarship.org/uc/item/0411897n#supplemental>

Peer reviewed|Thesis/dissertation

Elucidating Molecular Interactions of Fruit and Fungal Pathogens in a
Postharvest Context

By

SASKIA DESIREE MESQUIDA PESCI
DISSERTATION

Submitted in partial satisfaction of the requirements for the degree of

DOCTOR OF PHILOSOPHY

in

Plant Pathology

in the

OFFICE OF GRADUATE STUDIES

of the

UNIVERSITY OF CALIFORNIA

DAVIS

Approved:

Barbara Blanco-Ulate, Chair

Dario Cantu

Philipp Zerbe

Committee in Charge

2024

*To my parents, Pablo and Liliana, and my brother, Álvaro, for their unconditional love
and support.*

CONTENTS

List of Figures	vii
List of Tables	ix
Abstract	x
Acknowledgments	xiii
1 <i>Rhizopus stolonifer</i> exhibits necrotrophic behavior when causing soft rot in ripe fruit	1
1.1 Abstract	1
1.2 Introduction	2
1.3 Materials and Methods	4
1.3.1 Fungal and plant material	4
1.3.2 Fruit inoculations	4
1.3.3 Microscopy	4
1.3.4 Fungal DNA extraction, library preparation, and sequencing methods	5
1.3.5 Genome assembly	5
1.3.6 Genome repeat prediction	6
1.3.7 Gene prediction and functional annotation	6
1.3.8 Tissue sampling, RNA extraction, cDNA library preparation, and RNA sequencing	7
1.3.9 RNA-seq bioinformatics pipeline	8
1.3.10 RT-qPCR assessment of fungal transcriptional activity	9
1.4 Results	10
1.4.1 <i>Rhizopus stolonifer</i> successfully colonizes tissues from different fruit hosts over different periods	10
1.4.2 Novel genomic resources for <i>Rhizopus stolonifer</i>	11
1.4.3 Transcriptional profiles of <i>Rhizopus stolonifer</i> show distinct patterns of gene expression when infecting fruit hosts	13

1.4.4	<i>Rhizopus stolonifer</i> uses similar strategies when infecting different fruit hosts	16
1.5	Discussion	19
1.5.1	<i>Rhizopus stolonifer</i> displays distinctive rapid growth on different fruit hosts	19
1.5.2	Novel and high-quality genomic resources for <i>Rhizopus stolonifer</i> .	20
1.5.3	Cell wall degrading enzymes and redox processes play a relevant role in <i>Rhizopus stolonifer</i> infections of fruit	20
1.5.4	<i>Rhizopus stolonifer</i> interactions with its fruit hosts involve a comprehensive integration of external and internal signals	22
1.6	Conclusions	23
1.7	Data Availability	24
1.8	Acknowledgments	24
1.9	References	25
1.10	Supplementary Material	32
2	Fruit surface topography, timely transcriptional responses, and reduced susceptibility factors enhance anthracnose resistance in papaya	33
2.1	Abstract	33
2.2	Introduction	34
2.3	Materials and Methods	36
2.3.1	Plant material and experimental design	36
2.3.2	Image analysis to characterize the anthracnose disease severity, and anatomical and microstructural features of cuticle and cell wall . .	37
2.3.3	Analyses of fruit quality attributes	37
2.3.4	Characterization of fungal isolates	38
2.3.5	Microscopy analysis	38
2.3.6	Tissue sampling, RNA extraction, cDNA library preparation, and RNA sequencing	39
2.3.7	Functional annotations	40

2.3.8	RNA-seq bioinformatics pipeline	40
2.4	Results	41
2.4.1	Papaya genotypes display quantitative resistance to anthracnose disease	41
2.4.2	Surface topology and physicochemical properties provide insights into differences in resistant and susceptible genotypes	42
2.4.3	The response of resistant and susceptible genotypes to fungal infection varies in both timing and magnitude	46
2.4.4	Gene modules reveal trends of early and late gene expression associated with symptomatic and asymptomatic infections	48
2.4.5	Callose deposition is associated with resistance in papaya fruit	51
2.4.6	Highly expressed and induced genes reveal functions related to resistance and susceptibility to anthracnose	53
2.5	Discussion	55
2.5.1	Smoother and thicker fruit surfaces with fewer natural openings are associated with papaya resistance to <i>Colletotrichum</i>	55
2.5.2	Firm fruit with reduced sugars and higher acidity are more tolerant to <i>Colletotrichum</i> infections	58
2.5.3	Timing is crucial! Larger transcriptional responses to fungal infection do not ensure fruit resistance	59
2.5.4	Highly expressed genes during fruit infections provide clues about defense mechanisms and susceptibility factors	60
2.6	Conclusions	61
2.7	Data Availability	62
2.8	Acknowledgments	62
2.9	References	63
2.10	Supplementary material	71
3	Characterizing the early interaction between <i>Botrytis cinerea</i> and strawberry fruit to identify biomarkers for disease detection	72

3.1	Abstract	72
3.2	Introduction	73
3.3	Materials and Methods	75
3.3.1	Fungal and plant material	75
3.3.2	Fruit inoculations	76
3.3.3	Multispectral imaging for early infection detection	76
3.3.4	Volatile collection and analyses	77
3.3.5	Tissue sampling, RNA extraction, cDNA library preparation, and RNA sequencing	79
3.3.6	RNA-seq bioinformatics pipeline	80
3.4	Results	80
3.4.1	Fruit reflectance profiles reveal <i>Botrytis cinerea</i> presence before dis- ease symptoms are evident	80
3.4.2	Strawberry fruit inoculated with <i>Botrytis cinerea</i> have distinct pro- files of emitted volatile organic compounds	81
3.4.3	Early fruit transcriptional responses can shed light on the changes in surface properties and volatile profiles	84
3.5	Discussion	86
3.5.1	Multispectral features reveal <i>Botrytis cinerea</i> is active on straw- berry fruit in the early stages of infection	86
3.5.2	Infections of <i>Botrytis cinerea</i> lead to an increase in certain classes of volatile compounds	88
3.5.3	Pathways related to redox processes and synthesis of secondary metabolites are active early in the <i>Botrytis cinerea</i> -strawberry in- teraction	89
3.6	Conclusions	91
3.7	References	92
3.8	Supplementary Material	96

LIST OF FIGURES

1.1	<i>Rhizopus stolonifer</i> colonizes different fruit hosts	12
1.2	The genome of <i>Rhizopus stolonifer</i>	14
1.3	Patterns of up-regulated differentially expressed genes reveal distinct gene clusters acting throughout the course of <i>Rhizopus stolonifer</i> infection of fruit hosts	17
1.4	Expression patterns of genes encoding cell wall degrading enzymes present in the core infection toolbox of <i>Rhizopus stolonifer</i> on different fruit hosts	19
2.1	Quantitative resistance to <i>Colletotrichum gloeosporioides</i> and <i>C. truncatum</i> in seven papaya varieties	43
2.2	Fruit microstructural, anatomical, and physicochemical properties of the CI-05 resistant and CI-13 susceptible genotypes	45
2.3	Transcriptional profiling of the CI-05 resistant and CI-13 susceptible genotypes after natural infections with <i>Colletotrichum</i> spp.	49
2.4	Gene co-expression patterns reveal modules associated with papaya resistance and susceptibility to anthracnose	52
2.5	Host cell wall responses and fungal proliferation in the CI-05 resistant and CI-13 susceptible genotypes after <i>Colletotrichum gloeosporioides</i> and <i>C. truncatum</i> infections	54
2.6	Overview of highly expressed genes in the CI-05 resistant and CI-13 susceptible genotypes	56
3.1	Visualization of gray mold progression using multispectral imaging	82
3.2	Profiling of volatile organic compounds (VOCs) shows potential for early <i>Botrytis cinerea</i> detection	85
3.3	Transcriptional profiling of mock- and <i>Botrytis cinerea</i> -inoculated strawberry fruit	87

3.S1 Principal component analysis (PCA) of total mapped RNA-seq <i>Botrytis cinerea</i> and strawberry reads	96
--	----

LIST OF TABLES

1.1	Summary of core infection strategies used by <i>Rhizopus stolonifer</i> during infection of tomato, grape, strawberry, and plum fruit	19
-----	---	----

ABSTRACT

Elucidating Molecular Interactions of Fruit and Fungal Pathogens in a Postharvest Context

Worldwide, 20-25% of all fruit and vegetables are lost in the field and throughout the postharvest supply chain to rotting caused by fungal pathogens. This issue is particularly exacerbated in fleshy fruit, which become more susceptible to fungal pathogens as they ripen. Fungal pathogens with necrotrophic lifestyles are among the most devastating postharvest pathogens, as they actively kill the host tissues, resulting in extensive rotting. Plant defense responses to necrotrophs are complex and multi-layered, and a better understanding of the mechanisms behind the establishment of a compatible interaction between necrotrophs and fruit hosts is required for developing novel and effective management strategies.

The overarching goal of my Ph.D. dissertation was to understand the biology of the interactions between fruit and necrotrophic fungal pathogens to identify: 1) infection mechanisms deployed by fungal pathogens when interacting with fruit (Chapter 1); 2) constitutive, preformed, and induced plant defense mechanisms contributing to resistance to fungal pathogens in fruit (Chapter 2); and 3) features of early fungal pathogen-fruit interactions that can aid the timely detection of disease (Chapter 3).

In Chapter 1, I employed a genomic and transcriptomic approach to characterize the infection strategies of the impactful postharvest pathogen *Rhizopus stolonifer*, causal agent of soft rot, when infecting four fruit commodities of relevance to California agriculture (tomato, grape, strawberry, and plum). With collaborators, we developed publicly available, novel genomic resources that will further advance our understanding on how *R. stolonifer* interacts with its fruit hosts. I also performed a transcriptomics analysis that revealed that *R. stolonifer* possesses a necrotrophic core infection toolbox consisting of cell wall degrading enzymes, proteases, and oxidoreductases, that allow the fungus to macerate tissue and quickly colonize multiple hosts, and which have the potential to be targets for pathogen control. The knowledge generated in this study will aid the devel-

opment of better integrated pest management approaches to minimize losses due to soft rot.

In Chapter 2, I characterized the mechanisms underlying the resistance to anthracnose disease, caused by *Colletotrichum* spp., displayed by a pre-commercial papaya variety. With collaborators, we observed fruit surface and cuticular properties using confocal and scanning electron microscopy and analyzed fruit physicochemical properties. These analyses revealed the resistant variety has a thicker cuticular layer, lower stomatal density, greater firmness, and lower total soluble sugars, characteristics that can be considered preformed barriers or correlate with reduced susceptibility factors. I also performed differential gene expression and weighted gene co-expression network analyses to gain insight into induced defenses upon pathogen infection. The resistant variety seemed to respond earlier to fungal presence by synthesizing elements contributing to cuticular and cell wall integrity. On the other hand, the susceptible variety had a stronger immune response, but a higher presence of susceptibility factors and a delayed response to the pathogen that rendered it unable to control the disease. These results highlight the need to comprehensively characterize preformed and induced defenses, as well as susceptibility factors, to better understand fruit-pathogen interactions and inform breeding programs with strong targets for developing resistant varieties.

In Chapter 3, I utilized multispectral imaging (MSI) and volatile organic compound (VOC) profiling approaches to study biomarkers of early interactions between the necrotrophic fungus *Botrytis cinerea*, causal agent of gray mold, and strawberry fruit. With collaborators, I compared the spectral and VOC profiles of *B. cinerea*-inoculated and mock-inoculated fruit from 0 to 48 hours post inoculation (hpi). Reflectance profiles of *B. cinerea*-inoculated fruit differed from mock-inoculated ones as early as 12 hpi, and infected samples displayed distinct VOC profiles as early as 9 hpi, as well as emitted VOCs with antifungal activity. Lastly, I performed a transcriptomic study of strawberries mock- and *B. cinerea*-inoculated at early time points (3, 6, 12, and 24 hpi), which revealed differentially expressed genes involved in secondary metabolic pathways and redox processes that could explain the features revealed by the MSI and VOC analyses,

pointing to an early coordinated host response to *B. cinerea*. This research highlights the potential of complementary, non-destructive approaches for early detection of gray mold disease.

Taken together, the results of this thesis improve our understanding of the interactions between fruit and plant pathogenic fungi at a molecular level. Insights into the pathogen infection toolbox, the role of preformed and induced defenses and abundance of susceptibility factors, as well as how to leverage the molecular understanding of fruit-pathogen interactions for disease detection, are key for the development of novel and more efficient disease management strategies to minimize postharvest food losses.

ACKNOWLEDGMENTS

First of all, I would like to thank my professor and mentor, Bárbara Blanco-Ulate, for her invaluable guidance, support, and belief in me throughout my Ph.D. journey. She first welcomed me into her lab as a visiting scholar, and opened the opportunity for me to pursue my Ph.D. studies at UC Davis under her mentorship. I am deeply thankful for her encouragement to think creatively, for the countless hours she dedicated to exchanging ideas, and for the insight and intellect that she shared, which were instrumental in shaping my project. I admire her genuine care for her students and the collaborative lab culture that she has fostered, which have greatly shaped my growth as a scientist and as an individual.

I would like to thank my committee members, Dario Cantu and Philipp Zerbe, for their support and advice. I also appreciate the help from collaborators on various projects, particularly Pedro Bello, Eva Borrás, Abraham Morales-Cruz, Rosa Figueroa-Balderas, and David Pérez-Leyva. Thank you as well to Theresa Garcia for her administrative assistance.

A heartfelt thank you to my fellow Blanco Lab members and alumni for their friendship and support throughout this journey. Special thanks to Isabel Ortega-Salazar for being my first friend in Davis, and for all her love and encouragement over the years. A very big thanks to Jaclyn Adaskaveg for her friendship, support, and intellectual input that made data analysis less daunting. Thank you to Stefan Petrasch for his genuine and honest friendship and his support, regardless of distance. Thanks to Christian Silva for his help with bioinformatics, and for all the valuable conversations we shared during our time together. Lastly, warm thanks to Elia Gutiérrez-Baeza and Nathaly, Yiduo Wei, and Chris Preston Rubio for their technical and emotional support. A special thank you to Adrián Sbodio for all his invaluable technical assistance and for his friendship.

I am grateful to my former undergraduate assistants, Dilasha Shenaz and Benjamin Cohen Stillman, for their instrumental help with experiments and sample processing, as well as for inspiring me to become a better mentor. I also appreciate the friendship of Nancy Yip, Nancy Her, and all the visiting scholars who contributed to the Blanco Lab's

vibrant atmosphere: Kiko Fernández-Acero, Silvia Rodríguez-Pires, Lara O’Shea-Farren, Simone Piancatelli, Thomas Michelin, Valeria Imperiale, and Marta Balsells-Llauradó. I would like to thank as well the Mann Lab community, my cohort, and the friends in the Plant Pathology graduate group for their support.

A warm thank you to my housemates over the years, Best Yeemin, Immy Maneejantra, and Tianyue Wang, for making Davis feel like home. Thank you for the countless movie nights, the delicious food you shared with me, and for your love, friendship, and support at all times. A special thanks to my friends in the Davis Congregation, particularly Raquel Lee, for their love, support, and for being like family.

I also thank my friends from Wageningen, especially Laura, Si, Alisha, Ami, and William, for their continued support and love over the years. Thank you for keeping our friendship strong despite the distance, and for making the effort to come to see me on this side of the world. I would also like to thank my friends from home, Paloma, Beatriz, David, and Alba, whom despite the many years of physical separation make every reunion feel as though time had stood still.

Finally, I am deeply thankful to my family, who have been with me through every step of this journey. To my parents, Pablo and Liliana, thank you for always encouraging me to pursue what is best for me and for all your loving counsel, advice, and unconditional support. To my brother Álvaro, thank you for always being there for me, for lending a listening ear, and your loving advice and support, no matter the circumstances. I would not be the person I am today if it was not for them. Gracias de todo corazón.

Chapter 1

Rhizopus stolonifer exhibits necrotrophic behavior when causing soft rot in ripe fruit

1.1 Abstract

Rhizopus stolonifer is known for causing soft rot in fruit and vegetables during postharvest. Although it has traditionally been considered a saprophyte, it appears to behave more like a necrotrophic pathogen. In this study, we propose that *R. stolonifer* invades host tissues by actively killing host cells and overcoming the host defense mechanisms, as opposed to growing saprophytically on decaying plant matter. We tested this hypothesis by characterizing *R. stolonifer* infection strategies when infecting four fruit hosts (tomato, grape, strawberry, and plum). We started by generating a high-quality genome assembly for *R. stolonifer* using PacBio sequencing. This led to a genome size of 45.02 Mb, an N50 of 2.87Mb, and 12,644 predicted loci with protein-coding genes. Next, we performed a transcriptomic analysis to identify genes that *R. stolonifer* preferentially uses when growing in fruit versus culture media. We categorized these infection-related genes into clusters according to their expression patterns during the interaction with the host. Based on the expression data, we determined that *R. stolonifer* has a core infection toolbox consisting of strategies typical of necrotrophs, which includes a set of 33 oxidoreductases, 7 proteases, and 4 cell wall degrading enzymes to facilitate tissue breakdown and maceration across various hosts. This study provides new genomic resources for *R. stolonifer* and advances the knowledge of *Rhizopus*-fruit interactions, which can assist in formulating effective and sustainable integrated pest management approaches for soft rot prevention.

1.2 Introduction

Rhizopus stolonifer (Ehrenb.: Fr.) Vuill. is a plant pathogenic fungus belonging to the phylum Mucoromycota, naturally found in soil and plant debris, and able to grow on organic carbon sources, like bread. This fungus causes a disease known as soft rot or Rhizopus rot, which can affect many fruit and vegetables after they are harvested. Susceptible hosts include strawberries, bush berries, stone fruit, carrots, potatoes, sweet potatoes, cruciferous vegetables, and tomatoes (Bautista-Baños et al., 2014; Kwon et al., 2001; Lewthwaite et al., 2013; Northover and Zhou, 2002; Sallato et al., 2007; Tournas, 2005).

Due to the pervasiveness of its spores and its rapid growth, *R. stolonifer* is considered one of the most devastating postharvest pathogens worldwide (Bautista-Baños et al., 2014, 2008; Snowdon, 1990). Once the spores of *R. stolonifer* germinate under favorable conditions, rapid and extensive growth of mycelia occurs, spreading throughout the host tissues and other healthy hosts that are in direct contact with the affected one, a process known as nesting. The mycelial stolons attach to the host surface by means of complex, well-developed rhizoids (Feliziani and Romanazzi, 2016; Snowdon, 1990). The first visible sign of mycelial growth is a thin, white mass, which eventually turns dark when the columellate sporangia mature and bear the asexual sporangiospores. These spores are airborne and easily disseminate, contributing to the spread of the disease (Agrios, 2005; Schipper, 1984; Vicente et al., 2005).

Proper postharvest handling and storage are crucial to prevent soft rot (Bautista-Baños et al., 2014). Among the most effective strategies to minimize active infections of *R. stolonifer* are careful manipulation of the produce to avoid wounding, refrigeration during storage and transportation, maintaining relative humidity at optimal levels for fruit storage while limiting free water, and using fungicides (Bautista-Baños et al., 2014; Feliziani and Romanazzi, 2016). However, some commodities are sensitive to chilling temperatures or require high relative humidity during storage. Moreover, it has been reported that brief interruptions of the cold chain can favor infections (Bautista-Baños et al., 2008; Siefkes-Boer et al., 2009). Additionally, the use of synthetic fungicides is

subject to regulatory limitations and raises public health and environmental concerns (Bautista-Baños et al., 2014; Feliziani et al., 2015; Rezende et al., 2020; Salem et al., 2016; Xu et al., 2013).

R. stolonifer has traditionally been considered a saprophyte, meaning it cannot overcome host defenses or cause disease in living plants (Agrios, 2005). However, recent discoveries have shown that *R. stolonifer* can directly penetrate unwounded fruit using esterase enzymes (Baggio et al., 2016). It also utilizes redox processes and proteolysis when interacting with tomato fruit (Petrasch et al., 2019). These mechanisms are typical of necrotrophic fungal pathogens, which also release reactive oxygen species (ROS) and various cell wall degrading enzymes (CWDEs) to break down and consume host cells, causing significant tissue damage (Laluk and Mengiste, 2010; Liao et al., 2022; van Kan, 2006). Given these similarities, we hypothesized that *R. stolonifer*'s lifestyle aligns more closely with necrotrophy than saprotrophy. Here, we set out to generate novel genomic resources for *R. stolonifer* and study its pathogenicity mechanisms on different fruit hosts impacted by soft rot. We used a transcriptomic approach to identify infection strategies that the fungus is deploying commonly across all commodities, as well as any potential host-specific mechanisms. We first generated a highly contiguous genome and an improved predicted transcriptome from our previously published *R. stolonifer* transcriptome (Petrasch et al., 2019). We then evaluated *R. stolonifer* disease progression in four fruit crops highly valued in California and prone to soft rot: tomato, grape, strawberry, and plum. To determine if *R. stolonifer* changes its infection strategies according to the host, we analyzed the fungal transcriptome on each fruit host across four time points and compared it with the fungal behavior on growth media. Additionally, we examined virulence functions among the four hosts and searched for known necrotrophic infection strategies (Bi et al., 2023). This approach allowed us to identify core pathogenicity and virulence factors deployed by *R. stolonifer* and study how the fungus behaves in fruit environments. Overall, our research sheds light on *R. stolonifer*'s infection toolbox during interactions with different fruit and reveals key mechanisms that may be targeted to control soft rot.

1.3 Materials and Methods

1.3.1 Fungal and plant material

Rhizopus stolonifer strain BLUCD01 was obtained from postharvest infections of fruit and identified through morphological and sequencing methods (Petrasch et al., 2019). Axenic cultures of *R. stolonifer* were grown at room temperature (RT, approximately 20 °C) on 1% potato dextrose agar until sporulation. Sporangiospores were harvested using 0.01% Tween® 20 (Sigma-Aldrich, United States).

Tomato (*Solanum lycopersicum*) cv. Ailsa Craig fruit were grown under standard field conditions during the 2019 season in the Department of Plant Sciences Field Facilities at the University of California, Davis, United States. Red ripe fruit were harvested at 42 days post-anthesis. Strawberry (*Fragaria x ananassa*) cv. Portola fruit were obtained at commercial maturity from the UC Davis Strawberry Breeding Program. Japanese plum (*Prunus salicina* L.) cv. Fortune, and grape (*Vitis vinifera*) cv. Pristine® berries were commercially sourced.

1.3.2 Fruit inoculations

Fruit from all commodities were visually evaluated for uniform appearance and absence of wounds or symptoms of fungal infection. Fruit were disinfected in 0.6% sodium hypochlorite, wounded eight times within an area of approximately 4.9 cm² with a 1 mm sterile pipette tip to an approximate depth of 5-7 mm, and inoculated with 10 µl of a 30 spores/µl suspension of *R. stolonifer*. Tomato fruit were wounded on the blossom end, strawberry fruit were wounded near the center, and plum fruit and grape berries were inoculated on the equator. Inoculated fruit were incubated at RT in high-humidity containers (between 90% and 100% relative humidity), to mimic retail settings as well as create an environment favorable for fungal development. Progression of Rhizopus rot was monitored every 6 to 12 hours post-inoculation (hpi) until mature fungal mycelium covered the fruit surface.

1.3.3 Microscopy

Fruit tissues were observed and photographed using a Leica DVM6 Digital Microscope (Leica, Germany) with the 46X – 675X magnification objective. Fruit were inoculated as

described above and directly observed with the microscope at 6, 12, 24, and 48 hpi.

1.3.4 Fungal DNA extraction, library preparation, and sequencing methods

Around 100 mg of mycelium was collected in a 2 mL microcentrifuge tube and frozen in liquid nitrogen. High Molecular Weight (HMW) genomic DNA (gDNA) was extracted as previously described (Morales-Cruz et al., 2015). DNA purity and quantity were evaluated with a Nanodrop One spectrophotometer (Thermo Scientific, USA), and with a Qubit 2.0 Fluorometer (Life Technologies, USA). DNA integrity was verified by pulsed-field gel electrophoresis. 15 µg of HMW gDNA was cleaned with 0.45x AMPure PB beads (Pacific Biosciences, USA) before library preparation.

A SMRTbell template library was prepared using SMRTbell Express Template Prep Kit (Pacific Biosciences, USA) following the manufacturer’s instructions. For size selection, 4 µg of SMRTbell template were loaded on a Sage Blue Pippin (Sage Science, USA) and size-selected with a cut-off range of 25-80 Kbp. The size-selected library was cleaned with 1x AMPure PB beads (Beckman Coulter, USA). The SMRTbell library produced was sequenced in one SMRT cell on a PacBio Sequel I Platform (DNA Technology Core Facility, University of California, Davis).

1.3.5 Genome assembly

The genome of *R. stolonifer* BLUCD01v1 was assembled using SMRT reads with FALCON-Unzip ver. 2017.06.28-18.01 (Chin et al., 2016) adopting the custom pipeline published in Minio et al. (Minio, 2019a; Minio et al., 2019). Before performing error correction of the raw reads, repetitive regions were marked using the TANmask and REPmask modules from the DAMasker v1.0 (Myers, 2014), reducing the complexity of the read-to-read alignment phase. After error correction, reads were again marked before proceeding with the assembling phase. This additional repeat masking step increased assembly contiguity by reducing the complexity of the overlap graph.

FALCON was performed using different thresholds on seed-reads minimum length for overlap stage (`length_cutoff_pr` parameter) to find the least frag-

mented primary assembly. Parameter set includes: “falcon_sense_skip_contained = TRUE”, “falcon_sense_option = -output_multi -min_idt 0.70 -min_cov 4 -max_n_read 400”, “length_cutoff_pr = 27000”, “ovlp_DBSplit_option = -x500”, “ovlp_HPCdaligner_option = -mtan -mrep2 -v -B128 -M60 -t60 -k20 -h256 -e.9 -l1000 -s100 -T16”, and “overlap_filtering_setting = -max_diff 100 -max_cov 400 -min_cov 3”. The unzip step was skipped since *R. stolonifer* has a haploid genome. We used the long reads with Arrow (from ConsensusCore2 v.3.0.0) to polish the contigs and SSPACE-Longreads v.1.1 (Boetzer and Pirovano, 2014) to create the final scaffolds. The gene space completeness of the genome assemblies was evaluated using the BUSCO genes (Simão et al., 2015), specifically using BUSCO v5.0 and the “fungi_odb10” database. A full BUSCO report and genome statistics for *R. stolonifer* BLUCD01v1 can be found on Supplementary Tables S1 and S2. The same BUSCO analysis was run on two other available *R. stolonifer* genomes, RhiStoB9770 (https://www.ncbi.nlm.nih.gov/datasets/genome/GCA_000697035.1/) and NRRL66455 (<https://mycocosm.jgi.doe.gov/Rhisto1/Rhisto1.home.html>), together with scaffold statistics for comparison with BLUCD01v1 (Supplementary Table S3).

1.3.6 Genome repeat prediction

An initial run of RepeatMasker v4.0.6 (Smit, 2015) with the standard library was performed for the *R. stolonifer* BLUCD01v1 genome. The repeats predicted by this run were combined with the repeats from RepBase v22.04 (Bao et al., 2015) to create a new database using the de novo repeat predictor RepeatModeler v1.0.11 (Smit and Hubley, 2015). The classified consensus sequences were then used as a custom library for the final run of RepeatMasker with the BLUCD01v1 assembly.

1.3.7 Gene prediction and functional annotation

Three replicates of RNA-seq from previously published *R. stolonifer* BLUCD01 growing *in vitro* were combined (Petrasch et al., 2019). The 50 bp single-end reads were trimmed with Trimmomatic v0.36 (Bolger et al., 2014) with a 4-base wide sliding window, cutting

when the average quality per base drops below 15 and a minimum length of 40 bp. The trimmed reads were mapped to the reference genome with the splice-aware mapper HISAT2 v2.0.5 (Kim et al., 2019) using the single-end mode and the following arguments: “-k 1 -non-deterministic”. The alignment files with the splicing information were then used as hint for the gene predictor BRAKER1 v1.9 (Hoff et al., 2016) with the “-fungus” option to allow for potential overlapping genes on the soft-masked genome assemblies. The genes were filtered using the script “GFF_extract_features.py” from Minio et al. (Minio, 2019b; Minio et al., 2022) to obtain the final set of 13,114 predicted protein coding genes.

Functional annotations for Gene Ontology (GO) terms, Pfam families, Transporter Classification Database (TCDB), Pathogen-Host Interactions Database (PHI), and Fungal Peroxidase Database (fPox), as well as presence of secretion signal peptides, were carried out using the predicted transcriptome as previously described (Petrasch et al., 2019).

1.3.8 Tissue sampling, RNA extraction, cDNA library preparation, and RNA sequencing

Tissue samples were collected from the pericarp and epidermis of the blossom end of tomato fruit, the receptacle of strawberry fruit, and the exocarp and mesocarp of plum fruit and grape berries, including the inoculation points and lesion areas, at 6, 12, 24, and 48 hpi. Samples were immediately frozen in liquid nitrogen and stored at -80 °C until further processing. One biological replicate consisted of tissues of four independent fruit. Four separate biological replicates were obtained per commodity and time point.

Fruit tissues from all commodities were ground using a Retsch® Mixer Mill MM 400 (Retsch, Germany), and RNA was extracted from 1 g of ground tissue as previously described (Blanco-Ulate et al., 2013b). RNA purity and concentration were assessed with a NanoDrop One Spectrophotometer (Thermo Scientific, United States) and a Qubit 3 fluorometer (Invitrogen, United States), respectively. RNA integrity was confirmed by agarose gel electrophoresis.

Forty-eight barcoded cDNA libraries (four hosts, four time points per host, and three replicates per time point) were prepared using the Illumina TruSeq RNA Sample Preparation Kit v2 (Illumina, United States). Quality control of the cDNA libraries was per-

formed with the High Sensitivity DNA Analysis Kit in the Agilent 2100 Bioanalyzer (Agilent Technologies, United States). 150-bp paired-end libraries were sequenced on the HiSeq X Platform at IDSeq Inc. (Davis, CA, United States). In total, twelve libraries were sequenced per fruit commodity (three libraries per time point).

1.3.9 RNA-seq bioinformatics pipeline

Raw reads from the *Rhizopus*-infected fruit samples were quasi-mapped to combined transcriptomes of *R. stolonifer* and the four fruit commodities using Salmon (v. 1.10.3) (Patro et al., 2017). Parameter set includes: “-l A”, “-p 8”, and the “-validateMappings -posBias -seqBias -gcBias” flags. Mapping percentages and numbers of host and pathogen reads and genes for each sample can be found on Supplementary Table S4. The tomato transcriptome (*Solanum lycopersicum*, build SL4.0 with ITAG 4.0 annotations) (Tomato Genome Consortium, 2012) was obtained from https://solgenomics.net/organism/Solanum_lycopersicum/genome (accessed January 17, 2022). The strawberry transcriptome (*Fragaria x ananassa* Camarosa Genome Assembly v1.0 and Annotation v1.0.a1) was retrieved from https://www.rosaceae.org/species/fragaria_x_ananassa/genome_v1.0.a1 (accessed January 17, 2022). The plum transcriptome (*Prunus salicina* Zhongli No. 6 Whole Genome v1.0 Assembly and Annotation) was obtained from <https://www.rosaceae.org/Analysis/9019655> (accessed January 17, 2022). The grape transcriptome (*Vitis vinifera* PN40024 Genome 12x.V2) was retrieved from <http://www.grapegenomics.com/pages/PN40024/> (accessed January 17, 2022). For the *R. stolonifer* transcriptome, the predicted protein coding genes from the BLUCD01v1 genome were used. For downstream processing, infected and *in vitro* samples were quasi-mapped to the *R. stolonifer* transcriptome only. Count matrices were made from the Salmon output using the Bioconductor package tximport (Love et al., 2017) and are available in Supplementary Table S5 and in the Gene Expression Omnibus (GEO) database, under accession number GSE232735. Raw files containing host and pathogen reads are also located under GEO accession GSE232735.

Count matrices were used as input for differential expression analysis with the Bioconductor package DESeq2 (Love et al., 2014) in R. Reads were normalized for library

size. A subset of genes with an average of more than two reads per time point was used to evaluate the percentage of fungal annotations observed in active infections on each host out of the total annotations recorded for the transcriptome. Pairwise comparisons were made between the fungal gene expression at 6, 12, 24 or 48 hpi in each host against the previously published data of *R. stolonifer* BLUCD01 gene expression when grown in media prior to sporulation (also in three replicates), to compare the fungus deriving nutrients from a live host as opposed to growing saprophytically on readily available nutrients from culture media (Petrasch et al., 2019). Differentially expressed genes (DEGs) were those with a P_{adj} less than 0.05.

Selected GO terms were visualized using the Reduce + Visualize Gene Ontology Web server (<http://revigo.irb.hr/>). GO, Pfam, and CAZy terms that were common to all four hosts, and PHI and fPox annotations were used to manually assign genes to one or more of the following eleven categories: amino acid synthesis, cellular maintenance, cellular metabolism, transcription/translation, fungal cell wall (CW) metabolism, host CW degradation, oxidation-reduction process, proteolysis, signal transduction, transmembrane transport, and host-pathogen interaction. Enrichment analyses for these categories were performed using Fisher’s exact test ($P_{adj} < 0.05$).

1.3.10 RT-qPCR assessment of fungal transcriptional activity

cDNA was synthesized on 1 µg of RNA using the M-MLV Reverse Transcriptase (Promega, United States) in the SimpliAmp Thermal Cycler (Applied Biosystems, United States). Fungal biomass was quantified through Real-Time Quantitative PCR (RT-qPCR) using PowerSYBR Green PCR Master Mix (Applied Biosystems, United States) in the QuantStudio3 (Applied Biosystems, United States). Primers were designed using Primer-BLAST (Ye et al., 2012). Primer efficiency was confirmed to be higher than 90% using fourfold cDNA dilutions (0, 1:1, 1:4, 1:16, 1:64, and 1:256) in triplicate. Primer specificity was checked through melting curve analysis at different temperatures (60-95°C). Relative gene expression was calculated using the formula $2^{(\text{reference gene Ct} - \text{gene of interest Ct})}$, where “reference gene Ct” refers to the host reference gene and “gene of interest Ct” refers to *R. stolonifer ACT* (*RS_BLUCD01_v1_scf04.ver1.g049010.m01*, with $r = 0.947$

and p value = 2.69447E-11 between gene reads and total reads). The primers used in this study are listed in Supplementary Table S6.

1.4 Results

1.4.1 *Rhizopus stolonifer* successfully colonizes tissues from different fruit hosts over different periods

We visually assessed the development of soft rot on tomatoes, grapes, strawberries, and plums (Figure 1.1A) and quantified transcriptional activity of *R. stolonifer* in these four hosts via qRT-PCR (Figure 1.1B). No symptoms were visible up to 12 hours post-inoculation (hpi) in any of the hosts. At 24 hpi, advancing tissue maceration could already be observed in tomatoes, grapes, and strawberries. Aerial hyphae restricted to the inoculation area could be seen at around 30 hpi for tomato, together with cracking of the fruit surface, and at 36 hpi for grape and strawberry. Shortly afterward, tomato (36 hpi), grape, and strawberry (48 hpi) were completely covered by sporulating fungal mycelium, leading to extensive tissue rotting by 48 hpi (tomato) and 54 hpi (grape and strawberry). Although the mycelium was not visible in plum as early as the other commodities, extensive tissue maceration could be observed at 48 hpi, followed by the appearance of aerial hyphae at 72 hpi, and complete fruit maceration at 122 hpi. The progression of *R. stolonifer* infection symptoms was mirrored by the fungal transcriptional activity in each host (Figure 1.1B). For example, in strawberries, tomatoes, and grapes, the absence of visible fungal growth and incipient tissue maceration were matched by a moderate increase in fungal gene expression (*RsACT*, *RS_BLUCD01_v1_scf04.ver1.g049010.m01*) up to 24 hpi, followed by an exponential increase at 48 hpi concomitant with the rapid expansion of fungal mycelium on the fruit surface. Our observations indicate that, although *R. stolonifer* can successfully colonize diverse fruit commodities under conducive conditions, it does so to varying extents over different time frames.

We further examined *R. stolonifer* fungal structures throughout the course of infection using a digital microscope. Figure 1.1C shows these structures in tomato, where the surface texture and color facilitated better visualization. No germination was observed by

6 hpi, but incipient hyphal growth on the fruit surface was visible at 12 hpi (Figure 1.1C, left), though it was not macroscopically evident. Erect sporangiophores became visible at 24 hpi (Figure 1.1C, middle), coinciding with tissue cracking and the appearance of white mycelium on the fruit surface (Figure 1.1A), which had completely colonized the wounded area by 48 hpi (Figure 1.1C, right). We also observed immature columellate sporangia at 24 hpi, and the characteristic dark, mature sporangia bearing asexual sporangiospores were clearly visible at 48 hpi.

1.4.2 Novel genomic resources for *Rhizopus stolonifer*

We generated a haploid and highly contiguous reference genome for the strain BLUCD01 to support our research on the molecular mechanisms behind *R. stolonifer* infections of plant hosts. The reference assembly had a total size of 45.02 Mb, an N50 of 2.87 Mb, and a GC content of 35.42% (Figure 1.2A and B, Supplementary Table S2). In comparison with other available *R. stolonifer* genomes, BLUCD01 has a larger total size and an N50 value 3.2 times higher than the next largest N50 genome (NRRL66455) and is less fragmented, with 51 scaffolds as opposed to the next less fragmented genome with 326 (Supplementary Table S3). We detected 96.6% of the complete set of BUSCO genes in the genome, suggesting a comprehensive assembly of the gene space. BUSCO parameters were very similar to those of previously sequenced genomes (Supplementary Table S3). The final genome annotation resulted in a total of 12,644 predicted protein-coding genes.

We conducted an RNA-seq study to examine *R. stolonifer* during infection of four fruit hosts (tomato, grape, strawberry, and plum) (Supplementary Table S7). We included reads from *in vitro* samples as a reference for fungal behavior when growing in culture media (i.e., *in vitro*). The RNA-seq analysis showed that an increasing number of genes (~800) can be detected on all hosts from the start of the infection (6 hpi), when no evident fungal activity is visible. More genes were detected at later time points (ranging from 8,000 to 11,000 genes at 48 hpi) in all hosts, reflecting pathogen growth progression and colonization of the host tissues (Supplementary Table S4). We then determined the percentage of genes with functional annotations that were expressed in each host (Figure 1.2C). Overall, infections of all four fruit commodities seemed to induce the expression

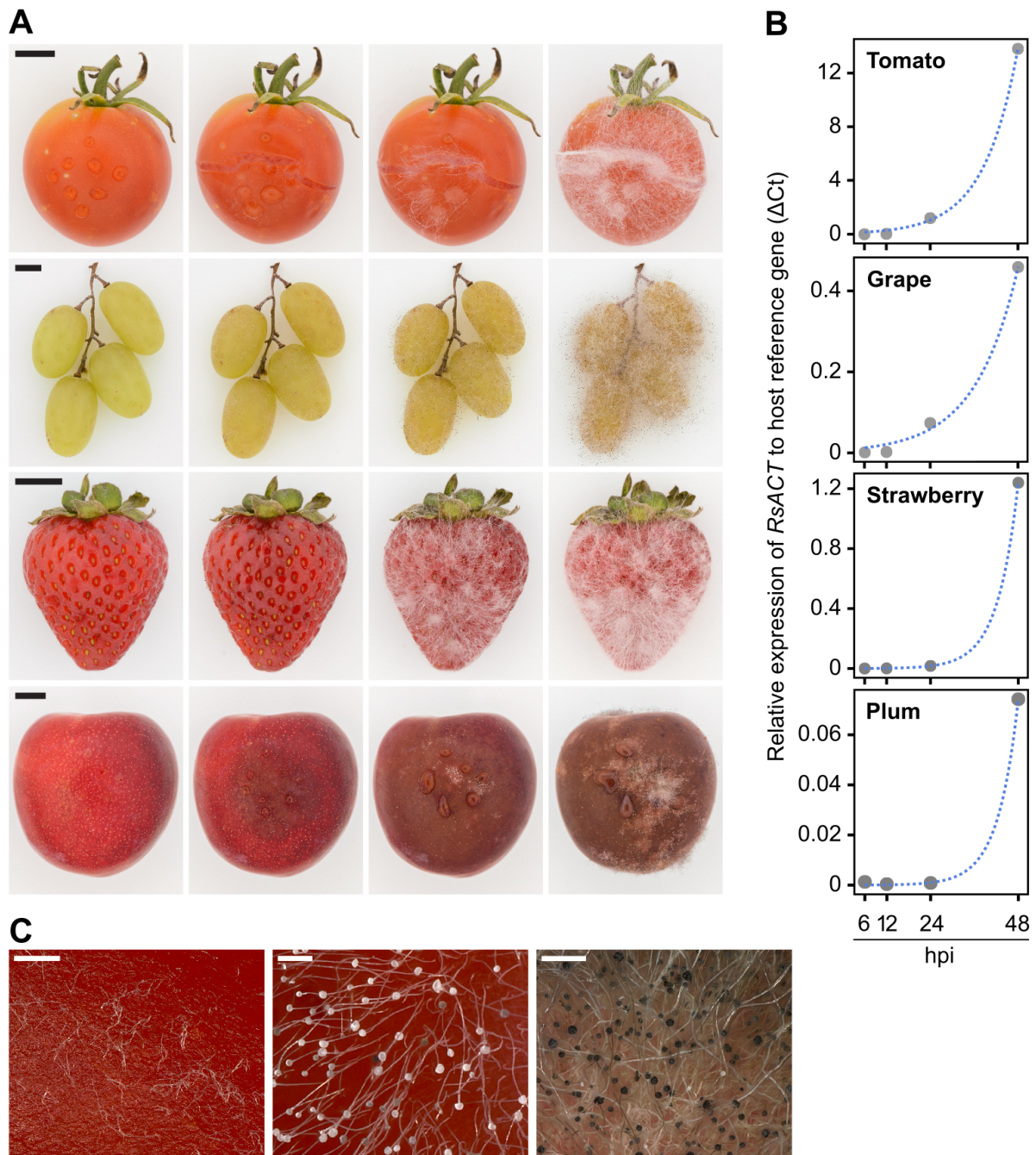


Figure 1.1: *Rhizopus stolonifer* colonizes different fruit hosts. (A) Progression of Rhizopus rot on tomato, grape, strawberry, and plum. Fruit were imaged at 6, 24, 36, and 48 hours post inoculation (hpi) for tomato; 6, 36, 48, and 72 hpi for grape; 6, 36, 48, and 54 hpi for strawberry; and 6, 48, 72, and 122 hpi for plum. Scale bars correspond to 1 cm. (Continued on following page)

Figure 1.1: (Continued from previous page) (B) Fungal transcriptional activity estimated by relative expression of the reference gene *RsACT*, normalized based on the reference genes *SlUBQ* (tomato), *VvACT* (grape), *FaDBP* (strawberry), and *PsEF-5A* (plum). All regressions exhibited an $R^2 = 0.99$. (C) *R. stolonifer* infection structures at 12 (left), 24 (middle), and 48 (right) hpi in tomato fruit visualized under the microscope. Scale bars correspond to 500 μm (12 hpi) and 250 μm (24 and 48 hpi).

of a subset ($< 25\%$) of the total genes, which could point towards the genes specifically needed for growth in the host, whereas those observed for *in vitro* growth ($> 75\%$) might be predominantly associated with growth on other substrates.

1.4.3 Transcriptional profiles of *Rhizopus stolonifer* show distinct patterns of gene expression when infecting fruit hosts

We identified differentially expressed genes (DEGs, $P_{adj} < 0.05$) by comparing the transcriptional profiles of *R. stolonifer* when inoculated in various fruit throughout time against the transcriptional profile of the fungus grown *in vitro* (Figure 1.3, Supplementary Table S7). We were interested in infection-related DEGs, defined as those significantly upregulated when *R. stolonifer* grows in the fruit versus on media (i.e., *in vitro*), as they may be linked to pathogenicity or virulence. We detected 1,594 infection-related DEGs in tomato, 1,248 in grape, 766 in strawberry, and 570 in plum (Supplementary Table S8). Infection-related DEGs were further classified into four different clusters (I-IV) according to their overall patterns of expression (Figure 1.3): Cluster I corresponded to genes that were primarily expressed at 6 hpi, Cluster II at 12 hpi, Cluster III at 24 hpi, and Cluster IV at 48 hpi. The presence of highly expressed DEGs even at 6 hpi confirmed that the fungus is active from the onset of the interaction despite the absence of visible symptoms (Figure 1.1A).

We explored the functions of infection-related DEGs with a particular focus on those related to fungal growth and host infection (Figure 1.3; Supplementary Table S9). In all hosts, early transcriptional responses captured in Cluster I were mainly enriched ($P_{adj} < 0.05$) in the initiation and maintenance of mycelial growth, such as ribosomal proteins, cell

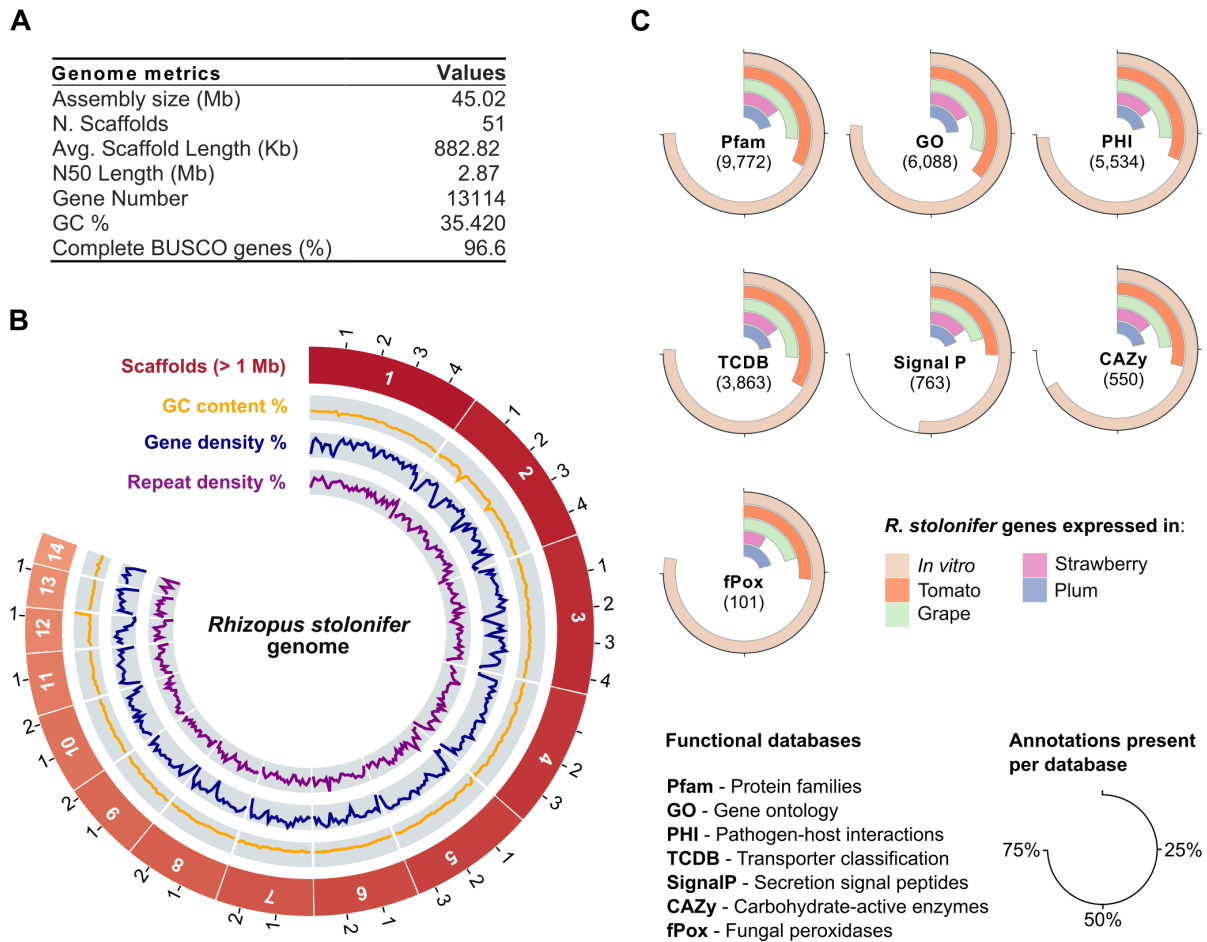


Figure 1.2: The genome of *Rhizopus stolonifer*. (A) Assembly metrics for the *R. stolonifer* BLUCD01v1 genome. A comparison between the BLUCD01v1 genome metrics and those of previously published *R. stolonifer* genomes can be found in Supplementary Table S3. (B) Circos plot representing (from outermost to innermost layer) scaffolds greater or equal in size to 1 Mb (14 out of 51 total), GC content (%), gene density (%), and repeat density (%). (C) Functional annotations from the 10,275 annotated *R. stolonifer* transcripts. Each category is represented by the total number of annotated genes and the percentage of genes present per database for each host and *in vitro* (calculated with the total number of genes with > 2 reads with annotations for a database and the total number of annotated genes for that database).

division, Acetyl-CoA metabolism, biosynthetic processes, and carbohydrate metabolism. For strawberry and plum, we additionally observed a small number of DEGs involved in fungal cell wall (CW) metabolism (mainly chitin deacetylases), and genes involved in oxidation-reduction processes (mainly dehydrogenases and peroxidases) in grape and plum.

Cluster II showed an increase in processes associated with infection of host tissues, with some growth-related functions seen in Cluster I (e.g., translation, cell division, biosynthetic processes, and carbohydrate metabolism) still happening at 12 hpi. In tomato, concomitant with the rapid colonization of the fruit tissue (Figure 1.1A), there was an enrichment in genes involved in host CW degradation. Among them were cell wall-degrading enzymes (CWDEs) such as polygalacturonases (PGs) (GH28) and other glycosyl hydrolases (GH43, GH45, GH134), xylan esterases (CE1), pectin methylesterases (CE8), and a pectate lyase (PL9). Enrichment of genes involved in oxidation-reduction processes, such as genes related with reactive oxygen species (ROS) production (oxidases) and detoxification (superoxide dismutase), was observed in most hosts. Genes involved in amino acid synthesis were enriched in tomato and grape, including redox-related amino acids, such as tryptophan and methionine.

Cluster III displayed a balance between fungal growth and host infection-related functions for most hosts, except strawberry. At 24 hpi in strawberries, *R. stolonifer* mainly expressed genes relating to cellular maintenance and transcription/translation (ribosomal proteins, translation, and cell division). This increase in fungal growth matches the onset of exponential growth observed for strawberry from 24 hpi – onwards (Figure 1.1B). Genes involved in oxidation-reduction processes were enriched in all hosts, and as in Cluster II, these included several dehydrogenases and cytochrome proteins, with the addition of thioredoxins and enzymes in the auxiliary activity family of CAZymes, which were involved in sugar metabolism (AA5, AA7) and protection of fungal cells from reactive quinone compounds (AA6). Although only significantly enriched in strawberry and plum, genes involved in proteolysis (e.g., aspartyl proteases, peptidases, and subtilases) were observed across hosts.

Cluster IV corresponded to late infection, when *R. stolonifer* had reached exponential growth and extensively colonized most of the host tissue, except for plum (Figure 1.1A and B). There was a decrease in genes associated with cellular maintenance and transcription/translation, while those involved in cellular metabolism (primarily carbohydrate metabolism) and fungal CW metabolism (mainly chitin deacetylases) increased (tomato and grape) or remained similar to their levels in Cluster III (strawberry and plum). Enrichment of genes involved in host CW degradation, oxidation-reduction processes, transmembrane transport, and host-pathogen interaction in all hosts seems to indicate that *R. stolonifer* is still actively colonizing the different fruit, and points to a balance between growth and infection. We observed a variety of CWDEs for all hosts, including several glycosyl hydrolases, pectinesterases, and cellobiose dehydrogenases, although this category was not enriched in strawberry. As for genes pertaining to oxidation-reduction processes, we found several ROS production (oxidases), detoxification (peroxidases), and signaling (thioredoxins) enzymes, and cytochrome proteins across hosts. Infections of grape and plum also exhibited genes involved in proteolysis (aspartyl proteases, subtilases, and various peptidases), and infections of tomato and grape displayed an enrichment of genes involved in signal transduction (kinases).

1.4.4 *Rhizopus stolonifer* uses similar strategies when infecting different fruit hosts

To gain insight into specific genes playing a relevant role in infection, we focused on the top 5 genes per host and cluster with the highest \log_2 - fold change and highest expression that fall within host-infection categories (Supplementary Table S10). To identify these genes, we calculated average normalized read count values for each gene per host and time point, and selected outliers (i.e., values above the 95th percentile) from a \log_{10} - distribution of the normalized read count data and from the \log_2 - fold change values per host and time point. Most of the highly expressed or highly induced genes belong to the host-pathogen interaction, oxidation-reduction process, and transmembrane transport categories. A gene encoding a polygalacturonase (*RS_BLUCD01_v1_scf03.ver1.g036800.m01*) was shared across all hosts, and expressed in Cluster I for tomato and grape, and Cluster IV for

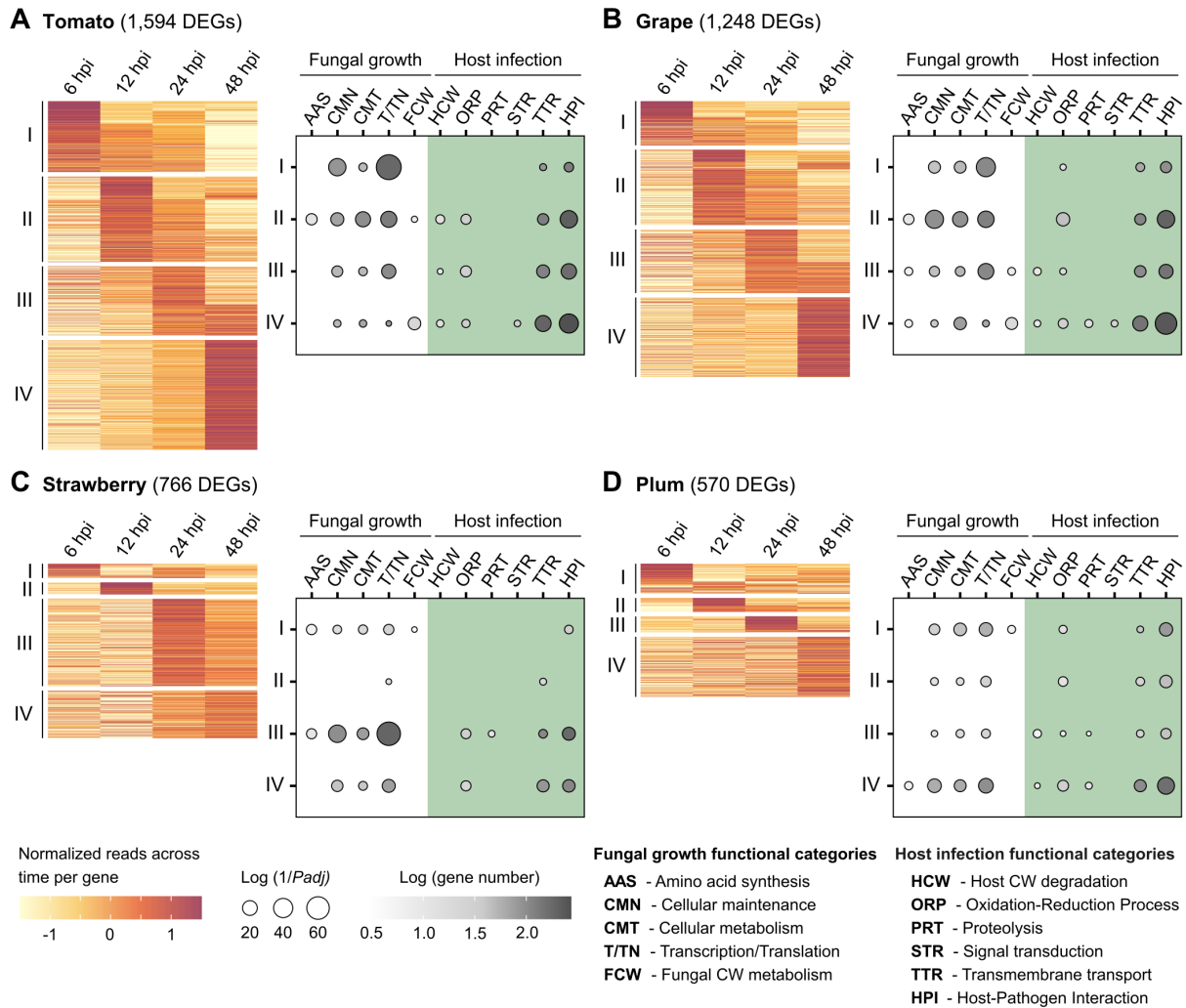


Figure 1.3: Patterns of up-regulated differentially expressed genes reveal distinct gene clusters acting throughout the course of *Rhizopus stolonifer* infection of fruit hosts. Heatmaps represent \log_{10} -transformed normalized read data of infection-related genes ($P_{adj} < 0.05$) from tomato (A), grape (B), strawberry (C), and plum (D) at 6, 12, 24, and 48 hours post-inoculation. Tables summarize the major functions represented in each cluster for the four hosts, as pertaining to two different categories: Fungal growth and Host infection. Roman numerals designate each gene cluster. DEGs = differentially expressed genes; hpi = hours post-inoculation. Numbers in parentheses indicate the number of upregulated DEGs for each host.

strawberry and plum. For genes involved in host CW degradation, proteolysis, oxidation-reduction processes, and transmembrane transport, although most shared genes were common to only two or three hosts, genes with similar annotations were found across hosts. This was the case for polygalacturonases, aspartyl proteases, dehydrogenases, and transmembrane transporters of the major facilitator superfamily. These results suggest that *R. stolonifer* is equipped with different genes that are fulfilling similar host infection purposes.

To identify core virulence strategies necessary for fruit colonization, we further examined infection-related genes that were common across all four hosts (Supplementary Table S11). Following the trends observed in Figure 1.3, most of these genes belonged to Cluster I in tomato, Cluster II in grape, Cluster III in strawberry, and Cluster IV in plum, further reflecting differences in the stage of Rhizopus rot progression on the various fruit hosts (Figure 1.1A and B). Only a small fraction of the common genes was observed in the same cluster (Clusters I and III) for all hosts. Common early functions were associated with fungal growth, mainly represented by ribosomal proteins and genes involved in cellular division, as well as ROS production and detoxification, and transmembrane transport. There were only 2 common genes associated with late infection for all hosts, and these were a ribosomal protein and a subtilase found in Cluster III.

We then focused on genes specifically related to host-infection functions. A summary of the infection strategies represented in the core set of common genes can be found in Table 1.1. In most cases, the number of reads is highest for tomato, followed by grape, strawberry, and plum, further reflecting the differences in progression of the infection previously observed (Figure 1.1A and B). In line with the earlier colonization of tomato fruit by *R. stolonifer*, for some genes, it is possible to observe an early peak in expression for tomato, which is mirrored later for the other hosts. Some of these trends are portrayed by genes encoding CWDEs (Figure 1.4). Taken together, these results suggest that *R. stolonifer* possesses a core infection toolbox consisting of CWDEs, oxidation-reduction and proteolytic enzymes, and transmembrane transporters, among others, that are differentially deployed across different time points depending on the fruit host environment.

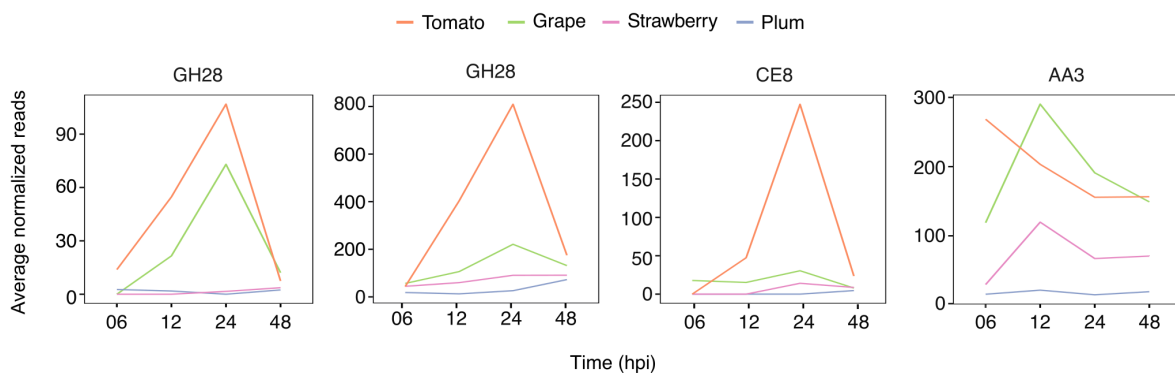


Figure 1.4: Expression patterns of genes encoding cell wall degrading enzymes present in the core infection toolbox of *Rhizopus stolonifer* on different fruit hosts. Showcased are two polygalacturonases (GH28, *RS_BLUCD01_v1_scf03.ver1.g036800.m01*, *RS_BLUCD01_v1_scf02.ver1.g020460.m01*), a pectinesterase (CE8, *RS_BLUCD01_v1_scf14.ver1.g123480.m01*), and a cellobiose oxidase (AA3, *RS_BLUCD01_v1_scf07.ver1.g080400.m01*). hpi: hours post inoculation.

Infection Strategies	Number of Genes	Example Functions
Cell wall degradation	4	Polygalacturonases (GH28), pectinesterase (CE8)
ROS production/detoxification	33	Dehydrogenases, glutathione peroxidase, peroxiredoxin, cytochromes
Proteolysis	7	Peptidases, metallopeptidases
Signal transduction	12	Protein kinases
Transmembrane transport	20	ABC transporters, permeases, Major Facilitator Superfamily

Table 1.1: Summary of core infection strategies used by *Rhizopus stolonifer* during infection of tomato, grape, strawberry, and plum fruit.

1.5 Discussion

1.5.1 *Rhizopus stolonifer* displays distinctive rapid growth on different fruit hosts

The high destructive power of *R. stolonifer* lies in its rapid growth and broad host range. Within 48 hours from inoculation, *R. stolonifer* exponentially progressed from no apparent signs of infection to a complete colonization of most fruit hosts. This fast growth is unique to *R. stolonifer* within the *Rhizopus* genus, with other species being less common

in foods and not as impactful (Pitt and Hocking, 2009), as well as when compared to other necrotrophs which progress more slowly over the same time span (Navarro et al., 2011; Petrasch et al., 2019). For tomato, grape, and strawberry, exponential growth was preceded by an enrichment in growth-related processes at 6, 12, and 24 hpi, respectively. For plum, we might have been unable to capture the onset of exponential growth as genes involved in growth- and infection-related processes had a similar weight throughout infection. Differences in the timing of disease progression could be attributed to varying anatomic characteristics between fruit hosts regarding protein and polysaccharide composition, cell wall (CW) structure, enzymatic metabolism, and softening mechanisms, among others (Goulao and Oliveira, 2008).

1.5.2 Novel and high-quality genomic resources for *Rhizopus stolonifer*

Despite the commercial impact of soft rot, relatively little is known about the biology of the infection process. We generated a new reference genome and predicted transcriptome for *R. stolonifer* strain BLUCD01 and compared to two previously published genomes (Supplementary Table S3). The genome size was more contiguous and larger than previously reported (Gryganskyi et al., 2018), being similar in size to other necrotrophic fungi such as *Botrytis cinerea* and *Sclerotinia sclerotiorum* (Amselem et al., 2011; Blanco-Ulate et al., 2013a). The high completeness denoted by the BUSCO score and high number of protein-coding genes predicted through RNA-seq make the *R. stolonifer* strain BLUCD01 genome and predicted transcriptome robust publicly available resources to further soft rot research.

1.5.3 Cell wall degrading enzymes and redox processes play a relevant role in *Rhizopus stolonifer* infections of fruit

R. stolonifer has traditionally been considered a saprotroph mainly growing on decaying fruit. However, in this study, we confirmed that *R. stolonifer* deployed a wide range of infection strategies characteristic of necrotrophic lifestyles, such as secretion of cell wall-degrading enzymes (CWDEs) and production of reactive oxygen species (ROS) (Rafiei

et al., 2021; van Kan, 2006; Zhao et al., 2014). We observed a variety of polygalacturonases (PGs), pectin methyl esterases (PMEs), xylanases, cellulases, and amylases, all of which are CWDEs previously described to play a role in tissue maceration and host colonization in *R. stolonifer* and other necrotrophic pathogens (Bautista-Baños et al., 2014; Petrasch et al., 2019). We detected five PG genes in tomato, four in grape, two in strawberry, and six in plum, with one gene encoding a GH28 being common across all hosts. Genes encoding PGs were also quite prevalent within the most expressed or most changing, with 12 genes being detected across all hosts. As for PMEs, we observed five genes in tomato, three in grape and plum, and two in strawberry, with one gene coding for a CE8 common to all. PGs are well-known virulence factors for numerous fungal pathogens, such as *B. cinerea*, and although PMEs do not appear to be necessary for virulence on fruit (Kars et al., 2005; Zhang and Van Kan, 2013), our observations suggest they could potentially play a relevant role in *R. stolonifer*. CWDEs were more predominantly expressed at late time points for grape, strawberry, and plum, and at earlier and late time points for tomato, where they were observed in higher numbers and more variety. This differential use of CWDEs across hosts could be due to differences in fruit CW composition characteristics (Zhang and Van Kan, 2013), as well as further indication that the pathogen adapts its infection mechanisms to the host. We found multiple genes involved in protein degradation, such as peptidases, metallopeptidases, endopeptidases, metalloendopeptidases, and aspartyl proteases, with nine genes common across hosts. Aspartyl proteases have been studied as virulence factors in various necrotrophic fungal pathogens, such as *Monilinia fructigena*, *B. cinerea* and *S. sclerotiorum*, and are proposed to play a role in facilitating tissue penetration and colonization through breakdown of proteins present in plant CWs (Mandujano-González et al., 2016). Our current observations, together with our prior findings of proteolysis related genes involved in *R. stolonifer*-fruit interactions, point to a relevant role of protein degradation in fruit infections by *R. stolonifer* (Petrasch et al., 2019).

Upon infection, plant cells respond with an oxidative burst, which involves rapid ROS production, mainly driven by respiratory burst oxidase homolog (RBOH) enzymes,

and triggers a hypersensitive response leading to programmed cell death (Siegmund and Viefhues, 2016). Pathogens with a necrotrophic lifestyle take advantage of the plant oxidative burst by producing their own ROS, enhancing host susceptibility (Siegmund and Viefhues, 2016; van Kan, 2006). Moreover, fungal pathogens are equipped with ROS-detoxifying systems against oxidative stress (Heller and Tudzynski, 2011). NADPH oxidases (Nox) are the most common enzymatic ROS-producing system (Siegmund and Viefhues, 2016; Takemoto et al., 2007). We detected genes associated with NoxC, which contains a Ca^{2+} -binding motif similar to plant RBOHs (Takemoto et al., 2007), and NoxR in tomato, grape, and strawberry. We also found genes associated with glutathione-S-transferases and glutathione peroxidases, detoxification enzymes that protect fungi against plant toxic metabolites and oxidative stress (Calmes et al., 2015; Morel et al., 2009; Shen et al., 2015; Wangsanut and Pongpom, 2022), with two genes common across hosts. We also observed genes encoding AA6 enzymes in tomato and grape, which showed similarity to the *Candida albicans* Pst2 flavodoxin-like protein, an antioxidant mechanism essential for virulence (Foderaro and Konopka, 2021). The number of ROS-producing and detoxifying systems varied across hosts, which might be due to varying plant CW composition and the need for different colonization tactics.

1.5.4 *Rhizopus stolonifer* interactions with its fruit hosts involve a comprehensive integration of external and internal signals

In line with the higher availability of sugars produced by CW degradation, there was an increase in chitin production and modification (Lenardon et al., 2010). Chitin constitutes a well-characterized microbe-associated molecular pattern recognized by plant cell surface receptors, triggering immune responses. To avoid recognition by the host, some fungal pathogens deploy LysM-containing effector molecules that protect fungal hyphae against host hydrolytic enzymes or scavenge chitin oligosaccharides (Kombrink and Thomma, 2013). We detected genes coding for LysM domain-containing proteins across all hosts, similar to *Penicillium expansum* and *Verticillium dahliae* LysM effectors (Kombrink and Thomma, 2013; Levin et al., 2017). While the putative LysM effectors in *P. expansum* had no significant effect on fungal pathogenicity and virulence, *V. dahliae* LysM effectors

were required for virulence in planta. Further analyses are required to determine the role of putative *R. stolonifer* LysM effectors in fruit pathogenicity.

Genes involved in signal transduction, mainly protein kinases, were consistently observed throughout infection. We observed multiple members of the Ras superfamily of small GTPases and their regulatory components, which are involved in fungal morphogenesis and virulence and function as signaling nodes (Dautt-Castro et al., 2021; Zong et al., 2023). The regulatory element RhoGAP, involved in the regulation of cellular redox state (Hobbs et al., 2014), was more prevalent from Cluster II – onwards, likely as a result of increasing oxidative stress. Genes in the Arf and Rab families, involved in vesicle trafficking (Dautt-Castro et al., 2021), were more predominant later in the infection, coinciding with an increase in transmembrane transport functions. These observations point to a comprehensive perception and transduction of various internal and external cues regulating the infection mechanisms mediating *R. stolonifer* – fruit interactions.

1.6 Conclusions

Taken together, our results support that *R. stolonifer* displays a clear necrotrophic behavior when infecting different fruit hosts in postharvest. A suite of cell wall degrading enzymes, ROS-producing and -scavenging systems, protein degradation, and sugar breakdown and uptake allows the fungus to macerate host tissues and quickly colonize a wide range of fruit. These infection strategies are also displayed by hemibiotrophic fungi, which start off as biotrophs, forming specialized infection hyphae or haustoria inside living host cells before switching to an aggressive necrotrophic stage where they secrete CWDEs and toxins to feed off dead tissue (Koeck et al., 2011). However, *R. stolonifer* has not been reported to exhibit the initial biotrophic phase nor form haustoria, which seems to further point to *R. stolonifer* behaving more as a necrotroph than a hemibiotroph or saprotroph. Finally, the publicly available genomic resources generated in this study will improve our understanding of how *R. stolonifer* interacts with its fruit hosts, which is key for the development of better integrated pest management approaches in postharvest and minimization of food loss due to soft rot.

1.7 Data Availability

The datasets generated in this study have been deposited in Zenodo (<https://doi.org/10.5281/zenodo.7630319>), the Sequence Read Archive (SRA) database (BioprojectID PRJNA1082801), and in the Gene Expression Omnibus (GEO) database (accession number GSE232735).

1.8 Acknowledgments

We would like to acknowledge Yiduo Wei and Dr. Stefan Petrasch for providing us assistance with data analysis and interpretation. We would like to thank Dr. Manon Paineau for providing advice on optimizing the bioinformatic pipeline. We thank Carlos Carachure, Juniper Piedmont, and Annie Willett for their review of the manuscript's narrative.

1.9 References

- Agrios, G. N. (2005). *Plant Pathology*. Elsevier.
- Amselem, J., Cuomo, C. A., Van Kan, J. A. L., Viaud, M., Benito, E. P., Couloux, A., Coutinho, P. M., De Vries, R. P., Dyer, P. S., Fillinger, S., Fournier, E., Gout, L., Hahn, M., Kohn, L., Lapalu, N., Plummer, K. M., Pradier, J.-M., Quévillon, E., Sharon, A., and Dickman, M. (2011). Genomic analysis of the necrotrophic fungal pathogens *Sclerotinia sclerotiorum* and *Botrytis cinerea*. *PLoS Genetics*, 7(8):e1002230.
- Baggio, J. S., Gonçalves, F. P., Lourenço, S. A., Tanaka, F. A. O., Pascholati, S. F., and Amorim, L. (2016). Direct penetration of *Rhizopus stolonifer* into stone fruits causing rhizopus rot. *Plant Pathology*, 65(4):633–642.
- Bao, W., Kojima, K. K., and Kohany, O. (2015). Repbase update, a database of repetitive elements in eukaryotic genomes. *Mobile DNA*, 6(1):11.
- Bautista-Baños, S., Bosquez-Molina, E., and Barrera-Necha, L. L. (2014). *Rhizopus stolonifer* (soft rot). In *Postharvest Decay*, pages 1–44. Elsevier.
- Bautista-Baños, S., Velaquez-Del Valle, M. G., Hernandez-Lauzardo, A. N., and Barka, E. A. (2008). The *Rhizopus stolonifer*-tomato interaction. In *12 The Rhizopus stolonifer-Tomato Interaction*.
- Bi, K., Liang, Y., Mengiste, T., and Sharon, A. (2023). Killing softly: A roadmap of *Botrytis cinerea* pathogenicity. *Trends in Plant Science*, 28(2):211–222.
- Blanco-Ulate, B., Allen, G., Powell, A. L. T., and Cantu, D. (2013a). Draft genome sequence of *Botrytis cinerea* bcdw1, inoculum for noble rot of grape berries. *Genome Announcements*, 1(3):e00252–13.
- Blanco-Ulate, B., Vincenti, E., Powell, A. L. T., and Cantu, D. (2013b). Tomato transcriptome and mutant analyses suggest a role for plant stress hormones in the interaction between fruit and *Botrytis cinerea*. *Frontiers in Plant Science*, 4.

- Boetzer, M. and Pirovano, W. (2014). Sspace-longread: Scaffolding bacterial draft genomes using long read sequence information. *BMC Bioinformatics*, 15(1):211.
- Bolger, A. M., Lohse, M., and Usadel, B. (2014). Trimmomatic: A flexible trimmer for illumina sequence data. *Bioinformatics*, 30(15):2114–2120.
- Calmes, B., Morel-Rouhier, M., Bataillé-Simoneau, N., Gelhaye, E., Guillemette, T., and Simoneau, P. (2015). Characterization of glutathione transferases involved in the pathogenicity of *Alternaria brassicicola*. *BMC Microbiology*, 15(1):123.
- Chin, C.-S., Peluso, P., Sedlazeck, F. J., Nattestad, M., Concepcion, G. T., Clum, A., Dunn, C., O’Malley, R., Figueroa-Balderas, R., Morales-Cruz, A., Cramer, G. R., Delle-donne, M., Luo, C., Ecker, J. R., Cantu, D., Rank, D. R., and Schatz, M. C. (2016). Phased diploid genome assembly with single-molecule real-time sequencing. *Nature Methods*, 13(12):1050–1054.
- Dautt-Castro, M., Rosendo-Vargas, M., and Casas-Flores, S. (2021). The small gtpases in fungal signaling conservation and function. *Cells*, 10(5):1039.
- Feliziani, E., Landi, L., and Romanazzi, G. (2015). Preharvest treatments with chitosan and other alternatives to conventional fungicides to control postharvest decay of strawberry. *Carbohydrate Polymers*, 132:111–117.
- Feliziani, E. and Romanazzi, G. (2016). Postharvest decay of strawberry fruit: Etiology, epidemiology, and disease management. *Journal of Berry Research*, 6(1):47–63.
- Foderaro, J. E. and Konopka, J. B. (2021). Differential roles of a family of flavodoxin-like proteins that promote resistance to quinone-mediated oxidative stress in *Candida albicans*. *Infection and Immunity*, 89(4):e00670–20.
- Goulao, L. and Oliveira, C. (2008). Cell wall modifications during fruit ripening: When a fruit is not the fruit. *Trends in Food Science & Technology*, 19(1):4–25.
- Gryganskyi, A. P., Golan, J., Dolatabadi, S., Mondo, S., Robb, S., Idnurm, A., Muszewska, A., Steczkiewicz, K., Masonjones, S., Liao, H.-L., Gajdeczka, M. T., Anike,

- F., Vuck, A., Anishchenko, I. M., Voigt, K., De Hoog, G. S., Smith, M. E., Heitman, J., Vilgalys, R., and Stajich, J. E. (2018). Phylogenetic and phylogenomic definition of *Rhizopus* species. *G3 Genes/Genomes/Genetics*, 8(6):2007–2018.
- Heller, J. and Tudzynski, P. (2011). Reactive oxygen species in phytopathogenic fungi: Signaling, development, and disease. *Annual Review of Phytopathology*, 49(1):369–390.
- Hobbs, G. A., Zhou, B., Cox, A. D., and Campbell, S. L. (2014). Rho gtpases, oxidation, and cell redox control. *Small GTPases*, 5(2):e28579.
- Hoff, K. J., Lange, S., Lomsadze, A., Borodovsky, M., and Stanke, M. (2016). Braker1: Unsupervised rna-seq-based genome annotation with genemark-et and augustus. *Bioinformatics*, 32(5):767–769.
- Kars, I., McCALMAN, M., Wagemakers, L., and van Kan, J. A. (2005). Functional analysis of *Botrytis cinerea* pectin methylesterase genes by pcr-based targeted mutagenesis: Bcpme1 and bcpme2 are dispensable for virulence of strain b05.10. *Molecular Plant Pathology*, 6(6):641–652.
- Kim, D., Paggi, J. M., Park, C., Bennett, C., and Salzberg, S. L. (2019). Graph-based genome alignment and genotyping with hisat2 and hisat-genotype. *Nature Biotechnology*, 37(8):907–915.
- Koeck, M., Hardham, A. R., and Dodds, P. N. (2011). The role of effectors of biotrophic and hemibiotrophic fungi in infection: Effectors of biotrophic fungi. *Cellular Microbiology*, 13(12):1849–1857.
- Kombrink, A. and Thomma, B. P. H. J. (2013). Lysm effectors: Secreted proteins supporting fungal life. *PLOS Pathogens*, 9(12):e1003769.
- Kwon, J.-H., Kang, S.-W., Kim, J.-S., and Park, C.-S. (2001). *Rhizopus* soft rot on cherry tomato caused by *Rhizopus stolonifer* in korea. *Mycobiology*, 29(3):176–178.
- Laluk, K. and Mengiste, T. (2010). Necrotroph attacks on plants: Wanton destruction or covert extortion? *The Arabidopsis Book*, 8:e0136.

- Lenardon, M. D., Munro, C. A., and Gow, N. A. (2010). Chitin synthesis and fungal pathogenesis. *Current Opinion in Microbiology*, 13(4):416–423.
- Levin, E., Ballester, A. R., Raphael, G., Feigenberg, O., Liu, Y., Norelli, J., Gonzalez-Candelas, L., Ma, J., Dardick, C., Wisniewski, M., and Droby, S. (2017). Identification and characterization of lysm effectors in *Penicillium expansum*. *PLOS ONE*, 12(10):e0186023.
- Lewthwaite, S. L., Wright, P. J., and Triggs, C. M. (2013). Sweetpotato cultivar susceptibility to postharvest soft rot caused by *Rhizopus stolonifer*. *New Zealand Plant Protection*, 66:223–228.
- Liao, C.-J., Hailemariam, S., Sharon, A., and Mengiste, T. (2022). Pathogenic strategies and immune mechanisms to necrotrophs: Differences and similarities to biotrophs and hemibiotrophs. *Current Opinion in Plant Biology*, 69:102291.
- Love, M. I., Huber, W., and Anders, S. (2014). Moderated estimation of fold change and dispersion for rna-seq data with *DESeq2*. *Genome Biology*, 15(12):550.
- Love, M. I., Soneson, C., and Robinson, M. D. (2017). Importing transcript abundance datasets with *tximport*. *bioRxiv*, 1(1):5.
- Mandujano-González, V., Villa-Tanaca, L., Anducho-Reyes, M. A., and Mercado-Flores, Y. (2016). Secreted fungal aspartic proteases: A review. *Revista Iberoamericana de Micología*, 33(2):76–82.
- Minio, A. (2019a). Falcon-unzip [computer software]. <https://github.com/andreaminio/FalconUnzip-DClab>.
- Minio, A. (2019b). Haplosync [computer software]. <https://github.com/andreaminio/HaploSync>.
- Minio, A., Cochetel, N., Vondras, A. M., Massonnet, M., and Cantu, D. (2022). Assembly of complete diploid-phased chromosomes from draft genome sequences. *G3 Genes/Genomes/Genetics*, 12(8):jkac143.

- Minio, A., Massonnet, M., Figueroa-Balderas, R., Castro, A., and Cantu, D. (2019). Diploid genome assembly of the wine grape carménère. *G3 Genes/Genomes/Genetics*, 9(5):1331–1337.
- Morales-Cruz, A., Amrine, K. C. H., Blanco-Ulate, B., Lawrence, D. P., Travadon, R., Rolshausen, P. E., Baumgartner, K., and Cantu, D. (2015). Distinctive expansion of gene families associated with plant cell wall degradation, secondary metabolism, and nutrient uptake in the genomes of grapevine trunk pathogens. *BMC Genomics*, 16(1):469.
- Morel, M., Ngadin, A. A., Droux, M., Jacquot, J.-P., and Gelhaye, E. (2009). The fungal glutathione s-transferase system. evidence of new classes in the wood-degrading basidiomycete *Phanerochaete chrysosporium*. *Cellular and Molecular Life Sciences*, 66(23):3711–3725.
- Myers, G. (2014). Efficient local alignment discovery amongst noisy long reads. In *International Workshop on Algorithms in Bioinformatics*, pages 52–67.
- Navarro, D., Díaz-Mula, H. M., Guillén, F., Zapata, P. J., Castillo, S., Serrano, M., Valero, D., and Martínez-Romero, D. (2011). Reduction of nectarine decay caused by *Rhizopus stolonifer*, *Botrytis cinerea* and *Penicillium digitatum* with aloe vera gel alone or with the addition of thymol. *International Journal of Food Microbiology*, 151(2):241–246.
- Northover, J. and Zhou, T. (2002). Control of rhizopus rot of peaches with postharvest treatments of tebuconazole, fludioxonil, and *Pseudomonas syringae*. *Canadian Journal of Plant Pathology*, 24(2):144–153.
- Patro, R., Duggal, G., Love, M. I., Irizarry, R. A., and Kingsford, C. (2017). Salmon provides fast and bias-aware quantification of transcript expression. *Nature Methods*, 14(4):417–419.
- Petrasch, S., Silva, C. J., Mesquida-Pesci, S. D., Gallegos, K., Van Den Abeele, C., Papin, V., Fernandez-Acero, F. J., Knapp, S. J., and Blanco-Ulate, B. (2019). Infection

- strategies deployed by *Botrytis cinerea*, *Fusarium acuminatum*, and *Rhizopus stolonifer* as a function of tomato fruit ripening stage. *Frontiers in Plant Science*, 10:223.
- Pitt, J. I. and Hocking, A. D. (2009). *Fungi and Food Spoilage*. Springer US.
- Rafei, V., Véléz, H., and Tzelepis, G. (2021). The role of glycoside hydrolases in phytopathogenic fungi and oomycetes virulence. *International Journal of Molecular Sciences*, 22(17):9359.
- Rezende, J. L., Fernandes, C. C., Costa, A. O. M., Santos, L. S., Vicente Neto, F., Sperandio, E. M., Souchie, E. L., Colli, A. C., Crotti, A. E. M., and Miranda, M. L. D. (2020). Antifungal potential of essential oils from two varieties of *Citrus sinensis* (lima orange and bahia navel orange) in postharvest control of *Rhizopus stolonifer* (ehrenb.: Fr.) vuill. *Food Science and Technology*, 40(suppl 2):405–409.
- Salem, E. A., Youssef, K., and Sanzani, S. M. (2016). Evaluation of alternative means to control postharvest *Rhizopus* rot of peaches. *Scientia Horticulturae*, 198:86–90.
- Sallato, B. V., Torres, R., Zoffoli, J. P., and Latorre, B. A. (2007). Effect of boscalid on postharvest decay of strawberry caused by *Botrytis cinerea* and *Rhizopus stolonifer*. *Spanish Journal of Agricultural Research*, 5(1):67.
- Schipper, M. (1984). A revision of the genus *Rhizopus*. i. the *Rhizopus stolonifer*-group and *Rhizopus oryzae*. *Stud Mycol*, 25:1–19.
- Shen, M., Zhao, D.-K., Qiao, Q., Liu, L., Wang, J.-L., Cao, G.-H., Li, T., and Zhao, Z.-W. (2015). Identification of glutathione s-transferase (gst) genes from a dark septate endophytic fungus (*Exophiala pisciphila*) and their expression patterns under varied metals stress. *PLOS ONE*, 10(4):e0123418.
- Siefkes-Boer, H. J., Boyd-Wilson, K. S. H., Petley, M., and Walter, M. (2009). Influence of coldstorage temperatures on strawberry leak caused by *Rhizopus* spp. *New Zealand Plant Protection*, 62:243–249.

- Siegmund, U. and Viefhues, A. (2016). Reactive oxygen species in the *Botrytis* - host interaction. In Fillinger, S. and Elad, Y., editors, *Botrytis – the Fungus, the Pathogen and its Management in Agricultural Systems*, pages 269–289. Springer International Publishing.
- Simão, F. A., Waterhouse, R. M., Ioannidis, P., Kriventseva, E. V., and Zdobnov, E. M. (2015). Busco: Assessing genome assembly and annotation completeness with single-copy orthologs. *Bioinformatics*, 31(19):3210–3212.
- Smit, A. (2015). Repeatmasker (version 4.0.6).
- Smit, A. and Hubley, R. (2015). Repeatmodeler (version 1.0.11).
- Snowdon, A. L. (1990). *A colour atlas of post-harvest diseases and disorders of fruits and vegetables. Volume 1: General introduction and fruits*. Wolfe Scientific Ltd.
- Takemoto, D., Tanaka, A., and Scott, B. (2007). NADPH oxidases in fungi: Diverse roles of reactive oxygen species in fungal cellular differentiation. *Fungal Genetics and Biology*, 44(11):1065–1076.
- Tournas, V. H. (2005). Spoilage of vegetable crops by bacteria and fungi and related health hazards. *Critical Reviews in Microbiology*, 31(1):33–44.
- van Kan, J. A. (2006). Licensed to kill: The lifestyle of a necrotrophic plant pathogen. *Trends in Plant Science*, 11(5):247–253.
- Vicente, A. R., Civello, P. M., Martínez, G. A., Powell, A. L. T., Labavitch, J. M., and Chaves, A. R. (2005). Control of postharvest spoilage in soft fruit. *Stewart Postharvest Review*, 1(4):1–11.
- Wangsanut, T. and Pongpom, M. (2022). The role of the glutathione system in stress adaptation, morphogenesis and virulence of pathogenic fungi. *International Journal of Molecular Sciences*, 23(18):10645.

- Xu, B., Zhang, H., Chen, K., Xu, Q., Yao, Y., and Gao, H. (2013). Biocontrol of postharvest rhizopus decay of peaches with *Pichia caribbica*. *Current Microbiology*, 67(2):255–261.
- Ye, J., Coulouris, G., Zaretskaya, I., Cutcutache, I., Rozen, S., and Madden, T. L. (2012). Primer-blast: A tool to design target-specific primers for polymerase chain reaction. *BMC Bioinformatics*, 13(1):134.
- Zhang, L. and Van Kan, J. A. L. (2013). 14 pectin as a barrier and nutrient source for fungal plant pathogens. In Kempken, F., editor, *Agricultural Applications*, pages 361–375. Springer Berlin Heidelberg.
- Zhao, Z., Liu, H., Wang, C., and Xu, J.-R. (2014). Erratum to: Comparative analysis of fungal genomes reveals different plant cell wall degrading capacity in fungi. *BMC Genomics*, 15(1):1–15.
- Zong, Y., Zhang, X., Gong, D., Zhang, F., Yu, L., Bi, Y., Sionov, E., and Prusky, D. (2023). Small gtpases *rasa* and *rasb* regulate development, patulin production, and virulence of *Penicillium expansum*. *Postharvest Biology and Technology*, 197:112192.

1.10 Supplementary Material

All supplementary tables can be accessed on <https://ucdavis.box.com/s/dof91jkyq83pay60ftqifh32jh0y260e>

Chapter 2

Fruit surface topography, timely transcriptional responses, and reduced susceptibility factors enhance anthracnose resistance in papaya

2.1 Abstract

Anthracnose disease, caused by *Colletotrichum* spp., leads to significant postharvest losses in papaya fruit. In this study, we identified a papaya genotype with quantitative resistance to anthracnose and investigated the mechanisms underlying this resistance using microscopy, fruit physicochemical analyses, and transcriptomics. The resistant genotype exhibited several beneficial traits compared to a susceptible genotype, including a thicker cuticular layer, lower stomatal density, greater firmness, and lower total soluble sugars. These characteristics can be considered preformed barriers or constitutive defenses, or correlate with reduced susceptibility factors. We also found that the resistant genotype responds more rapidly to fungal presence by synthesizing components that maintain surface and cell wall integrity, such as cutin and cuticular elements, and by depositing callose. In contrast, the susceptible genotype had accumulated more susceptibility factors, including elevated sugar content and activation of cell wall-degrading enzymes. While the susceptible genotype had a more robust immune response at the later stages of infection, the combination of susceptibility factors and a delayed response to the pathogen was insufficient to control the disease. This study highlights the need to characterize potential susceptibility factors and physicochemical traits to better understand fruit-pathogen interactions. Such knowledge can provide breeding programs with strong targets for de-

veloping crop varieties that are less susceptible to fungal diseases yet maintain quality traits that consumers expect.

2.2 Introduction

Papaya (*Carica papaya* L.) is an economically relevant tropical fruit due to its high nutritional and nutraceutical value (Evans and Ballen, 2012). Mexico leads the export market with an annual production of over 1.1 million tons, being the main papaya provider for the United States (SIAP, 2024). Anthracnose is the most common postharvest disease in papaya and results in significant yield losses worldwide. Particularly in Mexico, postharvest losses can exceed 50% (Rojo-Báez et al., 2017b). Anthracnose is caused by several *Colletotrichum* species, the most prevalent being *C. gloeosporioides* and *C. truncatum*, which infect the fruit in the field but only show symptoms after harvest (Dos Passos Braga et al., 2019; Maeda and Nelson, 2014; Singh and E.B., 2020). Symptoms manifest as rounded and water-sunken lesions, with the subsequent mycelium development (Ayón Reyna et al., 2022). Postharvest disease management relies on maintaining low temperatures and low relative humidity, together with fungicide applications (Hewajulige and Wijeratnam, 2010; Maeda and Nelson, 2014). However, the emergence of fungicide-resistant strains and growing concerns of consumers regarding fungicide residues have prompted the need for novel and more sustainable management practices (Hewajulige and Wijeratnam, 2010).

Colletotrichum spp. are plant pathogenic fungi that display hemibiotrophic lifestyles, first behaving as biotrophs and then switching to an aggressive necrotrophic phase (Canon et al., 2012). During the early stages of the biotrophic phase establishment, the pathogen can mask its presence by modifying the chitin of the fungal cell wall (CW), facilitating penetration into the host (Münch et al., 2008). Later, the formation of haustoria-like structures allows the maintenance of the pathogen by absorbing carbon and nitrogen (De Silva et al., 2017). The transition to the necrotrophic phase has been reported through the secretion of a large repertoire of proteins collectively known as the Biotrophy-Necrotrophy Switch (BNS) secretome (Bhadauria et al., 2011). In the necrotrophic phase, the pathogen releases a large arsenal of lytic enzymes capable of completely degrading

the host tissues, ultimately resulting in the development of lesions and extensive fungal growth (Gan et al., 2013). The duration of each phase varies, with onset of disease symptoms being often delayed and resulting in large losses postharvest, where apparently healthy produce decays in storage (Cannon et al., 2012).

Plants possess a diverse array of defense mechanisms to fend off pathogen infection: i) preformed physical and chemical barriers, such as the cuticle and CW layer, waxes, and toxic secondary metabolites, and ii) immune responses, such as the production of reactive oxygen species (ROS), release of signaling compounds, and CW reinforcements (Anil et al., 2014; Göhre and Robatzek, 2008). The balance between defenses (preformed and induced) and susceptibility factors is crucial in determining the outcome of plant-pathogen interactions, especially in ripening fruit (Silva et al., 2021). Susceptibility factors play a role in establishing a compatible interaction, which facilitates infections. This includes genes that contribute to the production of energy sources for the pathogen, as well as host CW degrading enzymes that can affect the integrity of structural barriers (Cantu et al., 2008; Koseoglou et al., 2022). Therefore, in the search for reliable and long-lasting sources of resistance for breeding purposes, it is essential to adopt a comprehensive strategy rather than solely relying on the traditional resistance gene approach.

In this study, we identified a resistant papaya genotype that shows quantitative resistance against *Colletotrichum* spp. We hypothesized that the fruit resistance to anthracnose was the result of i) differences in preformed structures and defenses, such as cuticle and CW characteristics, ii) induced defenses upon infection, and iii) absence or lower presence of susceptibility factors, such as fewer stomata and abundance of sugars (Chorolque et al., 2021; Gao et al., 2018). We compared the microstructure of the fruit cuticle and the structural changes in the CWs between the newly identified resistant genotype and a highly susceptible one using scanning electron microscopy and confocal microscopy. Additionally, we analyzed the expression of host genes in both papaya genotypes at two different time points: before the onset of symptoms and after symptoms became evident in the susceptible genotype. This approach allowed us to identify specific genes related to fruit cuticle composition, secondary metabolites, and various defense mechanisms, as well

as factors associated with structural or developmental processes that may promote fungal infections. Overall, our research deepens the understanding of papaya fruit interaction with two species of *Colletotrichum* and sheds light on the resistance mechanisms within papaya fruit. These insights can support breeding and management strategies aimed at reducing losses caused by anthracnose disease.

2.3 Materials and Methods

2.3.1 Plant material and experimental design

Papaya (*Carica papaya* L.) fruit from seven different pre-commercial and commercial genotypes grown under the same planting pattern and cultural management in orchards of Ixtlahuacan and Madrid, Colima State, Mexico, were harvested in stage 2 of ripeness (Barragán-Iglesias et al., 2018) under field conditions during the fall season in October 2019 and 2022, temperature of 28 °C, 95% relative humidity (RH), 1016 mbar. Fruits with uniform color and size, free of imperfections and mechanical injury, were selected, washed with distilled water and soap, and surface disinfected with 2% sodium hypochlorite for 2 min. To assess susceptibility to anthracnose, ripe fruit from each genotype (stage 5) (Barragán-Iglesias et al., 2018) were randomized in groups of three and inoculated with a 1x10⁶ conidia/mL suspension of *Colletotrichum gloeosporioides* CG13 (GeneBank accession number KF147905) or *Colletotrichum truncatum* CCM (GeneBank accession number KF147902) provided by Dr. Raúl Allende-Molar, and a mock-inoculated treatment with sterile distilled water was used. In total, nine fruit for each papaya genotype (three biological replicates and three fruit per replicate) were inoculated with each spore suspension to evaluate disease incidence and severity.

The CI-05 (most resistant) and CI-13 (most susceptible) genotypes were selected for subsequent study of natural infections. The fruit were harvested and sorted as stated above and incubated in a growth chamber with controlled conditions at 28 °C and 90% RH to favor infection development. Tissue samples were collected at 5 (asymptomatic) and 6 (asymptomatic for the CI-05 resistant genotype and symptomatic for the CI-13 susceptible genotype) days postharvest (dph). One biological replicate consisted of three

fruits, and four biological replicates per genotype and time point were obtained.

2.3.2 Image analysis to characterize the anthracnose disease severity, and anatomical and microstructural features of cuticle and cell wall

At 6 days after inoculation, four images of each fruit inoculated with each *Colletotrichum* species were captured with a 12-megapixel camera with no changes in ambient lighting. The data obtained were processed and cataloged as previously described (Kumara and Rawal, 2009). From confocal microscopy micrographs (section 2.4.5) cuticular thickness was determined using 2D images of the cross-sections stained with Auramine O. A total of ninety-six measurements were made (twenty-four for each biological replicate). Stomatal density was determined by quantifying the number of stomata in a total of seventy-two images for each genotype. The final result represented the number of stomata per area (mm^2). Callose deposition was identified using four of the cross-section images stained with Aniline blue, quantifying the total area of fluorescent pixels with respect to the total area of the image. CW thickness was determined by staining images of cross-sections with Calcofluor white, with a total of forty-two measurements for each treatment. All images were processed using ImageJ Software 1.52 (National Institute of Health, Bethesda, MD., USA.).

2.3.3 Analyses of fruit quality attributes

Fruit area (cm^2) was quantified using the ImageJ software. The color evaluation was performed with a CR-400 colorimeter (Konica Minolta, Japan), recording the L^* , a^* , and b^* parameters of the CIELab scale. Hue angle values were determined based on the following formula, where a^* is the degree of redness to greenness and b^* is the degree of yellowness to blueness (Adainoo et al., 2023).

$$\text{Hue angle} = \tan^{-1} (b^*/a^*)$$

These parameters were recorded from the outside of the fruit, taking readings from five equatorial points and three points in the areas adjacent to the pedicle on one side (basal constriction) and to the apex of each fruit on the other.

For measuring total soluble solids, a small amount of pulp juice was obtained from the equatorial region of the fruits, which was deposited in an Atago 3810 PAL-1 wide-range digital refractometer (ATAGO, Japan). Measurements were made in each biological replicate of both papaya genotypes.

pH measurements were carried out as previously described (Ruiz-Santiago et al., 2024), using 50 mL of pulp juice from each sample to measure the pH with a HI-2211 potentiometer (HANNA, Thailand). The same process was carried out for the determination of titratable acidity and pH. The results were calculated using the volume of NaOH spent by the sample with the following formula:

$$\text{Acidity (\%)} = (A * N * C) / D$$

Where A=Volume expended in mL, N= Normal alkaline, and C= Equivalent weight of organic acid.

2.3.4 Characterization of fungal isolates

Tissue sections consisting of 0.25 cm² of healthy tissue and 0.25 cm² of symptomatic tissue were collected using a scalpel. Samples were disinfected for 1 minute in sodium hypochlorite (1%), rinsed with sterile distilled water, and incubated on 1% potato dextrose agar (PDA) plates at 28 °C for 3 days. For isolate purification, a monosporic culture was carried out and the colonies were incubated for 7 days. The morphology of the colonies and conidia were characterized as previously described (Rojo-Báez et al., 2017a).

2.3.5 Microscopy analysis

For confocal laser scanning microscopy, the tissue was fixed in 10% formaldehyde and dehydrated in ethanol solutions (20, 30, 40, 50, 60, 70, 80, 90, and 100%). Subsequently, the sections were made transparent with ethanol-xylene solutions, and embedded in paraffin in the tissue embedding system KD-BM II (YONGFENG, China), and 20 µm thick cross-sections were made on a manual rotary microtome Leica RM2235 (Leica, Germany). To visualize the microstructure of the cuticle of both papaya genotypes, cross-sections were stained with Auramine O 0.01% w/v in 0.05 M Tris-HCl, pH 7.2 (Sigma, Germany) for 5 min. The 3D constructions of the cuticle were made using the z-stacks tool of the ZEN

2.3 SP1 software (Carl Zeiss, Germany). Cross-sections were excited in a range of 405-500 nm and visualized at an emission spectrum of 580 nm to determine possible differences in the cuticular microstructure of both papaya genotypes as previously described (Camacho-Vázquez et al., 2019). Calcofluor white staining at a concentration of 0.5% for 5 min in the dark was used to visualize cellulose in a range of 350-475 nm in a confocal-multiphoton microscope LSM 710 NLO (Carl Zeiss, Germany), and for the specific visualization of callose deposition in the cells, cross-sections were stained with 1% aniline blue for 5 min.

For electron microscopy, samples were fixed in 2% glutaraldehyde in phosphate buffer solution pH 7.4, and dehydrated in ethanol solutions (20, 30, 40, 50, 70, 80, 90, and 100%). Subsequently, samples were dried to the critical point with CO₂ in the Quorum K850 equipment (Quorumtech, United States) and covered with gold in a sputter vacuum chamber (SPI Supplies, United States). Finally, samples were mounted for visualization in a JSM 7800f scanning electron microscope (JEOL, Japan) at 5.0 Kv, as previously described (Ayón-Reyna et al., 2017; Camacho-Vázquez et al., 2019).

2.3.6 Tissue sampling, RNA extraction, cDNA library preparation, and RNA sequencing

Epicarp (skin) tissue was collected with a punch from the equatorial region of each fruit only. For asymptomatic fruit at 5 dph, random tissue was collected along the equatorial region. For the 6 dph fruit of the CI-13 susceptible genotype, tissue with characteristic symptoms of anthracnose disease was collected along the equatorial region, while for the CI-5 resistant genotype of the same treatment, tissue was collected randomly throughout the equatorial region due to the absence of visible symptoms.

Tissue was ground using a Retsch® Mixer Mill MM 400 (Retsch, Germany), and RNA was extracted from 1 g of ground tissue as previously described (Blanco-Ulate et al., 2013). RNA purity and concentration were assessed with a NanoDrop One Spectrophotometer (Thermo Scientific, United States) and a Qubit 3 fluorometer (Invitrogen, United States), respectively. RNA integrity was confirmed by agarose gel electrophoresis.

Twelve barcoded cDNA libraries were prepared using the Illumina TruSeq RNA Sample Preparation Kit v2 (Illumina, United States). Quality control of the cDNA libraries

was performed with the High Sensitivity DNA Analysis Kit in the Agilent 2100 Bioanalyzer (Agilent Technologies, United States). 150-bp paired-end libraries were sequenced on the HiSeq X Platform at IDSeq Inc. (Davis, CA, United States). In total, six libraries were sequenced per variety (three libraries per time point).

2.3.7 Functional annotations

Annotation of the *Carica papaya* SunUp genome (Yue et al., 2022) was performed using the OmicsBox software v3.1.2 (BioBam, Spain). First, ortholog genes were identified from the proteome with the BLASTp (McGinnis and Madden, 2004) suite in OmicsBox, with default parameters, using the UniProt Reviewed Swiss-Prot database (<https://www.uniprot.org/help/downloads>, accessed October 30th, 2023). Protein sequences were then mapped, annotated, and searched for gene ontology (GO) and protein family (Pfam) terms using the Blast2Go and InterProScan suites in OmicsBox, following the functional annotation pipeline with default parameters (Blum et al., 2021; Gotz et al., 2008). Kyoto Encyclopedia of Genes and Genomes (KEGG) pathways were identified using the Automatic Annotation Server (KAAS; v2.1; <http://www.genome.jp/kegg/kaas/>) with bi-directional best hit and BLAST as search program against papaya. Carbohydrate-active enzymes were annotated from the proteome with Trinotate (v3.2.2) (Bryant et al., 2017) using the hmmscan function against the Carbohydrate Active Enzymes database (CAZy, <http://www.cazy.org/>) with default settings.

2.3.8 RNA-seq bioinformatics pipeline

Raw reads were quasi-mapped to a combined papaya and *C. gloeosporioides* and *C. truncatum* transcriptome using Salmon (v.1.10.3) (Patro et al., 2017). Parameter set includes: “-l A”, “-p 8”, and the “-validateMappings -posBias -seqBias -gcBias” flags. Mapping percentages and numbers of host reads and genes for each sample can be found in Supplementary Table S1. The fungal transcriptomes were obtained from NCBI (https://www.ncbi.nlm.nih.gov/genome?LinkName=nucore_genome&from_uid=1826770863, https://www.ncbi.nlm.nih.gov/genome?LinkName=nucore_genome&from_uid=1893088450, accessed June 5th, 2023). Count matrices were made from the Salmon output using the

Bioconductor package tximport (Love et al., 2017) and are available in Supplementary Table S2.

Count matrices were used as input for differential expression analysis with the Bioconductor package DESeq2 in R (Love et al., 2014). Reads were normalized for library size. Gene expression comparisons were made for each variety between 6 dph and 5 dph samples and between genotypes (CI-13 and CI-05) at each time point. Differentially expressed genes (DEGs) were those with $P_{adj} < 0.05$. Normalized reads were then used for weighted gene co-expression network analysis (WGCNA) with the WGCNA package in R (Langfelder and Horvath, 2008). The analysis was conducted on both genotypes and time points together, and transcripts were filtered by the goodSamplesGenes functions. Network construction was conducted step by step, with soft thresholding power selected to obtain approximate scale-free topology and adjacency calculated with $power = soft\ power$. Both adjacency and TOM were calculated with signed type. Initial module eigengenes were detected by hierarchical clustering with default parameters and minModuleSize set to minimize redundancy of modules. Final module eigengenes were obtained by merging close modules with $cutHeight = 0.25$.

Enrichment analyses for GO, Pfam, KEGG, and CAZy terms were performed on module eigengenes using Fisher's exact test ($P_{adj} < 0.05$). Selected GO terms were visualized using the Reduce + Visualize Gene Ontology Web server (REVIGO, <http://revigo.irb.hr/>). GO terms belonging to the "Biological Process" semantic that were enriched in at least two hosts were chosen to graph the data.

2.4 Results

2.4.1 Papaya genotypes display quantitative resistance to anthracnose disease

Since the identification of papaya genotypes that display resistance to anthracnose could contribute significantly to the reduction of postharvest losses, we evaluated the resistance to anthracnose in a panel of seven pre-commercial and commercial papaya genotypes (named CI-02, CI-03, CI-05, CI-06, CI-07, CI-12, and CI-13), developed in Mexico for

domestic and international markets. We inoculated ripe (stage 5) papaya fruit with spore suspensions of *Colletotrichum gloeosporioides* and *C. truncatum* under postharvest conditions. These two species of *Colletotrichum* were selected because they were isolated from commercial papaya fields and are the most prevalent species found in Mexico (Figure 2.1).

At 6 days post inoculation (dpi), the isolates successfully infected all the evaluated genotypes, producing water-soaked lesions and, in most cases, visible mycelial growth. The exception was genotype CI-05, which showed little to no symptoms (Figure 2.1A). Six out of the seven evaluated genotypes demonstrated disease incidence values greater than 80% (Figure 2.1B). In contrast, the CI-05 genotype showed a disease incidence of 30% for *C. gloeosporioides* and 40% for *C. truncatum*. We also calculated the percentage disease index (PDI), which reflects the proportion of diseased tissue relative to healthy tissue. This classification helped assess the genotypes based on their susceptibility or resistance (Figure 2.1C). Genotypes CI-05 and CI-07 were identified as resistant, displaying low PDI values for both *Colletotrichum* species (Figure 2.1D), while CI-02 and CI-03 were moderately resistant. In contrast, genotypes CI-06 and CI-12 were classified as susceptible, and CI-13 as highly susceptible. Genotype CI-05 recorded the lowest average PDI at 7%, whereas CI-13 had the highest at 93%. Based on their contrasting disease incidence and PDI values, genotypes CI-05 and CI-13 were selected for further analysis.

2.4.2 Surface topology and physicochemical properties provide insights into differences in resistant and susceptible genotypes

Fruit surface properties are known to play a role in determining the compatibility outcomes between *Colletotrichum* spp. and fruit hosts (Bano et al., 2023). Given the significant arrest of disease symptoms in the resistant CI-05 genotype, we first considered that the cuticular properties of this genotype may differ significantly from the highly susceptible CI-13 genotype. To test this hypothesis, we examined cross-sections of the cuticle of both genotypes using confocal microscopy, as well as cuticular surface properties through scanning electron microscopy (SEM).

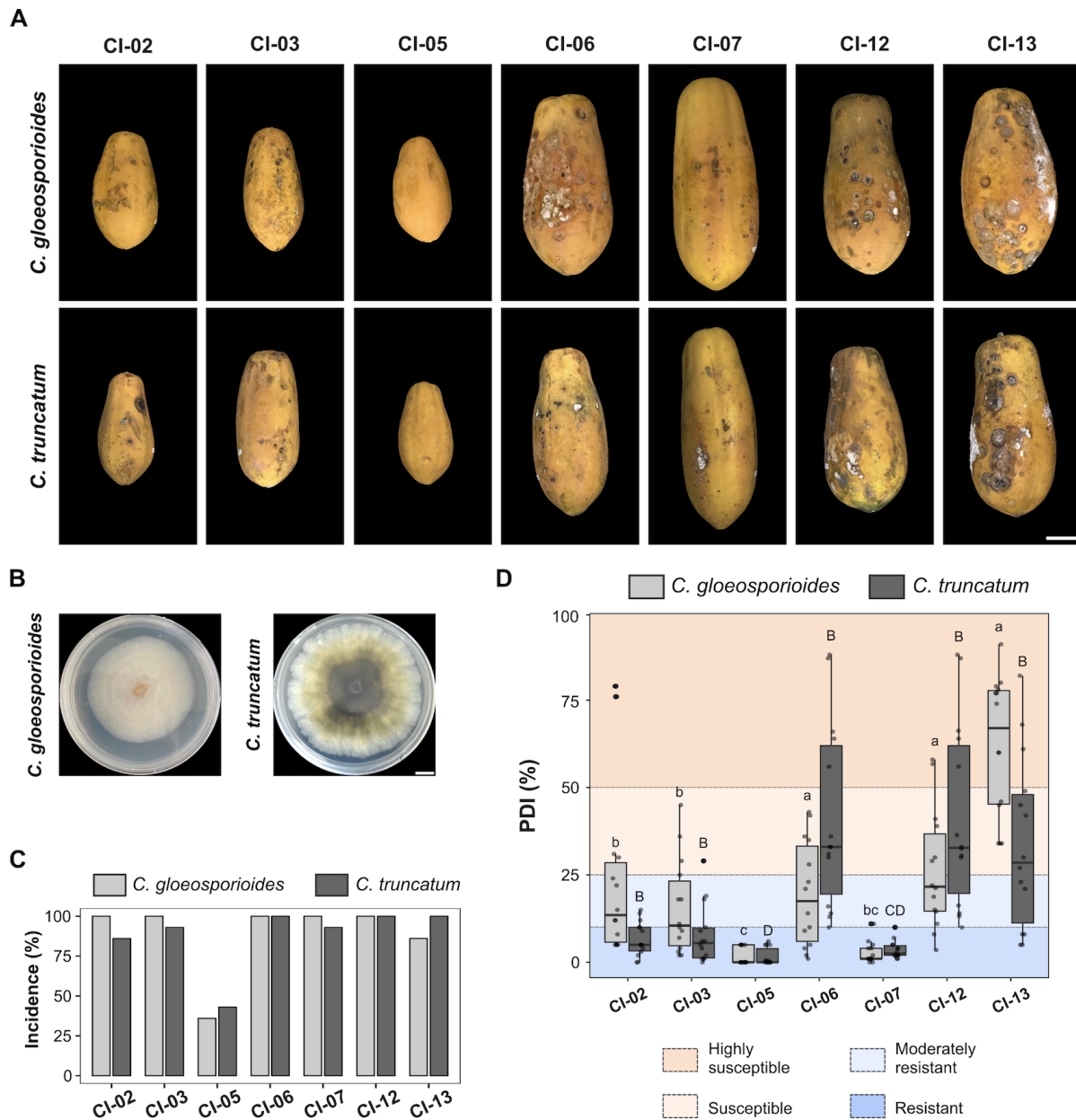


Figure 2.1: Quantitative resistance to *Colletotrichum gloeosporioides* and *C. truncatum* in seven papaya varieties. A) Development of anthracnose disease caused by *C. gloeosporioides* and *C. truncatum* in ripe papaya fruit at 6 days post-inoculation (dpi). The scale bar corresponds to 10 cm. The background of the photographs was digitally removed and replaced with black boxes. B) Axenic cultures of the *C. gloeosporioides* and *C. truncatum* isolates used in this study. Scale bar corresponds to 1 cm. (Continued on following page)

Figure 2.1: (Continued from previous page) C) Anthracnose disease incidence in the seven studied varieties (n=9 fruits per genotype). D) Percentage disease index (PDI) of anthracnose disease (n=9 fruits per genotype). Lowercase letters represent significant differences for *C. gloeosporioides* and capital letters for *C. truncatum* when comparing the genotypes (Tukey, $P < 0.05$).

A 3D model of the cuticle layer of both papaya genotypes (Figure 2.2A, top) showed a greater and more uniform deposition of cuticular components in the periclinal and anticlinal regions of the CWs of the resistant CI-05 genotype, leading to significantly greater ($P < 0.05$) cuticular thickness (Figure 2.2B, left). In contrast, the highly susceptible CI-13 genotype presented a thinner cuticle with fewer cuticular components in the anticlinal regions of the epidermal CWs. Anticlinal pegs surrounding the CWs were observed in both papaya genotypes.

SEM analysis showed differences in the microstructure of the cuticular surface between both papaya genotypes (Figure 2.2A, middle). Although both display a crust-like microstructure, with the presence of epicuticular wax crystalloids with a granular appearance, these wax crystalloids were more abundantly observed around the stomata in the highly susceptible CI-13 genotype (dotted circles). In contrast, in the resistant CI-05 genotype, these microstructures were uniformly distributed along the cuticular surface (Figure 2.2A, middle and bottom). Lastly, stomatal density was significantly lower in the resistant CI-05 genotype (Figure 2.2B, right).

Beyond surface properties, both papaya genotypes showed differences in fruit physicochemical characteristics (Figure 2.2C). The resistant CI-05 genotype produced significantly ($P < 0.05$) smaller and firmer fruit with less total soluble solids, higher titratable acidity, and lower pH compared to the highly susceptible CI-13 genotype. No statistically significant differences were found in skin color (i.e., hue angle).

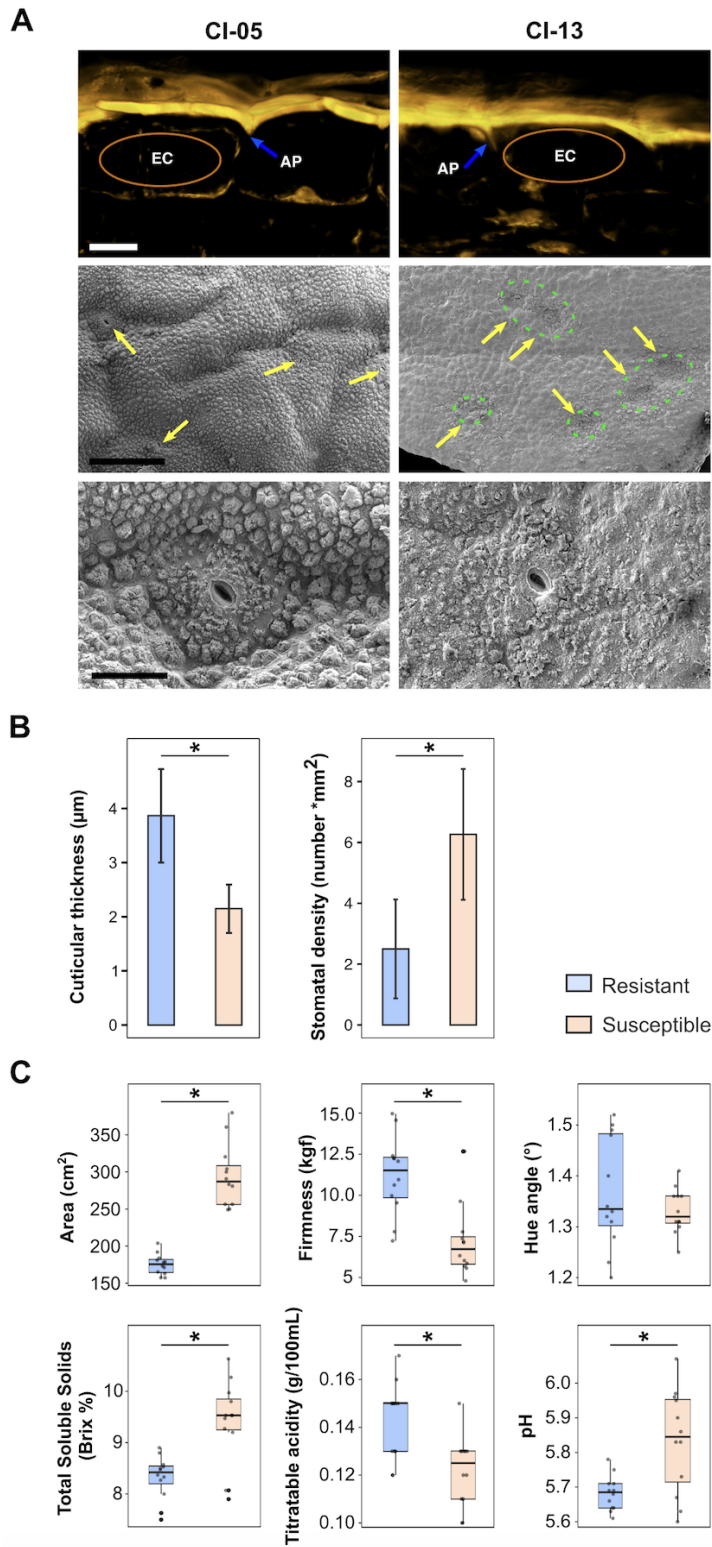


Figure 2.2: Fruit microstructural, anatomical, and physicochemical properties of the CI-05 resistant and CI-13 susceptible genotypes. (Continued on following page)

Figure 2.2: (Continued from previous page) A) Top: 3D reconstruction of the fruit cuticles using Auramine O fluorescence in confocal microscopy. Middle: Cuticular surface visualized by scanning electron microscopy. Bottom: Close-up of stomata on the fruit surface. AP: Anticlinal peg. EC: Epidermal cell. Blue arrows point towards anticlinal pegs. Solid orange circles designate the location of epidermal cells. Yellow arrows show the presence of stomata on the cuticular surface. Dashed green circles show the presence of cuticular projections in the surrounding areas of the stomata in the susceptible genotype. Black scale bars correspond to 200 μm (middle) and 50 μm (bottom), and the white scale bar corresponds to 10 μm . B) Fruit cuticular thickness (left, n=96 measurements per genotype) and stomatal density (right, n=72 images per genotype) in both papaya genotypes. Asterisks indicate significant differences in the comparison between resistant and susceptible genotypes (Cuticular thickness: Tukey $P < 0.05$; Stomatal density: T Student $P < 0.05$). C) Physicochemical properties in the resistant and susceptible genotypes (n= 12 fruit). Fruit area (top left), firmness (top middle), hue angle (top right), total soluble solids (Brix%, bottom left), titratable acidity (bottom middle), pH (bottom right). Asterisks indicate significant differences between genotypes (T Student, $P < 0.05$).

2.4.3 The response of resistant and susceptible genotypes to fungal infection varies in both timing and magnitude

The distinct surface characteristics and physicochemical properties of the resistant CI-05 genotype provide important evidence for its strong resistance to anthracnose. To further understand the molecular pathways and genes associated with these traits, as well as the immune responses of papaya to *Colletotrichum* spp. infection, we performed a genome-wide transcriptomic analysis of the pathosystem.

Using an RNA sequencing approach, we examined natural anthracnose infections in the two papaya genotypes, the resistant CI-05 and the highly susceptible CI-13 (Figure 2.3). We sampled the skins (exocarp) of the papayas at 5 and 6 days postharvest (dph). At 5 dph, none of the genotypes showed disease symptoms, while at 6 dph only the highly susceptible CI-13 showed growing *Colletotrichum* spp. lesions (Figure 2.3A). We focused on natural infections to study how papayas respond to the pathogen under field

conditions and during postharvest, while minimizing any disturbance to the fruit surface. We ensured that we had sufficient fruits for each biological replicate and genotype to accurately represent the conditions observed in the field.

A principal component analysis (PCA) for the quasi-mapped normalized reads of all papaya genes (Figure 2.3B) revealed that the major driver separating the data was the infection phenotype (PC1, 75%). Both genotypes clustered together at 5 dph, when no symptoms of the infection were evident in either, whereas both separated at 6 dph, when only the CI-13 susceptible genotype was symptomatic.

Although other microorganisms may be present in papaya tissues affected by anthracnose, we confirmed the transcriptional activity of *C. gloeosporioides* and *C. truncatum* in the samples from both genotypes. This was done by quasi-mapping all RNA-seq reads to a combined reference that included the genomes of papaya and the two *Colletotrichum* spp. (Figure 2.3C). Both fungal species were observed to have similar levels of transcriptional activity in the highly susceptible CI-13 genotype, while *C. gloeosporioides* seemed to be more abundant than *C. truncatum* in the resistant CI-05. We further confirmed the presence of *C. gloeosporioides* and *C. truncatum* by isolating them from the same papaya skins used in the RNA-seq experiment and evaluating their fungal morphology in culture.

We conducted differential expression analyses ($P_{adj} < 0.05$) to compare: (i) the highly susceptible CI-13 genotype with the resistant CI-05 genotype at each time point, and (ii) the two time points (6 dph versus 5 dph) within each genotype to identify the responses to infection (Figure 2.3D, Supplementary Table S3). The highest number of differentially expressed genes (DEGs) was found when comparing the symptomatic, highly susceptible CI-13 genotype with the asymptomatic, resistant CI-05 genotype at 6 dph. Similarly, when examining differential expression over time within each genotype, the highly susceptible CI-13 genotype showed a more pronounced response than the resistant genotype.

While there were some common genes identified across different comparison groups, the unique genes for each group significantly outnumbered the shared ones, particularly when comparing the two genotypes. For example, 3,502 differentially expressed genes (DEGs) were found to be more abundant in the highly susceptible CI-13 genotype com-

pared to the resistant CI-05 genotype. This finding suggests that the susceptible genotype has a stronger response to infection. Consequently, we examined the functions that were uniquely enriched ($P_{adj} < 0.05$) in the genes that were more prevalent in the susceptible versus the resistant genotypes at 6 dph. Both genotypes exhibited enrichments related to defense responses, ROS production and detoxification, hormone signaling pathways, the synthesis of secondary metabolites (phenylpropanoids, flavonoids, anthocyanins, green leaf volatiles, diterpenoids, saponins), fatty acid metabolism, and cuticle biosynthesis. Nevertheless, the highly susceptible CI-13 genotype at 6 dph specifically showed enrichment in the negative regulation of programmed cell death (GO:0043069), an induced defense response aimed at halting pathogen infection (Coll et al., 2011).

2.4.4 Gene modules reveal trends of early and late gene expression associated with symptomatic and asymptomatic infections

To identify biological processes and genes associated with papaya resistance or susceptibility to *Colletotrichum* spp., we identified groups of genes, i.e. co-expressed gene modules, in each genotype with high expression at each time point (Figure 2.4A, Supplementary Table S3). A total of eight modules were obtained and classified based on their associated phenotype (R-resistant or S-susceptible) and the timing when their expression peaked (E-early or 5 dph, L-late or 6 dph). The clusters associated with the A-asymptomatic phenotype included genes highly expressed in both resistant and susceptible genotypes before the appearance of symptoms (5 dph). Gene modules varied in size, with the largest being two associated with the susceptible phenotype, S-E-1 and S-L-1. The greater size of module S-L-1 ($n = 8,030$) indicates the great magnitude of the response mounted by the highly susceptible CI-13 genotype at late infection stages.

We analyzed each module to determine enriched ($P_{adj} < 0.05$) biological processes in the following categories: plant defense against pathogens, oxidative responses, primary and secondary metabolism, CW and fatty acid (FA) metabolism, and cuticle biosynthesis. We considered that these categories provide insights into potential preformed and induced defenses, as well as factors contributing to susceptibility (Figure 2.4B). Defense responses

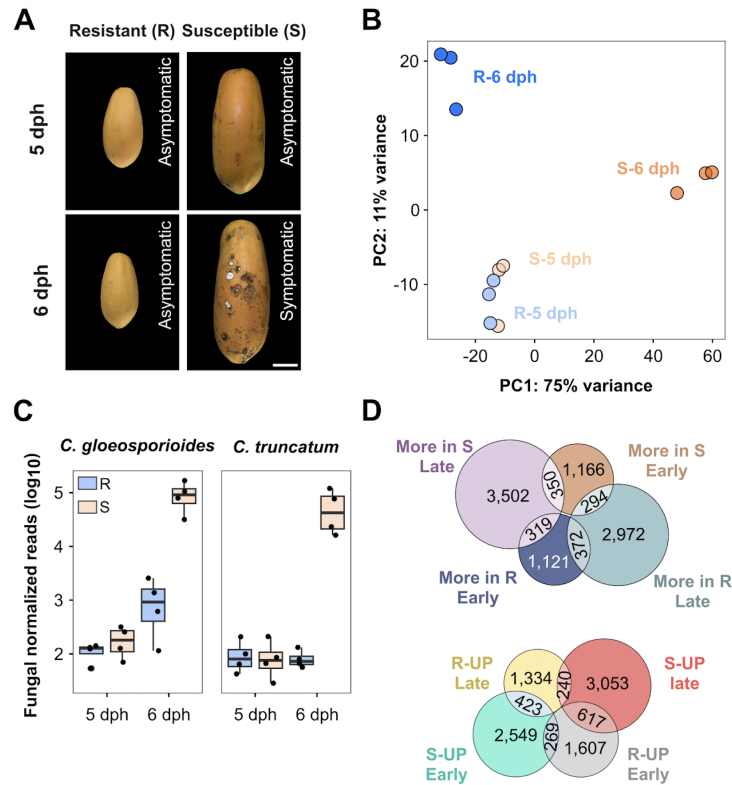


Figure 2.3: Transcriptional profiling of the CI-05 resistant and CI-13 susceptible genotypes after natural infections with *Colletotrichum* spp. A) Development of natural anthracnose infections in the resistant CI-05 (R) and highly susceptible CI-13 (S) papaya genotypes at 5 and 6 days postharvest (dph). Scale bar corresponds to 10 cm. The background of the photographs was digitally removed and replaced with black boxes. B) Principal component analysis (PCA) of total quasi-mapped RNA-seq papaya reads. C) Fungal load expressed as the \log_{10} of the normalized reads for each pathogen in resistant and susceptible papaya genotypes at 5 and 6 dph. D) Number of differentially expressed genes as a result of pairwise comparisons between susceptible (S) and resistant (R) genotypes at each time point (top) and comparisons between 6 dph and 5 dph within the genotypes (bottom).

to fungus (GO:0050832), responses to oxidative stress (GO:0006979), and various processes related to CW integrity were significantly enriched in all modules. This suggests that these factors are likely part of the core response of papaya to *Colletotrichum* spp., regardless of whether the genotype is resistant or susceptible.

Among all modules, S-L-1 showed the highest number of enriched biological processes across all categories. Since most processes were enriched in the S-L-1 module, we focused on identifying patterns of enrichment that contrasted between resistance and susceptibility phenotypes. The enrichment of primary CW organization or biogenesis (GO:0071554) was found exclusively in modules associated with susceptibility. This could be interpreted as a counter-response to the degradation of CWs during the infection process. Additionally, we observed a greater number of genes involved in the regulation of cellulose biosynthesis within the modules linked to susceptibility, even when enrichments were noted at later time points for both phenotypes (R-L-1, R-L-2, and S-L-1).

Regulation of CW pectin metabolism (GO:1902066) was enriched only at early time points in modules associated with resistance (R-E-1 and R-E-3). In contrast, lignin biosynthesis (GO:0009809) was enriched in both resistant and susceptible phenotypes at early and late time points. However, the regulation of this process (GO:1901141) occurred earlier (R-E-3) for the resistant phenotype than for the susceptible one (S-L-1). This suggests that the resistant CI-05 genotype can quickly induce lignification of the CW as a defense response at an earlier stage. Additionally, we observed an enrichment in callose synthases (GT48 CAZyme family) exclusively in the R-L-1 module. Together with lignin biosynthesis, this may create a mechanism to strengthen the CWs and limit fungal infection.

Cuticle hydrocarbon biosynthesis (GO:0006723) and cutin biosynthesis (GO:0010143), along with their regulation (GO:1901957), were found to be enriched early (R-E-3) in modules associated with resistance, and later (S-L-1) in those linked to susceptibility. These findings suggest that the highly susceptible CI-13 genotype does not actively maintain or replace its fruit cuticle before disease symptoms appear. However, once the lesions expand at 6 dph, wax biosynthesis becomes enriched in this genotype.

The R-E-2 module, which contains early-induced genes associated with resistance, showed enrichment in chitin responses (GO:0071323). In contrast, this term was only enriched in the S-L-1 module, which includes late-induced genes linked to susceptibility. This suggests that the resistant CI-05 genotype can recognize the presence of the fungus earlier, allowing it to mount an effective defense response both promptly and efficiently. Moreover, specific terms related to the production and detoxification of ROS were enriched at the early time point in the resistant phenotype. This includes the regulation of ROS metabolism (GO:2000377), the catabolism of hydrogen peroxide (GO:0042744), and the metabolism of glutathione (GO:0006749). These findings further indicate that the resistant CI-05 genotype exhibits an early oxidative burst response to fungal infection.

2.4.5 Callose deposition is associated with resistance in papaya fruit

Based on the results of the transcriptomic and enrichment analyses, we further investigated the host CW responses to infections by *Colletotrichum* species using microscopy. We inoculated fruits from two papaya genotypes, the resistant CI-05 and the highly susceptible CI-13, with *C. gloeosporioides* and *C. truncatum*. We then examined cross sections of the fruit’s epidermal layer with a confocal and scanning electron microscope (SEM).

Staining with aniline blue and calcofluor white observed by confocal microscopy revealed a more robust CW response in the resistant CI-05 genotype compared to the highly susceptible CI-13 genotype at 3 dpi, particularly in callose deposition (Figure 2.5A and B, left). We also observed that the resistant genotype had a thicker cell wall, even prior to inoculation ($6.31 \pm 2.03 \mu\text{m}$), compared to the susceptible one ($3.24 \pm 0.87 \mu\text{m}$) (Figure 2.5B, right).

Fungal proliferation was evident only in the highly susceptible CI-13 genotype at 3 dpi, as shown by the colored SEM images, which also revealed a cuticle rupture and loss of cellular structure in the susceptible genotype. In contrast, the resistant CI-05 maintained intact cellular structures without any signs of fungal proliferation (Figure 2.5A, right column).

To further support these observations, we analyzed the expression of the five most

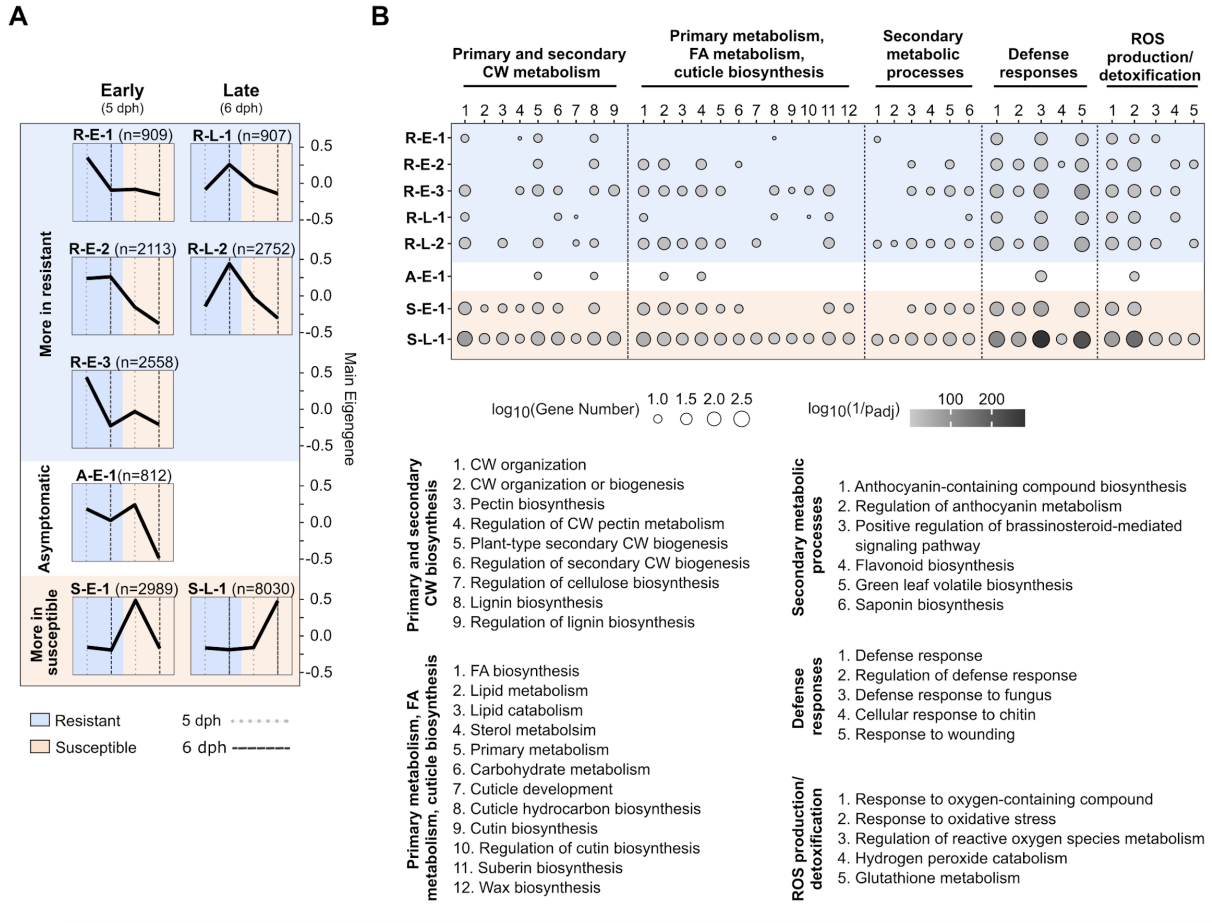


Figure 2.4: Gene co-expression patterns reveal modules associated with papaya resistance and susceptibility to anthracnose. A) Modules of co-expressed genes classified based on infection phenotype (R: resistant, A: asymptomatic, S: susceptible), and timing of gene expression (E: early, L: late). Blue-colored sections correspond to those associated with resistance, and orange-colored sections correspond to those associated with susceptibility. dph: days postharvest. B) Major functions represented in each gene module, as pertaining to five categories: Primary and secondary cell wall (CW) metabolism; Primary metabolism, fatty acid (FA) metabolism, and cuticle biosynthesis; Secondary metabolic process; Defense responses; and Reactive Oxygen Species (ROS) production and detoxification.

highly-expressed callose genes in both genotypes using the RNA-seq data (Figure 2.5C). Four of these genes were found in modules associated with resistance at both early and late time points, while only one was linked to the susceptible phenotype (S-L-1).

2.4.6 Highly expressed and induced genes reveal functions related to resistance and susceptibility to anthracnose

To identify specific genes that influence papaya fruit resistance or susceptibility to *Colletotrichum* spp., we hypothesized that DEGs exhibiting high baseline expression in resistance-related modules could act as potential defenses, either preformed or induced. Conversely, DEGs showing increased expression in susceptibility-related modules may function as susceptibility factors.

We selected all differentially expressed genes (DEGs) from the previously established comparisons and identified the genes with the highest expression levels by focusing on those within the 99th percentile of log₁₀-transformed expression data (Figure 2.6A). This led to a list of sixty-nine unique genes (Supplementary Table S4). The top twelve highest-expressed genes are shown in Figure 2.6B and represent four different modules. These include genes related to redox activity, ethylene biosynthesis genes, methyltransferase encoding genes, a gene coding for an invertase, and an endochitinase encoding gene.

To observe how gene responses were changing for each genotype and at each time point, we selected the genes with the highest log₂-fold change in each of the represented modules (Figure 2.6C). We observed two genes encoding a cytochrome P450 (*GWHTBFSC011082*, *GWHTBFSC022156*) and two genes encoding enzymes involved in CW remodeling and sugar metabolism with similar expression levels at 5 dph but different at 6 dph, pointing to the relevance of induced defenses in the late responses to the pathogen.

In addition to the highly expressed genes shown in (Figure 2.6), we identified two pectin-degrading enzymes, a rhamnogalacturonate lyase (RGL, *GWHTBFSC009260*) and a β -galactosidase (β -GAL, *GWHTBFSC018746*) in the S-L-1 module among the genes in the 99th percentile. These enzymes degrade the pectin backbone, likely contributing to pulp softening during ripening. Given the relevance of pectin integrity in defense against fungal pathogens, they constitute good candidates for susceptibility factors. Additionally,

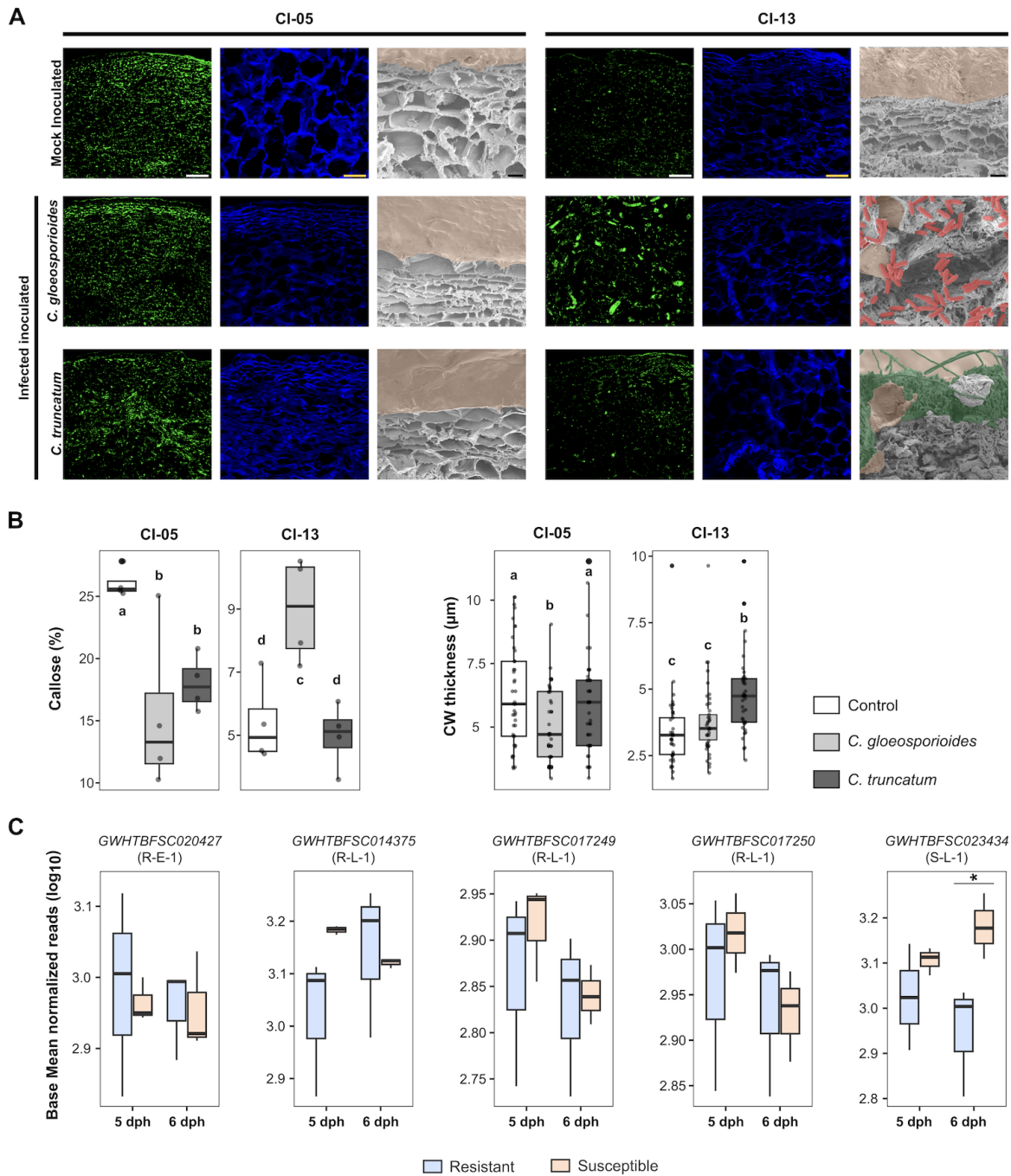


Figure 2.5: Host cell wall responses and fungal proliferation in the CI-05 resistant and CI-13 susceptible genotypes after *Colletotrichum gloeosporioides* and *C. truncatum* infections. (Continued on following page)

Figure 2.5: (Continued from previous page) A) Aniline blue staining for callose visualization (left column), calcofluor white staining for cell wall (CW) visualization (middle column), and colored scanned electron microscope (SEM) images showing fungal proliferation after fruit inoculation with *C. gloeosporioides* and *C. truncatum* infections (right column). Colored SEM images showing cuticular regions (orange), fungal conidia (red), and hyphae (green). White, yellow, and black scale bars correspond to 100 μm , 50 μm , and 10 μm , respectively. B) Percentage of callose in CI-05 resistant and CI-13 susceptible papaya genotypes during fungal infection (left). CW thickness of CI-05 resistant and CI-13 susceptible papaya genotypes (right). Small letters represent significant differences (T Student, $P < 0.05$). C) Overview of the top 5 expressed callose synthase genes. An asterisk indicates a significant difference between the susceptible and the resistant genotypes (T Student, $P < 0.05$).

we observed in resistance-associated modules an endoglucanase (*GWHTBFSC010245*), a sugar transporter (*GWHTBFSC006396*), a mannosidase (*GWHTBFSC013170*), and two NADP-dependent malic enzymes (*GWHTBFSC010791*, *GWHTBFSC018814*). The high expression of these genes involved in sugar and organic acid metabolism could correlate with the lower total soluble solids and higher titratable acidity recorded for the resistant CI-05 genotype.

2.5 Discussion

2.5.1 Smoother and thicker fruit surfaces with fewer natural openings are associated with papaya resistance to *Colletotrichum*

To successfully infect a fruit host, *Colletotrichum* spp. must first overcome the epicuticular wax and cuticular layer, the plant cell wall (CW), and preformed antifungal compounds present on the fruit surface. In our study, we identified the CI-05 papaya genotype, which exhibits quantitative resistance to *C. gloeosporioides* and *C. truncatum* (Figure 2.1). Analyzing the surface properties of the fruit revealed that the resistant CI-05 genotype had a greater and more evenly distributed deposition of cuticular components, resulting in in-

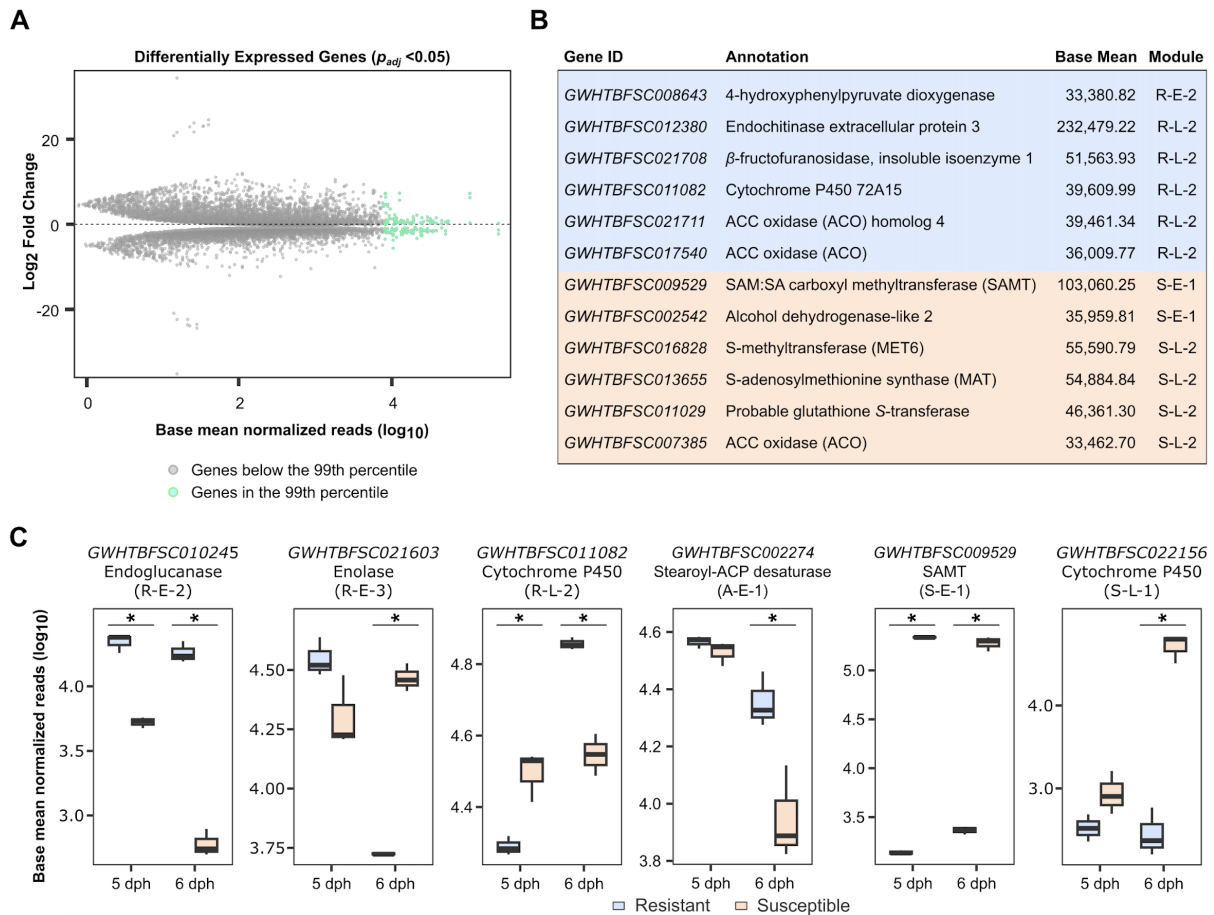


Figure 2.6: Overview of highly expressed genes in the CI-05 resistant and CI-13 susceptible genotypes. A) Scatterplot with all differentially expressed genes (DEGs). Those in the 99th percentile have been colored in green. B) Table with top-twelve expressed DEGs organized per module. C) Gene expression of the genes with the highest log₂-fold change per module. Asterisks indicate significant differences in the comparison between genotypes and infection status (T Student, $P < 0.05$).

creased cuticular thickness compared to the susceptible genotype (Figure 2.2). Previous research in other pathosystems indicates that cuticular thickness and integrity are key determinants of fruit resistance to fungal pathogens, particularly during the pre-penetration stages, which help slow down or halt the infection process (Kumara and Rawal, 2009; Lara et al., 2019; Ziv et al., 2018).

We also noted differences in the deposition of wax crystalloids between the two genotypes. In the highly susceptible CI-13 genotype, wax crystalloids were localized around the stomata. When *Colletotrichum* spp. adhere to the host cuticle and detect host-derived signals, they trigger conidia germination and the differentiation of melanized appressoria (Mendgen et al., 1996; Ryder and Talbot, 2015). Surface hydrophobicity, hardness, plant surface components, and topography are among the major host signals required for appressoria differentiation (Mendgen et al., 1996). For the necrotrophic fungus *Botrytis cinerea*, it has also been reported that sensing surface topography is key for directional growth and development. Synthetic surfaces that mimic leaf surfaces can stimulate germ tube development in *B. cinerea*, while flat surfaces do not have the same effect (Rombach et al., 2022). These observations suggest that the surface topography of the resistant CI-05 genotype may not be conducive to spore germination and appressoria differentiation, thereby delaying pathogen colonization at the cuticular level.

Interestingly, we found that genes related to wax biosynthesis were mainly enriched in gene modules associated with susceptibility (Figure 2.4). While wax synthesis has been shown to protect against fungal infections in some pathosystems (Cajuste et al., 2010), in others, surface hydrophobicity and cuticular wax appear to promote fungal infections (Tang et al., 2017). Considering the high susceptibility of the CI-13 genotype to both *Colletotrichum* spp., it seems that increased wax synthesis could actually be a factor contributing to its susceptibility and leading to a surface topography that facilitates infection.

Natural openings on the fruit surface, such as lenticels, stomata, and microfractures in the cuticle, greatly influence disease susceptibility, as they provide a quick entry route for pathogenic fungi (Chorolque et al., 2021; Gupt et al., 2021; Murria et al., 2019). Scanning

electron microscopy revealed that the resistant CI-05 genotype had a significantly lower stomatal density than the highly susceptible genotype (Figure 2.2). In papaya, it is important to note that the number of stomata is determined during anthesis and remains constant throughout fruit development (Hieke et al., 2002); therefore, this characteristic is dictated by the genotype from fruit set.

2.5.2 Firm fruit with reduced sugars and higher acidity are more tolerant to *Colletotrichum* infections

Certain physicochemical attributes of fruit are considered important factors in susceptibility to various pathosystems. These attributes include those that lead to increased production of metabolites that support pathogen growth and sugar transport, as well as CW degrading enzymes that facilitate CW loosening (Silva et al., 2021; Van Schie and Takken, 2014). In our study, the highly susceptible CI-13 genotype showed significantly higher total soluble solids and lower firmness. In contrast, the resistant CI-05 genotype exhibited lower pH, higher titratable acidity, and greater firmness. Higher total soluble solids, along with increased cellular respiration and ethylene production, have been positively correlated with *C. fioriniae* infection in apples, while firmness and titratable acidity maintained a negative correlation (Grammen et al., 2019). Among the highly expressed genes, we observed a series of CW degrading enzymes involved in pectin degradation that were highly expressed in the highly susceptible CI-13 genotype. These enzymes could be increasing the availability of carbohydrate substrates for further degradation to sugars through the action of other enzymes (Fanourakis et al., 2022). Additionally, the two observed highly expressed NADP-dependent malic enzymes could be contributing to the lower acidity of the resistant CI-05 genotype, as they have been reported to regulate cytosolic pH (Wheeler et al., 2005). Higher malic acid content in papaya juice has also been correlated with antimicrobial effects in papaya juice (Fanourakis et al., 2022).

Changes in the architecture and composition of the CW during ripening can also lead to fruit susceptibility to fungal infections. For instance, the suppression or knock-out of polygalacturonase (*SlPG2a*), expansin (*SlExp1*), and pectate lyase (*SlPL*) genes reduced the susceptibility to *B. cinerea* in tomato (Cantu et al., 2008; Silva et al.,

2021). In our differential gene expression analysis, we identified two genes encoding a β -galactosidase (β -GAL, *GWHTBFSC018746*) and a rhamnogalacturonate lyase (RGL, *GWHTBFSC009260*) among the genes with the highest expression. The high expression of these genes in the susceptible genotype could lead to the breakdown of pectin in the fruit primary CWs, resulting in tissue softening and increased susceptibility (Fanourakis et al., 2022). Knocking out a homolog of this gene in tomato resulted in increased fruit firmness and a longer shelf-life (Ochoa-Jiménez et al., 2018). Further functional validation assays are required to confirm the involvement of these two enzymes in the increased susceptibility of the CI-13 genotype.

2.5.3 Timing is crucial! Larger transcriptional responses to fungal infection do not ensure fruit resistance

The transcriptomics approach allowed us to gain insight into induced responses in each genotype upon fungal infection, as well as contrast both genotypes at each time point (Figure 2.3). The highly susceptible CI-13 genotype displayed the largest number of DEGs, which shows that it is undergoing a large transcriptional reprogramming and mounting defense responses, although the presence of the potential susceptibility factors discussed above might outweigh the induced defense mechanisms and result in disease. This is supported by our previous observations in nectarine and tomato, where the susceptible ripe fruit displayed a larger transcriptional response to infection when compared to the resistant unripe fruit (Balsells-Llauradó et al., 2020; Silva et al., 2021). In addition to the misregulation of various biological processes, we identified more genes involved in the negative regulation of programmed cell death (PCD) in the susceptible genotype. PCD plays a critical role in determining the outcomes of plant-pathogen interactions and is associated with resistance to necrotrophic pathogens when induced early in the interaction (Greenberg and Yao, 2004).

Core responses of papaya to *Colletotrichum* spp. infection, regardless of genotype, consisted of those terms that were similarly enriched in both genotypes, mainly associated with defense and oxidative stress responses, as well as secondary metabolic processes (Figure 2.4). However, the resistant genotype seemed to be able to respond to chitin

earlier. Recognition of chitin triggers a series of responses to restrict pathogen growth, characterized by CW thickening, callose deposition, and production of reactive oxygen species (ROS), among others (Anil et al., 2014). Although the susceptible genotype also displayed an oxidative burst, synthesis of cellulose, pectin, and lignin contributing to CW thickening, and synthesis of cutin and cuticle hydrocarbons, these processes probably took place too late when the pathogen had already established itself in the host tissues. Microscopy analyses confirmed greater callose deposition and CW thickening in both control and inoculated papaya fruit of the resistant CI-05 genotype (Figure 2.5). Although not all differences were statistically significant, four out of the top five callose synthase genes showed higher expression levels in the resistant genotype.

2.5.4 Highly expressed genes during fruit infections provide clues about defense mechanisms and susceptibility factors

The gene with the highest basal expression in our study was an endochitinase associated with the resistant phenotype (R-L-2 module). Plant chitinases are produced when fungi invade and can inhibit fungal spore germination, the formation of germ tubes, and the degradation of hyphal tips (Ntui et al., 2011). This suggests that the observed endochitinase likely serves as an induced defense response against *Colletotrichum* spp. in the resistant genotype. Genes encoding cytochrome P450 proteins were also highly expressed in both resistant and susceptible genotypes. Cytochrome P450 proteins are important in various detoxification and secondary metabolic pathways. We identified candidate genes encoding cytochrome P450 proteins belonging to the CYP71, 72, and 86, which are involved in the synthesis of terpenoids and fatty acids, including the biosynthesis of the triterpenoid saponins in the case of the CYP72 family (Chakraborty et al., 2023; Ghosh, 2017; Liu et al., 2019; Wang et al., 2024). Saponins are biologically active toxic compounds that healthy plants produce, which may possess antifungal properties (Minerdi et al., 2023; Zaynab et al., 2021). Genes involved in the synthesis of saponins were enriched in both genotypes at early and late time points, which points towards these toxic compounds as being induced defenses against *Colletotrichum* spp.

Ethylene biosynthesis genes, 1-aminocyclopropane- 1-carboxylate oxidases (ACOs),

were highly expressed in both genotypes. When a plant is infected by a pathogen, ethylene triggers the expression of defense response genes, especially against necrotrophic fungi. This is achieved through a signal transduction cascade and by affecting the production of other plant hormones that contribute to immune responses (Shekhawat et al., 2022). However, in climacteric fruits like papaya, increased ethylene can activate system 2 biosynthetic enzymes, resulting in further ripening or senescence. These developmental processes are known to increase susceptibility to fungal diseases (Li et al., 2024).

Lastly, the RGL enzyme, highly expressed in the susceptible genotype (mentioned above), ranks among the most highly expressed genes (top 1%). This enzyme targets the rhamnogalacturonan component of the pectin backbone and may affect the cohesion of pectin polymers during cell expansion and fruit softening as the fruit ripens (Molina-Hidalgo et al., 2013). Additionally, it can be induced by ethylene (Guillermo et al., 2017; Vicente et al., 2007). The increase in ethylene production may lead to enhanced expression of the RGL enzyme, resulting in greater CW degradation and increased susceptibility to disease in the CI-13 genotype. In contrast, the resistant CI-05 genotype exhibits increased ethylene biosynthesis but low expression of the RGL enzyme. This observation suggests an alternative regulatory mechanism regarding the RGL enzyme in this particular genotype.

2.6 Conclusions

Fruit susceptibility or resistance to pathogenic fungi is a complex trait influenced by a balance of several components, including constitutive and preformed barriers, induced defenses, and the presence of susceptibility factors. Our analysis of two papaya genotypes revealed that fruit traits like cuticular thickness, stomatal density, sugar content, and acidity affect the initial interaction with *Colletotrichum* spp. The highly susceptible genotype has a thinner cuticle, higher stomatal density, and lower firmness, creating a weaker barrier. Its higher sugar content, while appealing to consumers, may also support pathogen growth. Conversely, the resistant genotype, despite having slightly lower total soluble solids than preferred (>10% Brix) (Pereira Miranda et al., 2022), remains a valuable parental line for hybrid breeding programs due to its small size, high firmness, and

resistance to fungal disease. The resistant genotype can recognize pathogens early and trigger immune responses, including chitin degradation and reactive oxygen species (ROS) production. Although the susceptible CI-13 can mount a robust transcriptional response, its weaker constitutive barriers, along with susceptibility factors like the CW-degrading enzymes RGL and β -GAL, and higher sugar content, outbalance the induced defenses. Taken together, the results of this study shed light on the complex nature of papaya resistance to anthracnose. Rather than lack of defenses, the susceptibility of the CI-13 genotype seems to lie in the higher prevalence of factors that contribute to susceptibility to fungal infection, as well as the timing of the induced defense responses. These aspects highlight the importance of considering the weight of potential susceptibility factors in the outcome of plant-pathogen interactions as opposed to solely focusing on resistance factors. In the present study we have identified a series of constitutive and induced defenses as well as candidate susceptibility factors that can be jointly targeted in breeding efforts to improve resistance of papaya fruit to anthracnose.

2.7 Data Availability

The datasets generated in this study have been deposited in the Gene Expression Omnibus (GEO) database (accession number GSE281201).

2.8 Acknowledgments

We would like to acknowledge Adrián Sbodio for providing assistance with figure preparation and Madison Lalica for reviewing the manuscript's narrative.

2.9 References

- Adainoo, B., Thomas, A., and Krishnaswamy, K. (2023). A comparative study of edible coatings and freshness paper on the quality of fresh north american pawpaw (*Asimina triloba*) fruits using topsis-shannon entropy analyses. *Current Research in Food Science*, 7:100541.
- Anil, K., Das, S., and Podile, A. (2014). Induced defense in plants: A short overview. *Proceedings of the National Academy of Sciences, India Section B: Biological Sciences*, 84(4):669–679.
- Ayón-Reyna, L., González-Robles, A., Rendón-Maldonado, J., Báez-Flores, M., López-López, M., and Vega-García, M. (2017). Application of a hydrothermal-calcium chloride treatment to inhibit postharvest anthracnose development in papaya. *Postharvest Biology and Technology*, 124:85–90.
- Ayón Reyna, L., Uriarte Gastelum, Y., Camacho Díaz, B., Tapia Maruri, D., López López, M., López Velázquez, J., and Vega García, M. (2022). Antifungal activity of a chitosan and mint essential oil coating on the development of *Colletotrichum gloeosporioides* in papaya using macroscopic and microscopic analysis. *Food Bioprocess Technology*, 15:368–378.
- Balsells-Llauradó, M., Silva, C., Usall, J., Vall-llaura, N., Serrano-Prieto, S., Teixidó, N., Mesquida-Pesci, S., De Cal, A., Blanco-Ulate, B., and Torres, R. (2020). Depicting the battle between nectarine and *Monilinia laxa*: the fruit developmental stage dictates the effectiveness of the host defenses and the pathogen’s infection strategies. *Horticulture Research*, 7:167.
- Bano, A., Gupta, A., Prusty, M., and Kumar, M. (2023). Elicitation of fruit fungi infection and its protective response to improve the postharvest quality of fruits. *Stresses*, 3:231–255.
- Barragán-Iglesias, J., Méndez-Lagunas, L., and Rodríguez-Ramírez, J. (2018). Ripeness

- indexes and physicochemical changes of papaya (*Carica papaya* L. cv. maradol) during ripening on-tree. *Scientia Horticulturae*, 236:272–278.
- Bhadauria, V., Banniza, S., Vandenberg, A., Selvaraj, G., and Wei, Y. (2011). Cataloging proteins putatively secreted during the biotrophy-necrotrophy transition of the anthracnose pathogen *Colletotrichum truncatum*. *Plant Signaling & Behavior*, 6(10):1457–1459.
- Blanco-Ulate, B., Vincenti, E., Powell, A., and Cantu, D. (2013). Tomato transcriptome and mutant analyses suggest a role for plant stress hormones in the interaction between fruit and *Botrytis cinerea*. *Frontiers in Plant Science*, 4:142.
- Blum, M., Chang, H.-Y., Chuguransky, S., Grego, T., Kandasaamy, S., Mitchell, A., Nuka, G., Paysan-Lafosse, T., Qureshi, M., Raj, S., Richardson, L., Salazar, G., Williams, L., Bork, P., Bridge, A., Gough, J., Haft, D., Letunic, I., Marchler-Bauer, A., Mi, H., Natale, D., Necci, M., Orengo, C., Pandurangan, A., Rivoire, C., Sigrist, C., Sillitoe, I., Thanki, N., Thomas, P., Tosatto, S., Wu, C., Bateman, A., and Finn, R. (2021). The interpro protein families and domains database: 20 years on. *Nucleic Acids Research*, 49(D344–D354).
- Bryant, D., Johnson, K., DiTommaso, T., Tickle, T., Couger, M., Payzin-Dogru, D., Lee, T., Leigh, N., Kuo, T.-H., Davis, F., Bateman, J., Bryant, S., Guzikowski, A., Tsai, S., Coyne, S., Ye, W., Freeman, R., Peshkin, L., Tabin, C., Regev, A., Haas, B., and Whited, J. (2017). A tissue-mapped axolotl de novo transcriptome enables identification of limb regeneration factors. *Cell Reports*, 18(4):762–776.
- Cajuste, J., González-Candelas, L., Veyrat, A., García-Breijo, F., Reig-Armiñana, J., and Lafuente, M. (2010). Epicuticular wax content and morphology as related to ethylene and storage performance of ‘navelate’ orange fruit. *Postharvest Biology and Technology*, 55:29–35.
- Camacho-Vázquez, C., Ruiz-May, E., Guerrero-Analco, J., Elizalde-Contreras, J., Enciso-Ortiz, E., Rosas-Saito, G., López-Sánchez, L., Kiel-Martínez, A., Bonilla-Landa, I., Monribo-Villanueva, J., Olivares-Romero, J., Gutiérrez-Martínez, P., Tafolla-Arellano,

- J., Tiznado-Hernandez, M., Quiroz-Figueroa, F., Birke, A., and Aluja, M. (2019). Filling gaps in our knowledge on the cuticle of mangoes (*Mangifera indica*) by analyzing six fruit cultivars: Architecture/structure, postharvest physiology and possible resistance to fruit fly (*Tephritidae*) attack. *Postharvest Biology and Technology*, 148:83–96.
- Cannon, P., Damm, U., Johnston, P., and Weir, B. (2012). *Colletotrichum* – current status and future directions. *Studies in Mycology*, 73:181–213.
- Cantu, D., Vicente, A., Greve, L., Dewey, F., Bennett, A., Labavitch, J., and Powell, A. (2008). The intersection between cell wall disassembly, ripening, and fruit susceptibility to *Botrytis cinerea*. *Proceedings of the National Academy of Sciences*, 105:859–864.
- Chakraborty, P., Biswas, A., Dey, S., Bhattacharjee, T., and Chakrabarty, S. (2023). Cytochrome p450 gene families: Role in plant secondary metabolites production and plant defense. *Journal of Xenobiotics*, 13(3):402–423.
- Chorolque, A., Pozzo Ardizzi, M., and Hernández, L. (2021). Relación entre densidad de estomas y lenticelas en hojas y frutos del nogal (*Juglans regia L.*) y la severidad de *Xanthomonas arboricola* pv. *juglandis*. *Chilean Journal of Agricultural and Animal Sciences*, 37:65–73.
- Coll, N., Epple, P., and Dangl, J. (2011). Programmed cell death in the plant immune system. *Cell Death and Differentiation*, 18:1247–1256.
- De Silva, D., Crous, P., Ades, P., Hyde, K., and Taylor, P. (2017). Life styles of *Colletotrichum* species and implications for plant biosecurity. *Fungal Biology Reviews*, 31:155–168.
- Dos Passos Braga, S., Lundgren, G., Macedo, S., Tavares, J., Dos Santos Vieira, W., Câmara, M., and De Souza, E. (2019). Application of coatings formed by chitosan and mentha essential oils to control anthracnose caused by *Colletotrichum gloeosporioides* and *C. brevisporum* in papaya (*Carica papaya L.*) fruit. *International Journal of Biological Macromolecules*, 139:631–639.

- Evans, E. and Ballen, F. (2012). An overview of global papaya production, trade, and consumption. Series (FE913) from UF/IFAS University of Florida.
- Fanourakis, D., Nikoloudakis, N., Paschalidis, K., Christopoulos, M., Goumenaki, E., Tsantili, E., Delis, C., and Tsaniklidis, G. (2022). Gene expression, activity and localization of beta-galactosidases during late ripening and postharvest storage of tomato fruit. *Agriculture*, 12(6).
- Gan, P., Ikeda, K., Irieda, H., Narusaka, M., O’Connell, R., Narusaka, Y., Takano, Y., Kubo, Y., and Shirasu, K. (2013). Comparative genomic and transcriptomic analyses reveal the hemibiotrophic stage shift of *Colletotrichum* fungi. *New Phytologist*, 197:1236–1249.
- Gao, Y., Zhang, C., Han, X., Wang, Z., Ma, L., Yuan, D., Wu, J., Zhu, X., Liu, J., Li, D., Hu, Y., and Xuan, Y. (2018). Inhibition of *OsSWEET11* function in mesophyll cells improves resistance of rice to sheath blight disease. *Molecular Plant Pathology*, 19:2149–2161.
- Ghosh, S. (2017). Triterpene structural diversification by plant cytochrome p450 enzymes. *Frontiers in Plant Science*, 8:1886.
- Gotz, S., Garcia-Gomez, J., Terol, J., Williams, T., Nagaraj, S., Nueda, M., Robles, M., Talon, M., Dopazo, J., and Conesa, A. (2008). High-throughput functional annotation and data mining with the blast2go suite. *Nucleic Acids Research*, 36:3420–3435.
- Grammen, A., Van Campenhout, J., Geeraerd, A., and Keulemans, W. (2019). Susceptibility of apple fruits (*Malus x domestica* Borkh.) to the postharvest pathogen *Colletotrichum fioriniae*: cultivar differences and correlation with fruit ripening characteristics. *European Journal of Plant Pathology*, 155:801–816.
- Greenberg, J. and Yao, N. (2004). The role and regulation of programmed cell death in plant-pathogen interactions. *Cellular Microbiology*, 6:201–211.

- Guillermo, B.-V., Marisela, R.-D., Rosalba, T.-R., Reginaldo, B.-S., and Martín-Ernesto, T.-H. (2017). Physiological function of rhamnogalacturonan lyase genes based in the analysis of cis-acting elements located in the promoter region. *Research Journal of Biotechnology*, 12. No specific pages provided.
- Gupt, S., Chand, R., Mishra, V., Ahirwar, R., Bhatta, M., and Joshi, A. (2021). Spot blotch disease of wheat as influenced by foliar trichome and stomata density. *Journal of Agricultural and Food Research*, 6.
- Göhre, V. and Robatzek, S. (2008). Breaking the barriers: Microbial effector molecules subvert plant immunity. *Annual Review of Phytopathology*, 46:189–215.
- Hewajulige, I. and Wijeratnam, S. (2010). Alternative postharvest treatments to control anthracnose disease in papaya during storage. *Fresh Produce*, 4:15–20.
- Hieke, S., Menzel, C., and Ludders, P. (2002). Effects of leaf, shoot and fruit development on photosynthesis of lychee trees (*Litchi chinensis*). *Tree Physiology*, 22:955–961.
- Koseoglou, E., Van Der Wolf, J., Visser, R., and Bai, Y. (2022). Susceptibility reversed: modified plant susceptibility genes for resistance to bacteria. *Trends in Plant Science*, 27:69–79.
- Kumara, K. and Rawal, R. (2009). Screening of papaya cultivars against anthracnose disease caused by *Colletotrichum gloeosporioides* (penz.) penz. and sacc. *JSci-EUSL*, 6:27–33.
- Langfelder, P. and Horvath, S. (2008). Wgcna: an r package for weighted correlation network analysis. *BMC Bioinformatics*, 9.
- Lara, I., Heredia, A., and Domínguez, E. (2019). Shelf life potential and the fruit cuticle: The unexpected player. *Frontiers in Plant Science*, 10.
- Li, S., Zhao, Y., Wu, P., Grierson, D., and Gao, L. (2024). Ripening and rot: How ripening processes influence disease susceptibility in fleshy fruits. *Journal of Integrative Plant Biology*, 66:1831–1863.

- Liu, Q., Khakimov, B., Cárdenas, P. D., Cozzi, F., Olsen, C. E., Jensen, K. R., Hauser, T. P., and Bak, S. (2019). The cytochrome p450 cyp72a552 is key to production of hederagenin-based saponins that mediate plant defense against herbivores. *New Phytologist*, 222(3):1599–1609.
- Love, M., Huber, W., and Anders, S. (2014). Moderated estimation of fold change and dispersion for rna-seq data with *deseq2*. *Genome Biology*, 15.
- Love, M., Soneson, C., and Robinson, M. (2017). Importing transcript abundance datasets with *tximport*. *Dim Txi Inf Rep Sample 1*, 1.
- Maeda, C. and Nelson, S. (2014). Anthracnose of papaya in hawai'i. <https://www.ctahr.hawaii.edu/oc/freepubs/pdf/PD-103.pdf>.
- McGinnis, S. and Madden, T. (2004). Blast: at the core of a powerful and diverse set of sequence analysis tools. *Nucleic Acids Research*, 32:W20–W25.
- Mendgen, K., Hahn, M., and Deising, H. (1996). Morphogenesis and mechanisms of penetration by plant pathogenic fungi. *Annual Review of Phytopathology*, 34:367–386.
- Minerdi, D., Savoi, S., and Sabbatini, P. (2023). Role of cytochrome p450 enzyme in plant microorganisms' communication: A focus on grapevine. *International Journal of Molecular Sciences*, 24.
- Molina-Hidalgo, F., Franco, A., Villatoro, C., Medina-Puche, L., Mercado, J., Hidalgo, M., Monfort, A., Caballero, J., Muñoz-Blanco, J., and Blanco-Portales, R. (2013). The strawberry (*Fragaria × ananassa*) fruit-specific rhamnogalacturonate lyase 1 (*FaR-GLyase1*) gene encodes an enzyme involved in the degradation of cell-wall middle lamellae. *Journal of Experimental Botany*, 64:1471–1483.
- Murria, S., Kaur, N., Arora, A., and Arora, N. (2019). Microscopic and ultrastructural studies of grape cultivars (*Vitis vinifera* l.) with variable susceptibilities to anthracnose. *Indian Phytopathology*, 72:261–269.

- Münch, S., Lingner, U., Floss, D., Ludwig, N., Sauer, N., and Deising, H. (2008). The hemibiotrophic lifestyle of *Colletotrichum* species. *Journal of Plant Physiology*, 165:41–51.
- Ntui, V., Azadi, P., Thirukkumaran, G., Khan, R., Chin, D., Nakamura, I., and Mii, M. (2011). Increased resistance to fusarium wilt in transgenic tobacco lines co-expressing chitinase and wasabi defensin genes. *Plant Pathology*, 60:221–231.
- Ochoa-Jiménez, V.-A., Berumen-Varela, G., Burgara-Estrella, A., Orozco-Avitia, J.-A., Ojeda-Contreras, -J., Trillo-Hernández, E.-A., Rivera-Domínguez, M., Troncoso-Rojas, R., Báez-Sañudo, R., Datsenka, T., Handa, A., and Tiznado-Hernández, M.-E. (2018). Functional analysis of tomato rhamnogalacturonan lyase gene *Solyc11g011300* during fruit development and ripening. *Journal of Plant Physiology*, 231:31–40.
- Pereira Miranda, D., Christine Cancela Ramos, H., Santa-Catarina, R., Cesar Fiorio Vettorazzi, J., Santana, J., Pastana De Sousa Poltronieri, T., Azevedo Vimercati Pirovani, A., Oliveira Nunes Azevedo, A., Pereira Duarte, R., Souza Rodrigues, A., Bohry, D., and Gonzaga Pereira, M. (2022). Topcross hybrids in papaya (*Carica papaya* L.): evaluation of the potential for increasing fruit quality in new cultivars. *Archives of Agronomy and Soil Science*, 68:1473–1486.
- Rojo-Báez, I., García-Estrada, R., Sañudo-Barajas, J., León-Félix, J., and Allende-Molar, R. (2017a). Proceso de infección de antracnosis por *Colletotrichum truncatum* en papaya maradol. *Revista Brasileira de Fruticultura*, 39.
- Rojo-Báez, I., Álvarez Rodríguez, B., García-Estrada, R., León-Félix, J., Sañudo-Barajas, A., and Allende-Molar, R. (2017b). Situación actual de *Colletotrichum* spp. en México: Taxonomía, caracterización, patogénesis y control. *Revista Mexicana de Fitopatología / Mexican Journal of Phytopathology*, 35.
- Rombach, H., Alon, H., Shapiro, O., Elad, Y., and Kleiman, M. (2022). Elucidating the effect of tomato leaf surface microstructure on *Botrytis cinerea* using synthetic systems. *Frontiers in Plant Science*, 13.

- Ruiz-Santiago, F., Márquez-Rocha, F., García-Alamilla, P., Carrera-Lanestosa, A., Ramírez-López, C., Ocaranza-Sánchez, E., and Jiménez-Rodríguez, D. (2024). Physico-chemical and biochemical changes in cocoa during the fermentation step. *Fermentation*, 10.
- Ryder, L. and Talbot, N. (2015). Regulation of appressorium development in pathogenic fungi. *Current Opinion in Plant Biology*, 26:8–13.
- Shekhawat, K., Fröhlich, K., García-Ramírez, G., Trapp, M., and Hirt, H. (2022). Ethylene: A master regulator of plant–microbe interactions under abiotic stresses. *Cells*, 12.
- SIAP (2024). Panorama agroalimentario 2024. <https://online.pubhtml5.com/rsarc/ybn1/>. Servicio de Información Agroalimentaria y Pesquera.
- Silva, C., Van Den Abeele, C., Ortega-Salazar, I., Papin, V., Adaskaveg, J., Wang, D., Casteel, C., Seymour, G., and Blanco-Ulate, B. (2021). Host susceptibility factors render ripe tomato fruit vulnerable to fungal disease despite active immune responses. *Journal of Experimental Botany*, 72:2696–2709.
- Singh, H. and E.B. (2020). *Current Research and Innovations in Plant Pathology*. AkiNik, India.
- Tang, Y., Li, Y., Bi, Y., and Wang, Y. (2017). Role of pear fruit cuticular wax and surface hydrophobicity in regulating the prepenetration phase of *Alternaria alternata* infection. *Journal of Phytopathology*, 165:313–322.
- Van Schie, C. and Takken, F. (2014). Susceptibility genes 101: How to be a good host. *Annual Review of Phytopathology*, 52:551–581.
- Vicente, A., Saladié, M., Rose, J., and Labavitch, J. (2007). The linkage between cell wall metabolism and fruit softening: looking to the future. *Journal of the Science of Food and Agriculture*, 87:1435–1448.

- Wang, J., Yang, B., Zhang, F., Wang, J., Xue, K., Hussain Chang, B., Zhang, J., and Qin, X. (2024). Identification and expression analysis of cytochrome p450 genes probably involved in triterpenoid saponins biosynthesis in *Astragalus mongholicus*. *International Journal of Molecular Sciences*, 25(15):8333.
- Wheeler, M., Tronconi, M., Drincovich, M., Andreo, C., Flügge, U.-I., and Maurino, V. (2005). A comprehensive analysis of the nadp-malic enzyme gene family of *Arabidopsis*. *Plant Physiology*, 139:39–51.
- Yue, J., VanBuren, R., Liu, J., Fang, J., Zhang, X., Liao, Z., Wai, C., Xu, X., Chen, S., Zhang, S., Ma, X., Ma, Y., Yu, H., Lin, J., Zhou, P., Huang, Y., Deng, B., Deng, F., Zhao, X., Yan, H., Fatima, M., Zerpa-Catanho, D., Zhang, X., Lin, Z., Yang, M., Chen, N., Mora-Newcomer, E., Quesada-Rojas, P., Bogantes, A., Jiménez, V., Tang, H., Zhang, J., Wang, M.-L., Paull, R., Yu, Q., and Ming, R. (2022). Sunup and sunset genomes revealed impact of particle bombardment mediated transformation and domestication history in papaya. *Nature Genetics*, 54:715–724.
- Zaynab, M., Sharif, Y., Abbas, S., Afzal, M., Qasim, M., Khalofah, A., Ansari, M., Khan, K., Tao, L., and Li, S. (2021). Saponin toxicity as key player in plant defense against pathogens. *Toxicon*, 193:21–27.
- Ziv, C., Zhao, Z., Gao, Y., and Xia, Y. (2018). Multifunctional roles of plant cuticle during plant-pathogen interactions. *Frontiers in Plant Science*, 9.

2.10 Supplementary material

All supplementary tables can be accessed on <https://ucdavis.box.com/s/ti6jcz9koy5wdf5zcx7sv9uwz6v2vpqx>

Chapter 3

Characterizing the early interaction between *Botrytis cinerea* and strawberry fruit to identify biomarkers for disease detection

3.1 Abstract

Strawberries are a high-value soft fruit crop grown worldwide, but they suffer significant losses both before and after harvest due to gray mold disease, which is caused by the fungus *Botrytis cinerea*. The rapid development of fungicide resistance in *B. cinerea*, combined with the high susceptibility of strawberries, highlights the need for fast and non-destructive methods to detect gray mold disease. This is essential for effective decision-making and the implementation of integrated pest management strategies. Here, I hypothesized that infections by *B. cinerea* on strawberries result in changes to the plant defenses and metabolic pathways, which could be detected by analyzing alterations in fruit surface characteristics and the emission of volatile organic compounds (VOCs). To test this hypothesis, we employed multispectral imaging (MSI) and gas chromatography-mass spectrometry (GC-MS) to compare the spectral profiles of strawberries inoculated with *B. cinerea* against mock-inoculated fruit, from 0 to 48 hours post-inoculation (hpi). We sampled VOCs non-destructively at similar time points (9-24 hpi). Our results showed that the reflectance profiles of *B. cinerea*-inoculated strawberries differed from those of mock-inoculated ones as early as 12 hpi. A specific set of six wavelengths in the visible and infrared spectrum allowed for a significant distinction between infected and healthy fruit. Partial least squares discriminant analysis indicated that infected samples clustered

together as early as 9 hpi and emitted VOCs with antifungal properties, such as linalool, estragole, and nonanal. This suggests an early coordinated host response to *B. cinerea*. In addition, an RNA-seq study of mock-inoculated and *B. cinerea*-inoculated strawberries at early time points (3, 6, 12, and 24 hpi) identified differentially expressed genes in the infected strawberries that are involved in redox activity and secondary metabolic pathways. These gene changes can explain the observations made through the MSI and VOC analyses. Overall, this research underscores the potential for combining multiple approaches to achieve early detection of postharvest diseases and to enhance our understanding of fruit-pathogen interactions.

3.2 Introduction

Strawberries (*Fragaria x ananassa*) are an economically important soft fruit crop grown worldwide, highly appreciated for their nutritional value and flavor. The US ranks second globally for strawberry production, with 91% of that yield being produced in California (Hernández-Martínez et al., 2023). Strawberries are vulnerable to mechanical damage during harvest and in the postharvest supply chain, and are highly susceptible to several types of rotting pathogens. The most devastating of these pathogens is the ascomycete fungus *Botrytis cinerea*, a necrotrophic fungus with a broad host range that affects over 1,000 plant species (Elad et al., 2016).

B. cinerea is considered the primary pathogen of harvested strawberries, causing gray mold disease in fruit and senescing organs, as well as vegetative tissues (Petrasch et al., 2019). Gray mold can result from infection of flowers (primary infections) or infection of the fruit receptacle through direct penetration or wounds (Bristow et al., 1986). After infections of flowers or unripe fruit, *B. cinerea* enters a symptomless quiescent phase where growth is arrested until ripening or favorable conditions promote the transition of the pathogen to an aggressive infecting phase (Petrasch et al., 2019; Williamson et al., 2007). Current control practices to minimize gray mold disease include pre- and postharvest fungicide applications, hand harvesting to minimize wounding, and rapid and constant cooling of harvested fruit to reduce the activation of quiescent infections, among others

(Petrasch et al., 2019). However, these approaches are often ineffective and expensive and cannot completely eliminate the disease. Furthermore, with the growing concerns and limitations regarding fungicide use and the lack of strawberry cultivars with complete resistance to gray mold, reliable, fast, and non-destructive methods need to be in place for the early detection of gray mold disease.

Mechanisms leading to quiescence, as well as the switch from quiescent to aggressive infections, are not completely understood. Accumulation of phenolic compounds, such as proanthocyanidins and anthocyanins, together with the presence of preformed antifungal compounds, appear to play a role in establishing quiescence (Petrasch et al., 2019). It has been well established that phenylpropanoids, flavonoids, benzoic acids, and hydrolyzable tannins, collectively referred to as polyphenols, as well as terpenes and esters are involved in defense during fruit development and upon pathogen infection (Badmi et al., 2023; Li et al., 2020; Nagpala et al., 2016). Physiological changes in the host that occur during ripening are involved in the increased susceptibility of red fruit. Some of these changes include the polymerization of proanthocyanidins, with a consequent loss of their biological activity (Jersch et al., 1989). Additionally, an increase in the emission of volatile organic compounds (VOCs) is observed during ripening and after harvest (Forney et al., 2000). Around 360 volatile compounds with a wide range of biological activities have been identified in strawberry aroma (Junker and Tholl, 2013; Latrasse, 1991). Additionally, green leaf volatiles are among the most common compounds released upon damage or infection, and can act both as attractants and inducers of plant defenses (Scala et al., 2013). The interaction between strawberry fruit and *B. cinerea* affects the fruit VOC profile, resulting in a mushroom odor that is mainly caused by the fungal emitted 1-octen-3-ol, which has been observed to be highly abundant in fully infected strawberries (Morales-Valle et al., 2010; Vandendriessche et al., 2012). As strawberries affected by fungal decay present changes in physiological and quality attributes, such as pH, total soluble solids (TSS), titratable acidity (TA), and VOCs, I hypothesized that changes in the secondary metabolic profile of strawberries could serve as a tool to detect *B. cinerea* infection.

Here, we set out to explore the interaction between strawberry fruit and *B. cinerea*

at various time points after infection to determine how early the fungus can be detected before it is visible to the naked eye. We explored two non-destructive technologies to assess changes in fruit surface attributes and VOC emissions: multispectral imaging (MSI) and profiling of VOCs through gas chromatography-mass spectrometry (GC-MS). We compared the spectral and volatile profiles of mock- and *B. cinerea* inoculated fruit at several time points after infection, starting at 0 hours post inoculation (hpi) for MSI and 9 hpi for VOCs, and ending as late as 72 hpi for MSI and 24 hpi for VOCs. In parallel, we conducted an RNAseq study of mock- and *B. cinerea* inoculated fruit at 3, 6, 12, and 24 hpi, to gain insight into the molecular mechanisms underlying the changes observed through MSI and VOC profiling. This study highlights the potential of complementary non-destructive approaches for the timely detection of *B. cinerea* in postharvest and the study of fruit-pathogen interactions. Early detection of infected fruit is of key importance to the strawberry industry for the application of efficient disease management protocols and decision-making for distributing specific lots of fruit.

3.3 Materials and Methods

3.3.1 Fungal and plant material

Botrytis cinerea strain B05.10 was grown on 1% potato dextrose agar (PDA) plates at room temperature (RT) until sporulation. Conidia were harvested using 0.01% Tween® 20 (Sigma-Aldrich, United States).

Strawberry (*Fragaria x ananassa*) cvs. “Monterey”, “UCD Royal Royce”, and “Fronteras” were provided by the University of California, Davis Strawberry Breeding Program and grown under standard greenhouse conditions during the 2020 and 2021 seasons at the University of California, Davis, Orchard Park Greenhouse Complex, and harvested at commercial maturity, when they were uniformly red (50 days post anthesis). Strawberry cvs. “Monterey”, “San Andreas”, “Sweet Ann”, “UCD Victor”, and “Chandler” were commercially sourced during the 2023 season from fields located in Woodland, California.

3.3.2 Fruit inoculations

Strawberry fruit were visually evaluated for uniform appearance and absence of wounds or symptoms of fungal infection. Fruit were disinfected in 0.6% sodium hypochlorite, wounded once near the center with a 1 mm sterile pipette tip to an approximate depth of 5-7 mm, and inoculated with 10 μ l of *B. cinerea* conidia suspension (500 conidia/ μ l). The same procedure was followed for mock inoculations without adding the inoculum. Mock-inoculated and inoculated fruit were incubated at room temperature (RT, approximately 20 °C) in high-humidity containers (90-100% relative humidity).

3.3.3 Multispectral imaging for early infection detection

High-resolution multispectral images were taken using a VideometerLab 4 (Videometer A/S, Herlev, Denmark) and processed with the VideometerLab software version 3.22.29, as described in (Sbodio et al., 2024). Briefly, reflectance images were taken at 19 wavelengths (365, 405, 430, 450, 470, 490, 515, 540, 570, 590, 630, 645, 660, 690, 780, 850, 880, 940, and 970 nm), including the longpass filters for a total of 50 spectral bands. Multispectral images for mock- and *B. cinerea* inoculated fruit were taken with the wounded/inoculated area pointed up. One biological replicate consisted of four fruit, and three biological replicates were included per variety and time point.

Image analysis was carried out using the VideometerLab software (version 3.24.76). Pixels representing healthy and *B. cinerea*-infected tissues were collected from a subset of fruit images, and a normalized canonical discriminant analysis (nCDA) transformation based on the reflectance of each pixel was created to minimize the distance within classes (mock- vs. *B. cinerea*-inoculated) and to maximize the distance among classes. A region of interest (ROI) was obtained from all images by applying a mask to segment the fruit from the background. A further segmentation was applied to remove the fruit calix and achenes. A blob database was created with all images (216), and the infected areas were extracted from the healthy tissues based on the previously created nCDA transformation. Shape and spectral features were extracted from individual blobs, including area and tristimulus components of color (e.g. hue and saturation). The SpectralMean feature extracts the reflectance mean of each fruit for the 50 spectral bands. Region MSI_Mean

calculates a trimmed mean of transformed pixel values within the blob (each single fruit), and MSIThreshold measures the percentage or area of the blob region with a transformation value higher than the threshold, based on the nCDA model (derived from all the classes).

3.3.4 Volatile collection and analyses

Headspace sorptive extraction (HSSE) of strawberry fruit volatiles was performed non-destructively with polydimethylsiloxane-coated stir bars (Twisters®[®], Part 01222-001-00; Gerstel Inc., Linthicum, MD). To mimic retail conditions, strawberry fruit were placed inside a clamshell with three Twisters®[®] attached to the inside of the lid with a magnet. Fruit were either untreated (healthy) or wound-inoculated with *B. cinerea*. The clamshell was then placed inside a 1 L airtight glass container, and the Twisters®[®] were incubated with the fruit in 3 h intervals. Twisters®[®] were retrieved at 9, 12, 15, 18, 21, and 24 hpi and were placed in glass vials and stored at -20 °C until GC-MS analysis. A new set of technical triplicates of Twisters®[®] was added after each sampling time point to collect VOCs from the same fruit for the next 3 h incubation period. All Twisters®[®] were pre-conditioned prior to use, according to manufacturer specifications, and blank air samples were simultaneously collected using an empty clamshell. 10 µL of 2-hexanone-d5 were spiked into each clamshell before Twister®[®] exposure to use as the surrogate in each incubation round. As in the MSI approach, one biological replicate consisted of 4 fruit, and three biological replicates were included per variety and time point. In total, three different trials were conducted.

Before GC-MS analysis, each Twister®[®] was transferred into thermal desorption tubes where 1 µL of internal standard (500 ppb naphthalene-D8 in ethanol solution) was added. Each sample was thermally desorbed using a thermal desorption unit (TDU, Gerstel, US) and cooled injection system (CIS, Gerstel, US). The TDU was set to 50 °C for 0.2 min initially and heated at 60 °C min⁻¹ until reaching 250 °C and held for 4 min. Desorbed analytes were led into the CIS, which was held at -80 °C, and then heated at 12 °C s⁻¹ to 260 °C and was held for 3 min. Analytes were injected into the GC column in a splitless mode.

To separate analytes, an Agilent 7890A GC (Agilent Technologies Inc., Santa Clara, CA) equipped with a DB-5ms column (30 m \times 250 μ m \times 0.25 μ m, Agilent Technologies Inc., Santa Clara, CA) was used. The temperature gradient started at 40 °C for 5 min, then heated at 2.5 °C min⁻¹ to 100 °C and held for 1 min. Then, the oven arrived at 150 °C using 10 °C min⁻¹, and then was heated at 50 °C min⁻¹ to 300 °C and held for 2 min. Total runtime was 45 min. GC worked in constant flow mode at 1.5 ml min⁻¹ of helium. A 5975C single quadrupole mass spectrometer (MS, Agilent Technologies Inc., Santa Clara, CA) detected the VOCs using a mass range between 40 and 300 m/z. The source and quad were set to 230 °C and 150 °C, respectively. Clean blank Twisters® and external control solution (C8-C24 alkanes) were analyzed simultaneously with the samples to correct the background signal and instrument performance, respectively.

Raw chromatograms were initially inspected with the Agilent MassHunter Workstation Software Qualitative Analysis B.06.00 for qualitative reasons. Then, Profinder (Version B.08.00, Agilent Technologies Inc., Santa Clara, CA) and Mass Profiler Professional (MPP, V13.0, Agilent Technologies Inc., Santa Clara, CA) were used for GC-MS data deconvolution and alignment, which generated a peak table containing samples and features (compounds) with their corresponding intensities. Initial data was cleaned by removing siloxane peaks, as well as features that appeared in blank samples higher than 3 times (peak samples/blank ratio). A Twister® and the empty clamshell (air) blank were used to remove signals nonspecific to the fruit VOCs. All missing values were replaced by the minimum positive value divided by 10. Samples were normalized by the dry weight of the corresponding samples. Logarithm transformation was then applied to correct heteroscedasticity.

Statistical analyses were performed using Excel, MATLAB R2020a, and PLS Toolbox (Version 8.6, Eigenvector Research Inc., Manson, WA) software. Univariate t-test analysis was used to compare means and assess the significance of the fold change (FC) for the various compounds observed. FC and P-values were combined using Volcano Plots, which allow the detection of relevant features that explain significant differences (P < 0.05 and FC higher than 2). Then, multivariate analysis was applied to the data using principal

component analysis (PCA) and Partial Least-Squares Discriminant Analysis (PLS-DA). PCA was performed to visualize initial similarities between samples and detect potential outliers. PLS-DA was used as a supervised classification method. Classification ability is determined by sensitivity (probability to correctly detect a class), specificity (ability to correctly reject a class), and area under the curve (AUC, classification ability at different thresholds) values, which are defined by receiver operating characteristic (ROC) curves. Means and standard deviations of classification abilities were defined by cross-validation and prediction sets. For that, the data was randomly split 50 times using 67% for samples for a calibration training set and 33% for a prediction set (not included in building the model).

Lastly, the potential features of a defined class obtained from the PLS-DA were ranked by variable importance in projection (VIP) values. Identifications for relevant features with $VIP > 1$ were conducted by searching through a commercial database (NIST 20), along with a comparison of calculated Kovats Retention Index values to the ones reported in the literature. Tentative descriptions were performed when the similarity between experimental and theoretical spectral patterns (scores) of the compounds was higher than 65-70%.

3.3.5 Tissue sampling, RNA extraction, cDNA library preparation, and RNA sequencing

Tissue samples comprising the wounding/inoculation point and surrounding areas were collected at 3, 6, 12, and 24 hours post inoculation (hpi) and immediately frozen in liquid nitrogen and stored at -80°C until processing. One biological replicate consisted of an average of five fruit, and three biological replicates were obtained per time point. Samples were ground using a Retsch® Mixer Mill MM 400 (Retsch, Germany), and RNA was extracted from 1 g of ground tissue as described in (Blanco-Ulate et al., 2013). RNA purity and concentration were assessed with a NanoDrop One Spectrophotometer (Thermo Scientific, United States) and a Qubit 3 fluorometer (Invitrogen, United States), respectively. RNA integrity was confirmed by agarose gel electrophoresis.

Thirty-two barcoded cDNA libraries were prepared using the Illumina TruSeq RNA

Sample Preparation Kit v2 (Illumina, United States). Quality control of the cDNA libraries was performed with the High Sensitivity DNA Analysis Kit in the Agilent 2100 Bioanalyzer (Agilent Technologies, United States). 150-bp paired-end libraries were sequenced on the Element Bio AVITI 150 bp flow cell platform in the DNA Technologies Core of the UC Davis Genome Center (Davis, CA, United States). In total, three libraries were sequenced per treatment and time point.

3.3.6 RNA-seq bioinformatics pipeline

Raw reads from the *B. cinerea*-infected and mock-inoculated fruit samples were mapped to a combined transcriptome of *B. cinerea* and strawberry using Bowtie2 (Langmead and Salzberg, 2012). Mapping percentages and numbers of host reads and genes for each sample can be found in Supplementary Table S1. The strawberry transcriptome (*Fragaria x ananassa* Camarosa Genome Assembly v1.0 and Annotation v1.0.a2) was retrieved from <https://www.rosaceae.org/Analysis/9642085> (accessed April 4, 2024). The predicted transcriptome ASM83294v1 for *B. cinerea* strain B05.10 was obtained from http://fungi.ensembl.org/Botrytis_cinerea/Info/Index (Van Kan et al., 2017). Count matrices were made from the Bowtie2 results using sam2counts.py v0.919 (Buffalo, 2010) and are available in Supplementary Table S2. Count matrices were used as input for differential expression analysis with the Bioconductor package DESeq2 (Love et al., 2014) in R. Reads were normalized for library size. Enrichment analyses for GO, InterPro, and KEGG terms were performed on lists of differentially expressed genes (DEGs) in strawberry using Fisher’s exact test ($P_{adj} < 0.05$).

3.4 Results

3.4.1 Fruit reflectance profiles reveal *Botrytis cinerea* presence before disease symptoms are evident

To test our hypothesis that infections of *B. cinerea* cause changes in host tissues before they are noticeable to the naked eye, we monitored disease progression using multispectral imaging (MSI) at 0, 9, 12, 15, 18, 21, 24, 36, and 48 hours post inoculation (hpi, Figure 3.1). Mock- or *B. cinerea*-inoculated fruit from several commercial varieties of in-

terest to the California strawberry industry, greenhouse-grown and commercially sourced, were included to assess whether changes were variety-specific. On infected fruit, *B. cinerea* growth showed minimal growth progression, and incipient tissue damage was visible starting from 24 hpi and only limited to the wound-inoculated area. However, reflectance profiles of the *B. cinerea*-inoculated fruit revealed that changes in the surface characteristics at the whole-fruit level occurred as early as 12 hpi. Conversely, mock-inoculated fruit showed practically no changes.

Furthermore, a normalized canonical discriminant analysis (nCDA) transformation combining all wavelengths detected infected tissue areas where lesions would develop before they were large enough to be visible to the naked eye. These areas were calculated using a threshold (> 0) in the nCDA transformed scale ranging from healthy (-2) to infected (2) tissues. The highest separation potential (i.e., maximum eigenvalues) was obtained when combining about six wavelengths in the visible and near-infrared regions of the spectrum (470, 570, 590, 690, 880, 970 nm), with minor gain with additional wavelengths.

3.4.2 Strawberry fruit inoculated with *Botrytis cinerea* have distinct profiles of emitted volatile organic compounds

We non-destructively sampled VOCs emitted by healthy and *B. cinerea*-inoculated strawberries at 9, 12, 16, 20, and 24 hpi to assess changes in VOC profiles between treatments, as well as determine how early differences could be observed. Similarly to the MSI approach, fruit from several commercial strawberry varieties, greenhouse-grown and commercially sourced, were included to identify shared features enabling the distinction between mock- and *B. cinerea*-inoculated fruit. However, as wounding is a factor occurring in retail scenarios that increases the fruit susceptibility to the pathogen, we used healthy, non-wounded fruit as a control.

First, we performed a principal component analysis (PCA) to determine whether samples clustered based on class (healthy vs. *B. cinerea* - inoculated), variety, or time point and to identify outliers. Only clear differences by time point were observed, and no outliers were detected. Next, we built a partial least squares discriminant analysis (PLS-DA)

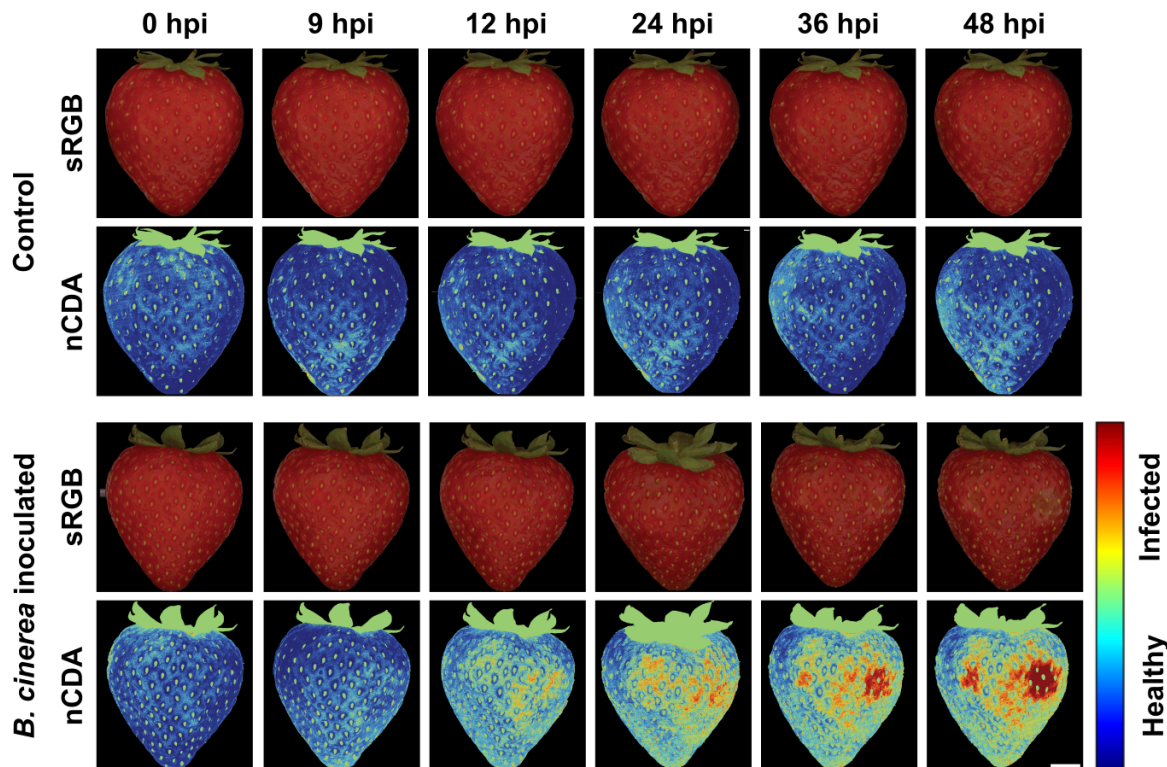


Figure 3.1: Visualization of gray mold progression using multispectral imaging. (A) Comparison of wounded control and *Botrytis cinerea*-inoculated strawberries across different time points with raw (sRGB) and corresponding transformed images (nCDA). Color scale refers to individual transformed pixel values from healthy (blue or -2) to infected (red or 2). Scale bar corresponds to 7.5 mm.

model for all time points and trials using two-thirds of the samples for calibration. This model represented a combination of VOCs considered to best explain the differences between healthy and *B. cinerea*-inoculated samples. Model accuracy, estimated based on sensitivity, specificity, and area under the curve (AUC), showed values equal to or higher than 0.7 (Figure 3.2A). Given the complexity of the data and to improve classification accuracy, we then built PLS-DA models for individual trials and time points. Similarly, the PCA analysis did not reveal differences by class or variety, and differentiation by time point depended on the trial. Model accuracies depended on the trial but were overall higher (0.86–0.96) than for all samples together. Overall, although there was some vari-

ation between trials, PLS-DA models were able to correctly classify samples as healthy or infected as early as 9 hpi, with higher accuracy at 16 and 24 hpi. Figure 3.2B shows the scores for the latent variables (LV) 1 and 2 of the PLS-DA models for Trial 3, including all time points. A clear distinction can be observed between healthy and *B. cinerea*-infected samples (Figure 3.2B, top). In contrast, no differences are observed among the three varieties tested (Figure 3.2B, bottom), showing the potential for these models to discriminate between healthy and infected samples regardless of variety. This result is relevant as the strawberry growers use a wide range of varieties every season, and therefore generating models that can be applied regardless of variety is of the utmost importance.

To determine whether there were any VOCs specific to *B. cinerea*-inoculated strawberries, we conducted t-tests to compare the abundance of each compound to healthy fruit at each time point. In total, we identified over 280 features representative of infection, with ~ 80 identified with scores $> 53\%$ (Supplementary Table S3). This dataset needs to be revisited to calculate false discovery rates for the multiple comparisons. We focused on those features that were upregulated at least at three different time points or across the three trials. This resulted in a list of 31 compounds that belonged to 9 different metabolite classes (Figure 3.2C). Out of these, esters were proportionally the most abundant class, mainly represented by fatty acid esters, followed by alcohols. Several of these compounds exhibited up- or down-regulation due to infection across the sampled times. To identify candidate VOCs that could serve as indicators of *B. cinerea* present, we focused on those compounds that were mostly up-regulated. This yielded 6 VOC candidates with potential for *B. cinerea* detection, which were mostly esters (Figure 3.2D). Morpholine 4-methyl, 4-oxide seemed to be consistently upregulated across all time points, with a particularly higher emission at 24 hpi. The esters butanoic acid, 3-methyl-, ethyl ester and 1-butanol, 3-methyl-, acetate seemed to follow a similar trend of higher expression at 24 hpi. On the other hand, octanoic acid, ethyl ester and the fatty acid butanoic acid, 2,2-dimethyl- seemed to be more prevalent at earlier time points. Overall, our observations point to esters being a prominent class in VOCs emitted upon *B. cinerea* infection as early as 9 hpi. With further validation, several of these compounds may serve as potential biomarkers

for the early detection of gray mold disease.

3.4.3 Early fruit transcriptional responses can shed light on the changes in surface properties and volatile profiles

To assess how early the pathogen induces changes in the fruit and to evaluate the molecular mechanisms that contribute to our observations in the MSI and VOC profiling approaches, we conducted a transcriptomic analysis of strawberry fruit mock- and *B. cinerea*-inoculated at 3, 6, 12, and 24 hpi (Supplementary Table S4). We first evaluated the overall transcriptional activity of *Botrytis cinerea* to confirm the presence of the pathogen at early time points by quantifying the total fungal normalized reads mapped to the combined genomes (Figure 3.3A). We observed that as early as 3 hpi, the levels of *B. cinerea* transcripts were significantly higher (ANOVA, $P < 0.05$) in the infected samples compared to the mock-inoculated samples. This finding confirms that the presence and activity of the pathogen can be detected in strawberries at very early stages. Additionally, we noted a baseline level of *B. cinerea* activity in samples that were not inoculated, indicating background fungal presence likely due to primary infections of flowers even after surface disinfection of the fruit.

Another key observation from our dataset was that the samples collected at 12 hpi, whether *B. cinerea*-inoculated or mock-inoculated, exhibited a distinct host transcriptional profile compared to the other samples. This is evident in a PCA of all strawberry normalized reads, where the 12 hpi samples were separated by PC 1, explaining 56% of the variance (Supplementary Figure 3.S1). The reason for this specific pattern is not yet clear and requires further investigation, though it could be related to circadian rhythms.

We determined differentially expressed genes (DEGs, $\text{padj} < 0.05$) between *B. cinerea*- and mock-inoculated fruit at each time point (Supplementary Table S4). Given the high variability in fungal growth among samples at early time points of infection, we detected only a very small number of total DEGs for the host and the pathogen (Figure 3.3B). At 12 hpi and 24 hpi, most DEGs belonged to the fungus, and the primary differences between the *B. cinerea*-inoculated and the mock-inoculated fruit for host DEGs were functions related to oxidation-reduction processes, transmembrane transport, and signal

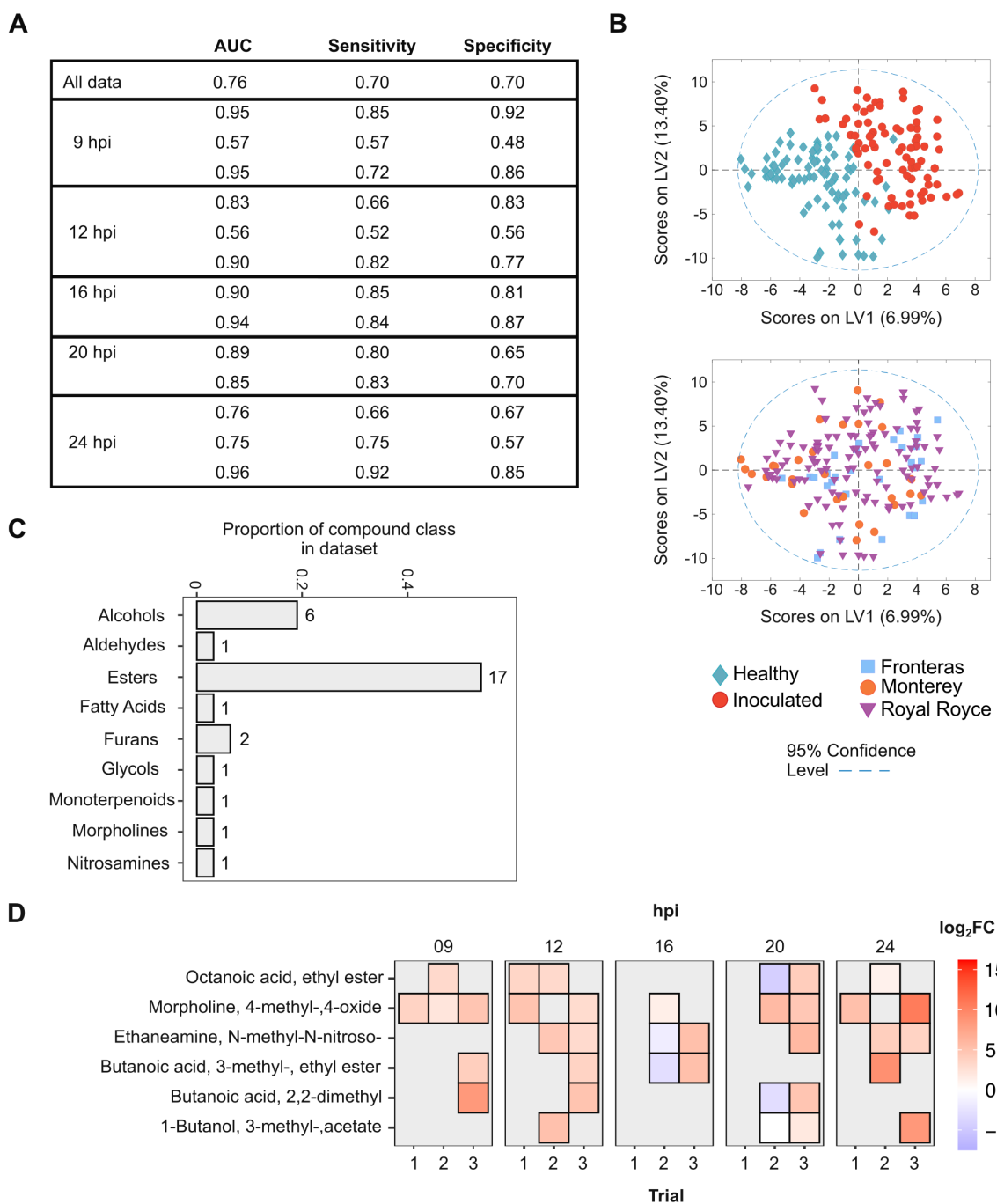


Figure 3.2: Profiling of volatile organic compounds (VOCs) shows potential for early *Botrytis cinerea* detection. (A) Estimation of partial least squares discriminant analysis (PLS-DA) model accuracies for all data points and each time point per trial. (B) PLS-DA score plot applied to only Trial 3 samples shows differences between healthy and infected samples, but no differences by variety. (Continued on following page)

Figure 3.2: (Continued from previous page) (C) Representation of different volatile classes in upregulated compounds across trials and time points. (D) Heatmap of the \log_2 of the ratio of the abundance of each compound in infected samples to the intensity in healthy samples (fold change). hpi: hours post inoculation; FC: fold change.

transduction by protein kinases. By 24 hpi, we only observed two DEGs in strawberry, with one being functionally annotated and involved in response to abscisic acid. We then evaluated the number of DEGs observed when performing comparisons between time points within each treatment, using 3 hpi as a reference, and evaluated whether these DEGs were commonly or uniquely expressed between treatments (Figure 3.3C). Within these DEGs we focused on those that were uniquely upregulated in *B. cinerea*-inoculated fruit, and that belonged to categories related to response to pathogens. We observed an enrichment in terms pertaining to oxidation-reduction processes across all three evaluated time points, which were represented by different oxidative enzymes and systems and constituted the main responses of fruit to infection at 6 and 12 hpi. By 24 hpi, although the number of DEGs was lower compared to 12 hpi, we observed a wider transcriptional response represented by different enriched categories, as expected, since the infection was well established and the symptoms were beginning to manifest. Functions activated due to *B. cinerea* infection at this last time point included defense responses, biosynthesis of phenylpropanoids, and MAPK signaling pathways.

3.5 Discussion

B. cinerea infections in strawberries are highly aggressive, and management options become limited once the pathogen is present, resulting in significant losses in both produce quality and economic value. This study examined early interactions between *B. cinerea* and strawberry fruit using MSI and VOC profiling for early gray mold detection.

3.5.1 Multispectral features reveal *Botrytis cinerea* is active on strawberry fruit in the early stages of infection

Spectral imaging is a non-invasive technology with great potential for phenotyping, assessment of crop physiological traits, and disease detection (Terentev et al., 2022). Here,

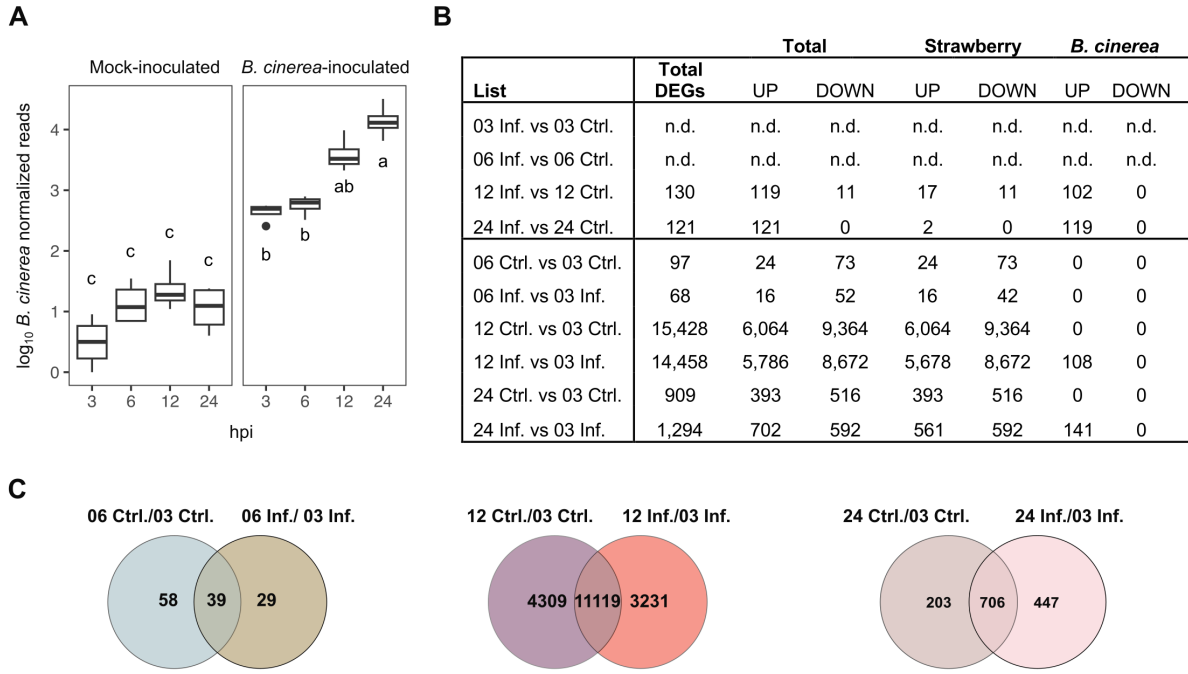


Figure 3.3: Transcriptional profiling of mock- and *Botrytis cinerea*-inoculated strawberry fruit. (A) *B. cinerea* transcriptional activity expressed as the \log_{10} of the fungal normalized reads in mock and inoculated samples. An ANOVA ($P < 0.05$) revealed normalized reads for the inoculated samples were significantly higher from the control. (B) Number of upregulated and downregulated host and pathogen differentially expressed genes (DEGs) of mock- and *B. cinerea*-inoculated fruit across different time points. Two types of comparisons were conducted: 1) infected (Inf.) vs. mock (Ctrl.) samples at each time point (top four comparisons), and 2) 6, 12, and 24 hours post inoculation (hpi) against 3 hpi for each treatment (bottom six comparisons). (C) Venn diagrams providing an overview of unique and shared DEGs for the second type of comparisons from panel B. Unique upregulated genes in infected fruit were further subjected to enrichment analyses.

we utilized high-resolution multispectral images that encompass 50 bands of the light spectrum to capture the early development of *B. cinerea* on strawberry fruit before it becomes visible to the naked eye. A normalized canonical discriminant analysis (nCDA) transformation of these images revealed a change in the reflectance profile of strawberries inoculated with *B. cinerea* at 9 hours post-inoculation (hpi), which was not observed in the mock-inoculated fruit. Beginning at 9 hpi, there was an increase in the number of pixels predicted as infected tissue by the nCDA model (with values shifting from blue toward red), and this increase was not restricted to the inoculated area. We achieved the maximum separation between healthy and infected tissue at six specific wavelengths across the visible and near-infrared regions of the spectrum: 470, 570, 590, 690, 880, and 970 nm. Previous studies on *B. cinerea* infections in cucumber plants and tomato leaves reported similar wavelengths for effectively distinguishing between pathogen-inoculated and mock-inoculated regions of interest (Fahrentrapp et al., 2019; Giakoumoglou et al., 2023). The ability to use a similar range and number of wavelengths for detecting *B. cinerea*-infected tissue before the onset of symptoms in various crops highlights the broad applicability of multispectral imaging (MSI) technology. Although MSI is limited to sensing at the surface level, the significant changes we observed in the reflectance profile of infected fruit demonstrate its potential for detecting latent *B. cinerea* infections, especially when the fungus transitions to its necrotrophic stage.

3.5.2 Infections of *Botrytis cinerea* lead to an increase in certain classes of volatile compounds

Additionally, we non-destructively analyzed the VOCs emitted by both healthy and *B. cinerea*-inoculated fruit at early time points. From approximately 280 features associated with *B. cinerea* infection, we successfully identified around 80 compounds representing a wide array of chemical classes typical of strawberry aroma. Notably, esters were the most abundant class of upregulated compounds observed across trials; they are known to dominate the volatile profile of strawberries and tend to increase as the fruit ripens (Azodanlou et al., 2004; Latrassé, 1991; Neri et al., 2015). Previous studies have also reported an increase in ester compounds upon *B. cinerea* infection and a correlation

between ester levels and spoilage rates (Li et al., 2022; Vandendriessche et al., 2012). To gain insight into specific compounds that could serve as potential biomarkers for *B. cinerea* infection, we focused on those that were consistently upregulated in infected tissues across multiple trials. Only six of the identified compounds met this requirement, and four of these were esters. Although not consistently upregulated across all time points and trials, we also observed other compounds previously reported to have antifungal effects against *B. cinerea* growth. These include the monoterpene linalool, the aldehyde nonanal, and the green leaf volatile 2-hexanol, which may signal the presence of an open wound to the pathogen (Neri et al., 2015). Additionally, we also detected 2,3-butanediol, which has been reported to be associated with latent *B. cinerea* infections in strawberry plants, as well as to induce phytohormone and antioxidant responses in response to disease (Hu et al., 2019; Shi et al., 2018). Despite the high variability of profiled VOCs due to the intrinsic natural variation of aroma compounds, partial least squares discriminant analysis (PLS-DA) models showed that it was possible to accurately classify samples as healthy or infected based on the aroma profile. Our data indicates that instead of using specific compounds as biomarkers for the presence of *B. cinerea*, there is greater potential for identifying increases in compound classes, such as esters.

3.5.3 Pathways related to redox processes and synthesis of secondary metabolites are active early in the *Botrytis cinerea*-strawberry interaction

Additionally, we performed a transcriptomic analysis on strawberry fruit that were either mock-inoculated or inoculated with *B. cinerea* at 3, 6, 12, and 24 hpi to better understand the molecular pathways involved in the early interactions between the fruit and the fungus. A principal component analysis of our samples (Supplementary Figure 3.S1) revealed that the time post-inoculation (hpi) accounted for a larger portion of the variance in our data (56%) compared to the type of infection (12%). This observation may be attributed to the fact that we assessed the interaction at an early stage. It is important to note that *B. cinerea* spores can require up to 8 hours of contact with a water film for successful germination (Jarvis, 1962). This suggests that the initial responses observed in both

mock-inoculated and *B. cinerea*-inoculated fruit are primarily reactions to the wounding inflicted during inoculation, implying that the pathogen's response did not significantly differ from the response to tissue damage at the onset of the interaction.

The very few differentially expressed genes (DEGs) could be attributed to the fact that the infection remained limited to the inoculation site. A more precise tissue dissection during sampling may be needed to ensure that the infected tissue is not diluted by the surrounding healthy tissue. As samples changed over time within each treatment group while still being categorized by infection status, we compared the 3 hpi time points with 6, 12, and 24 hpi. This analysis aimed to assess whether different molecular pathways were activated over time in the presence of the pathogen. DEGs from *B. cinerea*-inoculated samples at 6, 12, and 24 hpi were mainly enriched in functions related to oxidation-reduction processes, including several terms associated with glutathione S-transferases, thioredoxins, and oxidases. Oxidative stress is a well-known defense response aimed at halting pathogen infection and is also a consequence of fruit metabolism that continues after harvest (Peng et al., 2018; Zhang et al., 2023). The presence of free radicals can damage host cell membranes, leading to a decrease in fruit quality. This could explain the slight changes observed in the fruit reflectance profiles for the mock-inoculated fruit, as well as the more significant changes seen in the infected strawberries (Figure 3.1A). In line with the more advanced stage of the infection and the appearance of the first symptoms visible to the naked eye, the infected samples at 24 hpi displayed unique enrichments related to secondary metabolism, particularly in phenylpropanoid and steroid biosynthesis. The phenylpropanoid pathway leads to the synthesis of numerous chemical compounds that have antimicrobial properties, and some of these compounds, such as proanthocyanidins, function as pre-formed chemical barriers and have been correlated with resistance to gray mold, as well as synthesized upon *B. cinerea* infection in unripe fruit (Amil-Ruiz et al., 2011; Nagpala et al., 2016). Induction of phenylpropanoid biosynthesis could lead to changes in the fruit surface properties that could be picked up by MSI, as well as alterations of the aroma profile that could explain the separation we observed between healthy and infected samples. We also observed an enrichment at 12 hpi in the tricarboxylic acid

(TCA) cycle pathway, which provides the intermediate to fatty acid biosynthesis. Volatile compounds such as esters and green leaf volatiles are derived from fatty acid metabolism, which provides further support for the changes we observed in volatile profiles (Li et al., 2020; Scala et al., 2013).

3.6 Conclusions

Taken together, our results show the potential of using non-destructive approaches for the early detection of gray mold on strawberry fruit. MSI revealed the presence of *B. cinerea* at 12 hpi, when pathogen presence was not visible to the naked eye. Similarly, by profiling aroma signatures we were able to accurately distinguish infected strawberries from healthy fruit at 9 hpi, even earlier than in the MSI approach. Our transcriptomics approach revealed that oxidative responses and synthesis of secondary metabolic compounds more prevalent in infected samples could explain the signals picked up by our two non-destructive approaches. Refining our sampling method will allow for a more accurate study of early fruit molecular responses to *B. cinerea* infection, and reveal processes altered by the fungus that can be leveraged for disease detection. The integration of these two approaches can lead to more accurate and earlier assessment of gray mold in strawberries, which can aid in better disease management practices and decision-making on distribution of certain lots of fruit, minimizing food and monetary losses.

3.7 References

- Amil-Ruiz, F., Blanco-Portales, R., Muñoz-Blanco, J., and Caballero, J. L. (2011). The strawberry plant defense mechanism: A molecular review. *Plant and Cell Physiology*, 52(11):1873–1903.
- Azodanlou, R., Darbellay, C., Luisier, J.-L., Villettaz, J.-C., and Amadò, R. (2004). Changes in flavour and texture during the ripening of strawberries. *European Food Research and Technology*, 218:167–172.
- Badmi, R., Gogoi, A., and Doyle Prestwich, B. (2023). Secondary metabolites and their role in strawberry defense. *Plants*, 12(18):3240.
- Blanco-Ulate, B., Vincenti, E., Powell, A., and Cantu, D. (2013). Tomato transcriptome and mutant analyses suggest a role for plant stress hormones in the interaction between fruit and *Botrytis cinerea*. *Frontiers in Plant Science*, 4:142.
- Bristow, P. R., McNICOL, R. J., and Williamson, B. (1986). Infection of strawberry flowers by *Botrytis cinerea* and its relevance to grey mould development. *Annals of Applied Biology*, 109(3):545–554.
- Buffalo, V. (2010). sam2counts.py—convert sam mapping results to reference sequence counts. Computer software.
- Elad, Y., Pertot, I., Cotes Prado, A. M., and Stewart, A. (2016). Plant hosts of *Botrytis* spp. In Fillinger, S. and Elad, Y., editors, *Botrytis – the Fungus, the Pathogen and its Management in Agricultural Systems*, pages 413–486. Springer International Publishing.
- Fahrentrapp, J., Ria, F., Geilhausen, M., and Panassiti, B. (2019). Detection of gray mold leaf infections prior to visual symptom appearance using a five-band multispectral sensor. *Frontiers in Plant Science*, 10.
- Forney, C. F., Kalt, W., and Jordan, M. A. (2000). The composition of strawberry aroma is influenced by cultivar, maturity, and storage. *HortScience*, 35(6):1022–1026.

- Giakoumoglou, N., Pechlivani, E. M., Sakelliou, A., Klaridopoulos, C., Frangakis, N., and Tzovaras, D. (2023). Deep learning-based multi-spectral identification of grey mould. *Smart Agricultural Technology*, 4.
- Hernández-Martínez, N. R., Blanchard, C., Wells, D., and Salazar-Gutiérrez, M. R. (2023). Current state and future perspectives of commercial strawberry production: A review. *Scientia Horticulturae*, 312:111893.
- Hu, Z., Chang, X., Dai, T., Li, L., Liu, P., Wang, G., Liu, P., Huang, Z., and Liu, X. (2019). Metabolic profiling to identify the latent infection of strawberry by *Botrytis cinerea*. *Evolutionary Bioinformatics*, 15:1176934319838518.
- Jarvis, W. (1962). The infection of strawberry and raspberry fruits by *Botrytis cinerea* fr. *Annals of Applied Biology*, 50(3):569–575.
- Jersch, S., Scherer, C., Huth, G., and Schlösser, E. (1989). Proanthocyanidins as basis for quiescence of *Botrytis cinerea* in immature strawberry fruits/proanthocyanidine als ursache der quieszenz von *Botrytis cinerea* in unreifen erdbeerfrüchten. *Zeitschrift für Pflanzenkrankheiten und Pflanzenschutz/Journal of Plant Diseases and Protection*, pages 365–378.
- Junker, R. R. and Tholl, D. (2013). Volatile organic compound mediated interactions at the plant-microbe interface. *Journal of Chemical Ecology*, 39(7):810–825.
- Langmead, B. and Salzberg, S. L. (2012). Fast gapped-read alignment with bowtie 2. *Nature Methods*, 9(4):357–359.
- Latrasse, A. (1991). *Fruits III*. Routledge.
- Li, H., Larsen, D. H., Cao, R., Van De Peppel, A. C., Tikunov, Y. M., Marcelis, L. F. M., Woltering, E. J., Van Kan, J. A. L., and Schouten, R. E. (2022). The association between the susceptibility to *Botrytis cinerea* and the levels of volatile and non-volatile metabolites in red ripe strawberry genotypes. *Food Chemistry*, 393:133252.

- Li, Z., Wang, Z., Wang, K., Liu, Y., Hong, Y., Chen, C., Guan, X., and Chen, Q. (2020). Co-expression network analysis uncovers key candidate genes related to the regulation of volatile esters accumulation in woodland strawberry. *Planta*, 252(4):55.
- Love, M. I., Huber, W., and Anders, S. (2014). Moderated estimation of fold change and dispersion for rna-seq data with *DESeq2*. *Genome Biol.*, 15:550.
- Morales-Valle, H., Silva, L. C., Paterson, R. R. M., Oliveira, J. M., Venâncio, A., and Lima, N. (2010). Microextraction and gas chromatography/mass spectrometry for improved analysis of geosmin and other fungal “off” volatiles in grape juice. *Journal of Microbiological Methods*, 83(1):48–52.
- Nagpala, E. G., Guidarelli, M., Gasperotti, M., Masuero, D., Bertolini, P., Vrhovsek, U., and Baraldi, E. (2016). Polyphenols variation in fruits of the susceptible strawberry cultivar alba during ripening and upon fungal pathogen interaction and possible involvement in unripe fruit tolerance. *Journal of Agricultural and Food Chemistry*, 64(9):1869–1878.
- Neri, F., Cappellin, L., Spadoni, A., Cameldi, I., Algarra Alarcon, A., Aprea, E., Romano, A., Gasperi, F., and Biasioli, F. (2015). Role of strawberry volatile organic compounds in the development of *Botrytis cinerea* infection. *Plant Pathology*, 64(3):709–717.
- Peng, Y., Van Wersch, R., and Zhang, Y. (2018). Convergent and divergent signaling in pamp-triggered immunity and effector-triggered immunity. *Molecular Plant-Microbe Interactions*(®), 31(4):403–409.
- Petrusch, S., Knapp, S. J., Van Kan, J. A. L., and Blanco-Ulate, B. (2019). Grey mould of strawberry, a devastating disease caused by the ubiquitous necrotrophic fungal pathogen *Botrytis cinerea*. *Molecular Plant Pathology*, 20(6):877–892.
- Sbodio, A. O., Mesquida-Pesci, S. D., Yip, N., Alvarez-Rojo, I., Gutierrez-Baeza, E., Tay, S., Bello, P., Wang, L., and Blanco-Ulate, B. (2024). Non-wounding contact-based inoculation of fruits with fungal pathogens in postharvest. *Plant Methods*, 20(1):83.

- Scala, A., Allmann, S., Mirabella, R., Haring, M., and Schuurink, R. (2013). Green leaf volatiles: A plant's multifunctional weapon against herbivores and pathogens. *International Journal of Molecular Sciences*, 14(9):17781–17811.
- Shi, Y., Liu, X., Fang, Y., Tian, Q., Jiang, H., and Ma, H. (2018). 2, 3-butanediol activated disease-resistance of creeping bentgrass by inducing phytohormone and antioxidant responses. *Plant Physiology and Biochemistry*, 129:244–250.
- Terentev, A., Dolzhenko, V., Fedotov, A., and Eremenko, D. (2022). Current state of hyperspectral remote sensing for early plant disease detection: A review. *Sensors*, 22(3):757.
- Vandendriessche, T., Keulemans, J., Geeraerd, A., Nicolai, B. M., and Hertog, M. L. A. T. M. (2012). Evaluation of fast volatile analysis for detection of *Botrytis cinerea* infections in strawberry. *Food Microbiology*, 32(2):406–414.
- Williamson, B., Tudzynski, B., Tudzynski, P., and Van Kan, J. A. L. (2007). *Botrytis cinerea*: The cause of grey mould disease. *Molecular Plant Pathology*, 8(5):561–580.
- Zhang, X., Wang, M., Gan, C., Ren, Y., Zhao, X., and Yuan, Z. (2023). Riboflavin application delays senescence and relieves decay in harvested strawberries during cold storage by improving antioxidant system. *LWT*, 182:114810.

3.8 Supplementary Material

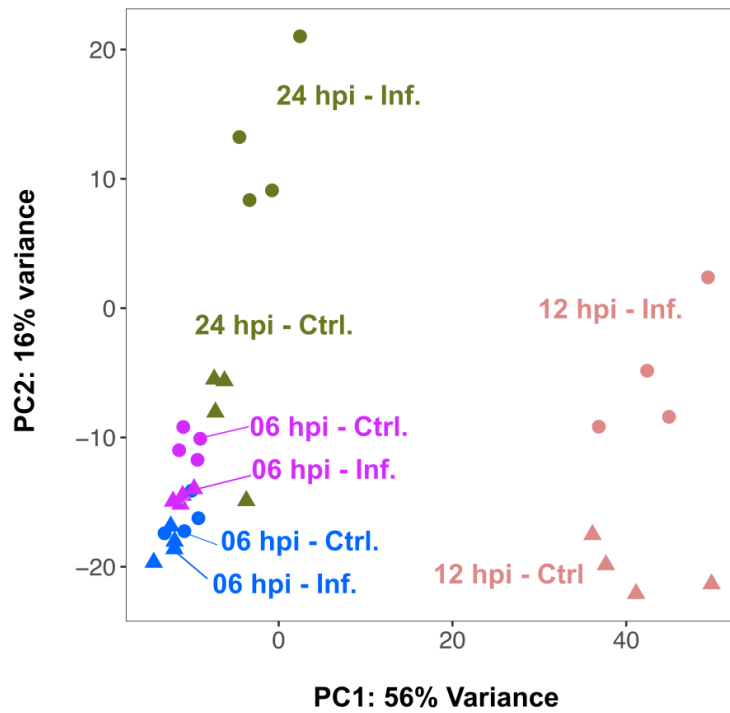


Figure 3.S1: Principal component analysis (PCA) of total mapped RNA-seq *Botrytis cinerea* and strawberry reads. Triangles denote mock-inoculated (Ctrl.) samples, and circles denote *B. cinerea*-inoculated (Inf.) samples. hpi = hours post inoculation.

All supplementary tables can be accessed on <https://ucdavis.box.com/s/zowp2bchu9f3mdakyn2u3def6ky2jotk>